

# **Mechanisms of Engine Blow-By Aerosol Formation and Resulting Strategies for their Reduction**

Zur Erlangung des akademischen Grades eines  
DOKTORS DER INGENIEURWISSENSCHAFTEN (DR.-ING.)

von der KIT-Fakultät für Chemieingenieurwesen und Verfahrenstechnik des  
Karlsruher Instituts für Technologie (KIT)

genehmigte

DISSERTATION

von

Dipl.-Ing. Niclas Giovanni Jorg Pino Nowak  
aus Reutlingen

Tag der mündlichen Prüfung: 01.07.2024

Erstgutachter: Prof. Dr. Gerhard Kasper

Zweitgutachter: Prof. Dr. Dieter Stapf







# Preface

I owe the success of this work to the support of wonderful people.

I would like to thank my doctoral supervisor, Prof. Gerhard Kasper, for the numerous valuable suggestions and enriching discussions. Especially the close cooperation within the "Crankcase Ventilation Consortium" have helped me both professionally and personally.

I would like to thank Prof. Thomas Koch for the very good cooperation and valuable input. It was a great pleasure to work with him as a team.

I would like to thank Prof. Dieter Stapf for reviewing my doctoral thesis.

I would like to thank Prof. Achim Dittler for supporting this work.

I would like to thank Dr. Jörg Meyer for the frequent and invaluable professional exchange, as well as his great support. Many thanks also to Jürgen Pfeil for his contributions.

I would especially like to thank my colleague and friend Dipl.-Ing. Kai-Michael Scheiber for the great cooperation. I could not have wished for a more pleasant and competent project partner than him.

I would also like to thank all my student thesis writers, whose work contributed significantly to the success of this dissertation. In particular, I would like to emphasize the valuable cooperation with Tabea Sinn and Christian Straube.

I would like to thank all colleagues from the administration, engineering, workshops, and laboratories of the MVM institute for their great cooperation and support.

I would like to thank UT99 AG for the valuable cooperation in the "Crankcase Ventilation Consortium" and the support to complete this project.

From the bottom of my heart, I would like to thank my parents Nelida and Karl, who have always supported me fully.

My dearest thanks go to my wife Carolin, who has always supported and motivated me.

Karlsruhe, February 2024

Niclas Nowak



# Declaration of independent work

I hereby declare that I completed this work independently and that I have used no aids other than those referenced. The parts of the work, which include phrases or points taken from other sources, are clearly marked with the origin of the information.

Karlsruhe, February 2024

Niclas Nowak



# Abstract

The formation of blow-by aerosols poses a risk to sustainable engine operation. These aerosols contribute to particulate matter (PM) emissions and gaseous (e.g., methane slip) emissions in combustion engines with open crankcase ventilation systems. In engines with closed crankcase ventilation, these aerosols form deposits that reduce engine efficiency, performance, and reliability. To avoid such issues, highly efficient oil mist filters and in-engine reduction strategies based on a quantitative understanding of aerosol sources and formation mechanisms in the crankcase environment are key.

However, obtaining accurate measurements of particle size distributions (PSDs) in engine blow-by aerosols is challenging due to several factors such as high number concentrations, elevated temperatures, the presence of saturated vapor, and unsteady flow conditions. To address these challenges, a comprehensive study was conducted using a commercial optical particle counter (OPC). In this study, single-stage (1:9) and double-stage (1:80) sampling, dilution, and conditioning systems were devised and characterized to determine their effectiveness in the OPC sensor range of 0.3 to 17  $\mu\text{m}$ . Correcting for particle losses, primarily due to inertia, was crucial for reliable PSD measurements, with losses exceeding 90% at 10  $\mu\text{m}$ . The impact of saturated oil vapor on droplet growth during the cooling and dilution of the sample flow was investigated based on actual vapor concentration data. Results showed that droplet growth became significant above 100  $^{\circ}\text{C}$ , but diluting the sample flow with 20  $^{\circ}\text{C}$  air at a 1:20 ratio suppressed growth. Tests conducted with engine blow-by aerosols using the overall sampling and dilution strategy demonstrated excellent reproducibility and good agreement (after loss corrections) with reference data regarding PSD in the 0.3-10  $\mu\text{m}$  range and total mass. However, the actual engine blow-by PSD was broader, exceeding the measurement range of the OPC on both ends. Converting OPC data from particle number to mass underestimated the total mass by 10% to 20% compared to weighed filter samples, unless contamination with oil deposits on the OPC was avoided. A re-calibration procedure is proposed to address pressure pulsations resulting from engine operation.

Based on these findings, a comprehensive study was carried out with the same OPC on a medium-duty 4-cylinder 5.1-liter diesel engine. The influence of oil temperature, engine load and engine speed on the blow-by aerosol properties was investigated. Increasing the engine load at 1200 rpm from 0 to 880 Nm at a free-moving oil temperature of up to 117 °C resulted in a 64% higher concentration of particles smaller than 1.2  $\mu\text{m}$ . At a constant oil temperature of 93 °C, the same test resulted in a 50% higher concentration. Lowering the oil temperature to 48 °C almost completely prevented the formation of submicron particles. When the engine speed is increased from 1400 to 2400 rpm, the concentration below 2.7  $\mu\text{m}$  increases significantly. Both the increase in engine load and the increase in engine speed resulted in an increase in the blow-by gas flow rate and thus more aerosol emissions from the crankcase. To determine the aerosol contribution of the turbocharger, experiments were conducted by coupling and decoupling the turbocharger. The results show that the turbocharger is a negligible aerosol source at nominal engine power but contributes significantly to the blow-by gas flow, up to 30%. The location of the blow-by aerosol sources within the engine was determined by varying the OPC sampling points and introducing dilution air into different sections of the crankcase. The lower crankcase compartment was found to be the major source of submicron aerosols. Introducing air into this compartment caused particles to be flushed through the riser ducts into the upper crankcase section. This did not result in the dilution of the aerosol, but the mass rates increased in proportion to the dilution factor. Analysis of the separation characteristics of the risers showed inertial behavior and very low efficiencies of less than 10% at 10  $\mu\text{m}$ , resulting in most particles <10  $\mu\text{m}$  passing through the ducts unhindered. The upper part of the crankcase proved to be a source of particles larger than 2.7  $\mu\text{m}$  and even larger than 10  $\mu\text{m}$ . These particles were captured by a filter integrated directly into the valve cover.

Information on the contribution of single aerosol sources in the lower crankcase compartment was obtained from a 1.3-L single-cylinder engine under well-defined conditions in the 0.01 to 10  $\mu\text{m}$  size spectrum. The formation of supermicron particles in the crankcase was mainly attributed to cooling jet break-up when the piston was at top dead

center (TDC). Conversely, aerosol generation decreased by approximately 90% at bottom dead center (BDC) due to the shorter and more stable oil jet. Motoring the engine resulted in an additional peak around  $0.7\ \mu\text{m}$ , associated with oil atomization at the piston rings, which increased significantly with cylinder peak pressure. No significant contribution from bearings was identified at peak pressures below 116 bar, and engine speed had a minor effect on aerosol properties. Operating the engine in fired mode substantially increased submicron aerosol concentration, likely due to higher peak pressures promoting aerosol generation at the piston rings and the formation of additional particles from recondensing oil vapor generated at hotspots. Soot or ash aerosols were not detected in the crankcase aerosol, possibly because they were integrated into the bulk oil.

The formation mechanisms involving nucleation and growth by vapor condensation, with and without pre-existing nuclei, were investigated experimentally and through one-dimensional simulations under engine-like conditions using actual engine oil and hexadecane. The equilibrium saturation levels at temperatures ranging from  $100\ ^\circ\text{C}$  to  $130\ ^\circ\text{C}$  were well-defined, and cooling occurred in laminar tube flow at a controlled rate. Nucleation and growth of pre-existing nuclei resulted in separate peaks around  $0.25 \pm 0.1\ \mu\text{m}$  and  $0.7 \pm 0.2\ \mu\text{m}$ , respectively, which closely matched actual engine data. The position of the latter peak was relatively insensitive to the primary nuclei size within the range of  $0.04$  to  $0.2\ \mu\text{m}$ . Increasing vapor concentration (via more volatile oil or higher temperature) or decreasing the cooling rate slightly enlarged the nucleation peaks ( $0.15\ \mu\text{m}$  to  $0.35\ \mu\text{m}$ ) but significantly reduced peak concentrations by a factor of 10. This counterintuitive result can be explained by shifts in the supersaturation profile during cool-down. It should be noted that in both experiment and simulation, spontaneous nucleation was limited to pre-existing nuclei concentrations below approximately  $2 \times 10^5$  to  $5 \times 10^5\ \text{cm}^{-3}$  at engine oil temperatures of  $100\ ^\circ\text{C}$  or higher. Vapor losses to system walls during cool-down were found to be a significant factor in both actual engine environments and laboratory settings, and they must be considered for realistic simulations, as they affect the actual number concentrations more than the peak location.

Effective in-engine strategies for reducing blow-by aerosols were developed. They involve the optimization of piston ring design, as these rings are identified as the primary contributors to submicron crankcase aerosol. Minimizing blow-by gas flow at the piston rings is crucial for effective reduction. Additionally, reducing the brake mean effective pressure (BMEP) of the engine is beneficial, as crankcase emissions increase exponentially with BMEP. Enhancing piston cooling, particularly by reducing the oil temperature of the cooling jet, is a more viable approach. Specifically, decreasing the oil temperature of the cooling jet on a single-cylinder diesel engine from 80 °C to 50 °C resulted in a 33% reduction in mass emissions in the 0.7 μm mode, while reducing the oil temperature on a 4-cylinder diesel engine from 93 °C to approximately 70 °C led to a 50% decrease in particles smaller than 1 μm. The impact of the oil cooling nozzle, which generates a mode around 2 μm by forming satellite drops during the break-up of the oil jet is also addressed. Improving jet stability by reducing the distance between the nozzle and the piston helps minimize the impact of this source. Regarding the turbocharger, its contribution to aerosol mass was found to be less than 20%, but it accounted for up to 30% of the blow-by gas flow. Introducing this gas flow in the lower region of the crankcase did not dilute the blow-by aerosol but rather flushed out additional particles. On the other hand, directing gases from the turbocharger or other sources to the upper region of the crankcase is beneficial as it led to the expected dilution of the blow-by aerosol. However, this approach requires that the entrance of the ventilation system is in the upper crankcase region. The work highlights the saturated environment of the crankcase, which contains a significant amount of oil vapor. At crankcase temperatures around 120 °C, condensation of this vapor during cooling substantially increases the aerosol mass of existing nuclei and possibly also forms new particles. Therefore, lower bulk oil temperatures and fewer engine hotspots play a vital role in reducing crankcase aerosol concentration. The impact of less volatile engine oils is less straightforward, as higher vapor pressure leads to the formation of fewer but larger droplets through nucleation and growth of existing aerosols. Larger droplets are easier to remove using most abatement devices. Lower cooling rates are also beneficial for similar reasons, although controlling them in engine design poses challenges.

# Kurzfassung

Die Bildung von Blow-By-Aerosolen stellt eine Gefahr für den nachhaltigen Betrieb von Verbrennungsmotoren dar. Diese Aerosole tragen zu den Emissionen von Partikeln und gasförmigen Stoffen (z.B. Methanschleupf) bei, wenn ein offenes Kurbelgehäuseentlüftungssystem Verwendung findet. In Motoren mit geschlossener Kurbelgehäuseentlüftung bilden diese Aerosole Ablagerungen, die die Effizienz, Leistung und Zuverlässigkeit des Motors negativ beeinträchtigen. Um solche Probleme zu vermeiden, sind hoch effiziente Ölnebelfilter und innermotorische Reduktionsstrategien auf Basis eines quantitativen Verständnisses der Aerosolquellen und Bildungsmechanismen im Kurbelgehäuse entscheidend.

Die genaue Messung von Partikelgrößenverteilungen (PGV) von Blow-By-Aerosolen ist jedoch aufgrund mehrerer Faktoren wie hohe Anzahlkonzentrationen, hohe Temperaturen, dem Vorhandensein von gesättigtem Dampf und instabilen Strömungsbedingungen, herausfordernd. Um diesen Herausforderungen zu begegnen, wurde eine umfassende Studie mit einem kommerziellen optischen Partikelzähler (OPC) durchgeführt. In dieser Studie wurde ein einstufiges (1:9) und ein zweistufiges (1:80) Probenahme-, Verdünnungs- und Konditionierungssystem entwickelt und charakterisiert, um ihre Wirksamkeit im OPC-Sensorbereich von 0.3 bis 17  $\mu\text{m}$  zu bestimmen. Die Korrektur von Partikelverlusten, hauptsächlich aufgrund von Trägheit, war entscheidend für zuverlässige PGV-Messungen, wobei die Verluste bei 10  $\mu\text{m}$  mehr als 90% betragen. Der Einfluss von gesättigtem Öldampf auf das Tropfenwachstum während der Abkühlung und Verdünnung des Probenstroms wurde experimentell untersucht. Die Ergebnisse zeigen, dass das Tropfenwachstum oberhalb von 100 °C signifikant ist, aber die Verdünnung des Probenstroms mit 20 °C Luft im Verhältnis von 1:20 das Wachstum unterdrückt. Tests mit Motor-Blow-By-Aerosolen unter Verwendung der erarbeiteten Probenahme- und Verdünnungsstrategie zeigten eine ausgezeichnete Reproduzierbarkeit und gute Übereinstimmung (nach Verlustkorrekturen) mit Referenzdaten bezüglich der PGV im Bereich von 0.3 bis 10  $\mu\text{m}$  und der Gesamtmasse. Die tatsächliche Blow-By-PGV am Motor war

jedoch breiter und übertraf den Messbereich des OPC auf beiden Seiten. Die Umrechnung von OPC-Daten von der Partikelanzahl in die Masse unterschätzte die Gesamtmasse um 10% bis 20% im Vergleich zu gewogenen Filterproben, es sei denn, eine Kontamination des OPC durch Ölablagerungen wurde vermieden. Ein Neukalibrierungsverfahren wurde erarbeitet, um Messartefakte durch Druckpulsationen beim Betrieb des Motors zu verhindern.

Auf Grundlage dieser Erkenntnisse wurde eine umfassende Studie mit demselben OPC an einem 4-Zylinder-5.1-Liter-Dieselmotor durchgeführt. Der Einfluss der Öltemperatur, der Motorlast und der Motordrehzahl auf die Eigenschaften der Blow-By-Aerosole wurde untersucht. Eine Erhöhung der Motorlast bei 1200 U/min von 0 auf 880 Nm bei einer variablen Öltemperatur von bis zu 117 °C führte zu einer 64% höheren Konzentration von Partikeln kleiner als 1.2 µm. Bei einer konstanten Öltemperatur von 93 °C führte derselbe Test zu einer 50% höheren Konzentration. Eine Verringerung der Öltemperatur auf 48 °C verhinderte nahezu vollständig die Bildung von submikronen Partikeln. Bei Erhöhung der Motordrehzahl von 1400 auf 2400 U/min stieg die Konzentration unter 2.7 µm signifikant an. Sowohl die Erhöhung der Motorlast als auch die Erhöhung der Motordrehzahl führten zu einer Zunahme des Blow-By-Volumenstroms und somit zu mehr Aerosolemissionen aus dem Kurbelgehäuse. Um den Beitrag des Turboladers zum Aerosolausstoß zu bestimmen, wurden Experimente durchgeführt, indem der Turbolader gekoppelt oder entkoppelt wurde. Die Ergebnisse zeigen, dass der Turbolader eine vernachlässigbare Aerosolquelle bei nomineller Motorleistung ist, aber bis zu 30% zum Blow-By-Gasvolumenstrom beiträgt. Der Ort der Blow-By-Aerosolquellen im Motor wurde durch Variation der OPC-Probenahmestellen und das Einbringen von Verdünnungsluft in verschiedene Bereiche des Kurbelgehäuses bestimmt. Es stellte sich heraus, dass der untere Kurbelgehäusebereich die Hauptquelle für submikrone Aerosole ist. Das Einbringen von Luft in diesem Bereich führte dazu, dass Partikeln durch die Steigrohre in den oberen Kurbelgehäusebereich gespült wurden. Dies führte nicht zur Verdünnung des Aerosols, sondern der Massenstrom erhöhte sich proportional zum Verdünnungs-

faktor. Die Analyse der Abscheideeigenschaften der Steigrohre zeigte sehr geringe Effizienzen von weniger als 10% bei 10  $\mu\text{m}$ , wodurch die meisten Partikeln  $<10 \mu\text{m}$  ungehindert durch die Rohre hindurchtraten. Der obere Teil des Kurbelgehäuses erwies sich als Quelle von Partikeln größer als 2.7  $\mu\text{m}$  und sogar größer als 10  $\mu\text{m}$ . Diese Partikeln wurden von einem direkt in die Ventilabdeckung integrierten Filter erfasst.

Informationen über den Beitrag einzelner Aerosolquellen im unteren Kurbelgehäusebereich wurden unter definierten Bedingungen an einem 1.3-Liter-Einzylinder-Motor im Größenbereich von 0.01 bis 10  $\mu\text{m}$  gewonnen. Die Bildung von supermikronen Partikeln im Kurbelgehäuse wurde hauptsächlich dem Zerfall des Kühlstrahls zugeschrieben, wenn der Kolben den oberen Totpunkt erreichte. Umgekehrt nahm die Aerosolerzeugung beim unteren Totpunkt aufgrund des kürzeren und stabileren Ölstrahls um etwa 90% ab. Der geschleppte Betrieb des Motors führte zu einem zusätzlichen Peak bei etwa 0.7  $\mu\text{m}$ , der mit der Ölzerstäubung an den Kolbenringen zusammenhängt und mit dem Zylinder-Spitzendruck signifikant ansteigt. Es wurde kein signifikanter Beitrag von Lagern bei Spitzendrücken unter 116 bar identifiziert, und die Motordrehzahl hatte nur einen geringen Einfluss auf die Aerosoleigenschaften. Der befeuerte Betrieb des Motors erhöhte die Konzentration von submikronen Aerosolen erheblich, vermutlich aufgrund höherer Spitzendrücke, die die Aerosolerzeugung an den Kolbenringen förderten und zusätzliche Partikeln aus rekondensierendem Öldampf bildeten, der an heißen Stellen entstand. Ruß- oder Ascheaerosole wurden im Kurbelgehäuseaerosol nicht nachgewiesen, möglicherweise weil sie in das flüssige Öl eingetragen wurden.

Die Nukleation und das Wachstum durch Dampfkondensation, mit und ohne vorhandenen Keimen, wurde als relevanter Bildungsmechanismus von Kurbelgehäuseaerosolen erkannt und sowohl experimentell als auch durch eindimensionale Simulationen unter motorähnlichen Bedingungen untersucht. Dabei wurde sowohl Motoröl als auch Hexadecan zu Modellbildungszwecken verwendet. Eine Luftatmosphäre wurde bei Temperaturen von 100 °C bis 130 °C gesättigt, und die Abkühlung erfolgte in laminarem Rohrfluss mit kontrollierter Rate. Nukleation und Wachstum von vorhandenen Keimen führten zu separaten Moden bei etwa  $0.25 \pm 0.1 \mu\text{m}$  und  $0.7 \pm 0.2 \mu\text{m}$ , die eng mit tatsächlichen

Motordaten übereinstimmten. Die Position des letzteren Peaks war relativ unempfindlich gegenüber der Größe der primären Keime im Bereich von 0.04 bis 0.2  $\mu\text{m}$ . Eine Erhöhung der Dampfkonzentration (durch leicht flüchtigeres Öl oder höhere Temperatur) oder eine Verringerung der Abkühlrate vergrößerten die Nukleationspeaks leicht (0.15  $\mu\text{m}$  bis 0.35  $\mu\text{m}$ ), reduzierten aber die Spitzenkonzentrationen signifikant um den Faktor 10. Dieses Ergebnis lässt sich durch Veränderungen der Übersättigung während der Abkühlung erklären. Sowohl im Experiment als auch in der Simulation wurde gezeigt, dass homogene Nukleation bei Fremdkeimkonzentrationen kleiner  $2 \times 10^5$  bis  $5 \times 10^5 \text{ cm}^{-3}$  und Motoröltemperaturen von 100 °C oder höher auftritt. Dampfverluste an Systemwänden während der Abkühlung stellten sich sowohl in realen Motoren als auch im Labor als bedeutender Faktor heraus und muss für realistische Simulationen berücksichtigt werden, da sie die tatsächlichen Partikelkonzentrationen stärker beeinflussen als die Peak-Position.

Effektive innermotorische Strategien zur Reduzierung von Blow-By-Aerosolen wurden entwickelt. Sie beinhalten die Optimierung des Kolbenringdesigns, da sie als Hauptverursacher von submikronen Kurbelgehäuseaerosolen identifiziert wurden. Die Minimierung des Blow-By-Gasstroms an den Kolbenringen ist entscheidend für eine effektive Reduzierung der Emissionen. Zusätzlich ist die Verringerung des effektiven Mitteldrucks des Motors vorteilhaft, da Kurbelgehäuseemissionen exponentiell mit dem effektiven Mitteldruck ansteigen. Eine vielversprechendere Methode ist die Verbesserung der Kolbenkühlung, insbesondere durch die Reduzierung der Öltemperatur des Kühlstrahls. Konkret führte die Verringerung der Öltemperatur des Kühlstrahls an einem Einzylinder-Dieselmotor von 80 °C auf 50 °C zu einer 33%igen Reduzierung der Massenemissionen in der 0.7  $\mu\text{m}$  Mode. Eine Reduktion der Öltemperatur an einem Vierzylinder-Dieselmotor von 93 °C auf etwa 70 °C führte zu einer 50%igen Abnahme der Partikelmasseemissionen kleiner als 1  $\mu\text{m}$ . Auch dem Beitrag der Ölkühldüse, der durch die Bildung von Satellitentröpfchen während des Zerfalls des Ölstrahls eine Mode um 2  $\mu\text{m}$  erzeugt, kann entgegengewirkt werden. Die Verbesserung der Strahlstabilität durch Verringe-

rung des Abstands zwischen Düse und Kolben hilft, den Einfluss dieser Quelle zu minimieren. Hinsichtlich des Turboladers wurde festgestellt, dass sein Beitrag zur Aerosolmasse weniger als 20% beträgt, jedoch bis zu 30% des Blow-by-Gasstroms ausmacht. Das Einleiten dieses Gasstroms im unteren Bereich des Kurbelgehäuses verdünnte nicht das Blow-By-Aerosol, sondern spült zusätzliche Partikeln heraus. Es ist vorteilhaft, Gase vom Turbolader oder anderen Quellen in den oberen Bereich des Kurbelgehäuses zu leiten, da dies zur erwarteten Verdünnung des Blow-By-Aerosols führte. Diese Methode erfordert jedoch, dass der Eingang der Entlüftung im oberen Bereich des Kurbelgehäuses liegt. Die Arbeit hebt die gesättigte Umgebung des Kurbelgehäuses hervor, die eine erhebliche Menge an Öldampf enthält. Bei Kurbelgehäusetemperaturen von etwa 120 °C führt die Kondensation dieses Dampfes während des Abkühlens wesentlich zu einer Erhöhung der Aerosolmasse bestehender Keime und möglicherweise auch zur Bildung neuer Partikeln. Daher spielen niedrigere Öltemperaturen und weniger heiße Stellen im Motor eine entscheidende Rolle bei der Reduzierung der Konzentration von Kurbelgehäuseaerosolen. Der Einfluss von weniger flüchtigen Motorölen ist weniger eindeutig, da ein höherer Dampfdruck zu weniger, jedoch größeren Tropfen durch die Keimbildung und das Wachstum bestehender Aerosole führt. Größere Tropfen lassen sich leichter mit den meisten Abscheidevorrichtungen entfernen. Niedrigere Kühlraten sind aus ähnlichen Gründen vorteilhaft, jedoch lassen sie sich in der Motorumgebung nur schwer kontrollieren.



# Contents

<b>Preface .....</b>	<b>i</b>
<b>Declaration of independent work.....</b>	<b>iii</b>
<b>Abstract.....</b>	<b>v</b>
<b>Kurzfassung .....</b>	<b>ix</b>
<b>Contents .....</b>	<b>xv</b>
<b>List of abbreviations.....</b>	<b>xix</b>
<b>1 Introduction .....</b>	<b>1</b>
1.1 Project structure, scope, and aim .....	2
1.2 Characterization methods for blow-by aerosols .....	4
1.3 Formation mechanisms of blow-by aerosols .....	9
1.4 Literature review on blow-by aerosol size distributions .....	16
1.5 References .....	24
<b>2 Sampling and conditioning of engine blow-by aerosols for representative measurements by optical particle counters .....</b>	<b>29</b>
2.1 Abstract .....	29
2.2 Introduction .....	30
2.3 Experimental materials, methods, and procedures .....	33
2.4 Results and discussion .....	41
2.5 Summary and conclusions .....	52
2.6 References .....	55
<b>3 Blow-by aerosol spectra from a 4-cylinder 5.1-liter diesel engine .....</b>	<b>59</b>
3.1 Introduction .....	59
3.2 Engine characteristics and test stand .....	60
3.3 Influence of oil temperature, engine load, and speed on aerosol .....	64
3.4 Experiments to locate aerosol sources within the engine .....	75
3.5 Contribution of the turbocharger to the aerosol load .....	87
3.6 Aerosol sources beyond the optical particle counter measuring range .....	90
3.7 References .....	95
<b>4 On blow-by aerosol sources in a single-cylinder crankcase environment.....</b>	<b>97</b>
4.1 Abstract .....	97
4.2 Introduction .....	98

4.3	Materials and methods .....	100
4.4	Results and discussion .....	105
4.5	Summary and conclusions .....	113
4.6	Acknowledgements.....	114
4.7	UT99 AG .....	114
4.8	References .....	115
<b>5</b>	<b>On aerosol formation by condensation of oil vapor in the crankcase of combustion engines .....</b>	<b>117</b>
5.1	Abstract.....	117
5.2	Introduction .....	118
5.3	Materials and methods.....	124
5.4	Results and discussion .....	132
5.5	Summary and conclusions .....	144
5.6	References .....	147
5.7	List of symbols.....	150
<b>6</b>	<b>Summary and conclusions .....</b>	<b>153</b>
6.1	Strategies for reducing blow-by aerosol formation.....	158
	<b>List of publications.....</b>	<b>165</b>





# List of abbreviations

APS	aerodynamic particle sizer
BDC	bottom dead center
BMEP	brake mean effective pressure
CPC	condensation particle counter
DMA	differential mobility analyzer
DMS	differential mobility spectrometer
EEPS	engine exhaust particle sizer
ELPI	electrical low pressure impactor
GC	gas chromatography
ICE	internal combustion engine
Oh	Ohnesorge number
OPC	optical particle counter
PM	particulate matter
PSD	particle size distribution
QCM	quartz crystal monitor
Re	Reynolds number
S	saturation
SMPS	scanning mobility particle sizer
St	Stokes number
TDC	top dead center



# 1 Introduction

Since the end of the 19<sup>th</sup> century internal combustion engines (ICEs) have revolutionized the transportation of people and goods. Advancements in material sciences, thermodynamics, manufacturing processes, and the development of transportation infrastructure greatly expanded the practicality of these engines, leading to their widespread adoption throughout the 20<sup>th</sup> century (Basshuysen et al., 2015). However, in recent years, this technology has faced growing public criticism due to its environmental impact resulting from unsustainable fuels and harmful emissions. In order to maintain the competitiveness of combustion engines against alternative propulsion concepts while complying with an increasingly stringent legal framework (e.g., EU, EPA, IMO), the main focus of technological development is now on introducing renewable fuels, implementing in-engine measures to reduce emissions, and optimizing the exhaust gas treatment system.

Open crankcase ventilation systems contribute to particulate matter (PM) and gaseous emissions. These systems are a significant source for methane slip (Nigel et al., 2017). In engines with a closed ventilation system, crankcase aerosols can form deposits that reduce engine efficiency, performance, and reliability (Lakshmanan et al., 2019; Uy et al., 2017; Jaroszczyk et al., 2006). In addition, crankcase aerosol residues from combustion contain CaSO<sub>4</sub> and zinc phosphates (Dittler, 2012) that impact on the performance of aftertreatment systems negatively (Sauter, 2004; Yilmaz et al., 2002) and pose a risk to sustainable engine operation. To avoid these issues, the key lies in implementing both highly efficient oil mist separators as well as in-engine reduction strategies based on a comprehensive understanding of aerosol sources and formation mechanisms in the crankcase environment.

However, there is currently limited knowledge available in this area. It is understood that when an engine operates normally, gases originating from the combustion chamber leak through the piston rings, turbocharger bearings, and valve stems before reaching the crankcase. These gases, known as blow-by gases, contain particles that are formed

within the crankcase through processes such as vapor condensation or mechanical atomization (Johnson, 2012). Such particles consist primarily of oil, with traces of soot, ash, fuel, and water. This thesis focuses on blow-by aerosol. It examines suitable characterization methods for such aerosols, their formation mechanisms, and proposes strategies for reducing its formation rate within the crankcase.

### 1.1 Project structure, scope, and aim

**Chapter 1** presents information on commonly employed methods for aerosol characterization, the mechanisms of blow-by aerosol formation, and a comprehensive literature review concerning the particle size distributions of blow-by aerosols. Building upon this foundation, the subsequent chapters give new insights regarding measurement methods and generation mechanisms of blow-by aerosols, as well as strategies for reducing their formation.

In **Chapter 2**, a specific optical particle counter (OPC) from Palas® GmbH undergoes extensive validation to ensure its suitability for measuring blow-by aerosols in a combustion engine environment. Two dilution systems, one with a single stage and another with two stages, are developed to reduce the aerosol concentration by ratios of 1:9 or 1:80, respectively. The OPC, measuring procedures, and the associated sampling and conditioning system are tested using actual blow-by aerosols obtained from a medium-duty four-cylinder 5.1-liter diesel engine.

**Chapter 3** showcases particle size distribution (PSD) data collected from the same 4-cylinder engine, now operating at various points across the engine map, covering a wide range of engine speeds, loads, and oil temperatures. Additionally, aerosols are characterized at different points within the engine in order to locate their sources. The study also includes a discrete analysis of the turbocharger to gain insights into its contribution to the overall aerosol load. Furthermore, open face filter samples are taken and electrical mobility measurements are conducted to complement the aerosol data beyond the upper and lower limits of the OPC's measurement range.

**Chapter 4** concentrates on a single-cylinder engine setup that is operated in motored or fired mode to gain further understanding of mechanical atomization processes occurring at the oil-spattering nozzle, piston rings, and bearings. This setup is also utilized to explore the potential entry of soot and ash into the crankcase.

Given the limited knowledge available on blow-by aerosol generation through condensation, **Chapter 5** places significant emphasis on this topic, both experimentally and theoretically. Chemical analysis using gas chromatography provides evidence of aerosol formation through condensation within the crankcase. Experiments involving surrogate aerosols and saturated oil vapor contribute to a better understanding of the thermodynamic conditions that lead to homogeneous and heterogeneous condensation. Additionally, a calculation model based on classical nucleation theory is developed to gain further insights into these processes.

**Chapter 6** presents a summary of the findings and concludes with remarks on aerosol reduction strategies.

Note that Chapters 2, 4, and 5 have been taken from publications.

The objective of this predominantly experimental study is to obtain and analyze a comprehensive and reliable set of aerosol data generated by one specific (and typical) diesel engine, rather than to compare aerosol emission data from various engines with each other. While the data obtained from this research may be valuable for designing separators for crankcase ventilation systems, here the primary aim is to understand the underlying mechanisms of aerosol formation and to identify the relevant internal sources. This understanding points to in-engine strategies for reducing aerosol formation on the basis of an optimized engine design, process parameters, and operating fluids. While the implementation of such changes is ultimately the responsibility of engine manufacturers, the aim of this dissertation is to provide the necessary understanding as well as experimental tools.

## 1.2 Characterization methods for blow-by aerosols

A prerequisite for characterizing aerosol sources and formation mechanisms in the crankcase is obtaining reliable data on aerosol size and concentration. Since blow-by aerosols can range in size from about 10 nm to several 100  $\mu\text{m}$ , various measurement methods are required to cover the entire size spectrum. Typical blow-by aerosol number concentrations exceed  $10^6 \text{ cm}^{-3}$  and necessitates dilution in most measurement setups. However, there are additional challenges associated with high crankcase gas temperatures (usually 90 to 120  $^{\circ}\text{C}$ ) and significant concentrations of condensable vapor, which can alter aerosol properties during sampling if not handled carefully. The pulsatile nature of the blow-by gas stream also poses challenges to isokinetic sampling and may affect the accuracy of aerosol spectrometers. Therefore, obtaining reliable and representative data on blow-by aerosols is a highly demanding task.

The measurement conditions for exhaust emissions (Burtscher, 2005) and crankcase emissions are similar in terms of high particle concentrations in the submicron and low micron range, as well as high temperatures. However, there are differences in the nature of the particles between the two. Exhaust particles are in a solid aggregate state while in the crankcase, they exist mostly if not entirely as liquid droplets. As a result, the measurement system needs to be tailored accordingly. Dealing with liquid aerosols presents its own challenges, such as wetting (if not flooding) of surfaces in contact with the droplets, which can act as sources of accumulated secondary aerosols. Additionally, the presence of condensable vapor poses a well-known challenge in aerosol technology. It can negatively affect the accuracy of the measurement device and potentially falsify the particle size distribution due to condensation. Generally, the sampling and dilution system must consider inertial losses, including those caused by bends in the sampling setup (Pui et al., 1987).

Over the past decades, several measurement techniques have been employed to characterize blow-by aerosols. These techniques are based on distinguishing physical fea-

tures such as particle inertia, light-matter interactions, or electrical mobility. Instruments using particle inertia include impactors and the APS (TSI Inc.), while aerosol spectrometers based on light-matter interactions utilize techniques like scattered light detection (e.g., OPC) and extinction measurement. Electric mobility methods rely on the mobility of charged particles in an electric field and include instruments such as SMPS, EEPS (TSI Inc.), and DMS500 (Cambustion Ltd.). Furthermore, data on total concentration without particle size information can be obtained through gravimetric analysis (mass) or condensation particle counters (number). Each instrument has specific advantages and disadvantages and requires different conditioning of the sample streams. The size determined by these measuring systems is typically an equivalence diameter. Nevertheless, converting this equivalence diameter to the geometric diameter is relatively straightforward for oil droplets since they are spherical in shape.

**Impactors** operate on the principle of inertial separation, typically by a sharp change in flow direction, in order to separate, size, and collect particles. The equivalent diameter obtained from these devices is the so-called aerodynamic diameter. One major advantage of impactors is their wide measurement range, which can span from 0.01 to 20  $\mu\text{m}$ . By adjusting the particle collection time, impactors can be adapted easily to different aerosol concentrations. Generally, impactors require a predetermined sample volume flow and can withstand high temperatures. A drawback is the reduced size resolution of commercial low-pressure impactors which typically have 8 to 12 stages with cut points decreasing by a factor of 2. Additionally, the presence of an oil film on the impaction plates can lead to the formation of secondary aerosol and subsequently to measuring artifacts. Most impactors require a gravimetric evaluation of deposits which is laborious and lacks temporal resolution to capture fluctuations in the aerosol concentration. Some impactors such as quartz crystal monitor (QCM) cascade impactors address this issue by employing a piezoelectric sensor to detect the mass increase on each impaction plate. Electrical low-pressure impactors (ELPI) are another alternative, which measure the deposited charges instead of particle mass, but require an aerosol with predefined electrical charge. ELPIs offer reliable detection of very small particles and

provide high temporal resolution. However, these systems have other limitations, including a maximum concentration limit imposed by the charge as well as challenges associated with the sensitivity of the charger to vapors and/or high temperatures.

**Electrical mobility spectrometers** are widely used to characterize submicron or nanoscale aerosols. Similar to a gas chromatograph, they consist of several components needed to impart a defined electrical charge on the particles, to separate them by mobility, and then to detect each size fraction. For instance, the scanning mobility particle sizer (SMPS) consists of a radioactive source that induces a Boltzmann charge distribution in the aerosol, a size separation unit known as a differential mobility analyzer (DMA), and a condensation particle counter (CPC) to measure concentration per size class. Through the electrostatic classification process in the DMA, the SMPS determines an electric mobility diameter (=equivalent diameter) based on the motion characteristics of a spherical, charged particle in an electric field. The SMPS is employed for measuring very small particles ranging from approximately 2 to 1000 nm. It is particularly notable for its excellent size resolution and its capability to measure high concentrations ranging up to  $1 \times 10^7 \text{ cm}^{-3}$ . One major drawback of the SMPS system is the inherent need to scan all size classes sequentially. A complete scan typically takes one minute, during which the aerosol source must not change. Additionally, an SMPS can only be operated near room temperature, because the condensation counter, a crucial system component, can only operate in that range. An alternative solution is the DMS500 by Cambustion, utilized by Tatli and Clark (2008) as well as Johnson et al. (2011), and discussed by Burtscher (2005) as a fast particle spectrometer. This system functions similarly to an SMPS and operates in the same particle size range but can be utilized at temperatures up to 150 °C, because the CPC is replaced by numerous sensitive electrometers. One per size class. This allows for significantly improved real-time measurements, but at the cost of reduced size resolution. Moreover, the unipolar corona charging mechanism employed by this device tends to introduce greater inaccuracies caused by an increased occurrence of multiple charged particles.

**Extinction meters** gather data about an aerosol by measuring the decrease in intensity of a beam of light that passes through it, typically monochromatic laser light. By applying Lambert-Beer's law, a total particle concentration can be inferred from the extinction, provided the average extinction cross section of all particles is known. However, if information about the size distribution is not available, an extinction measurement at one specific wavelength alone cannot provide absolute concentration information. In such cases, the wavelength dependence of the extinction can be utilized, as demonstrated in the three-wavelength extinction method by Schaber et al. (1994), to gather details about size and concentration. However, in general, only average particle diameter values can be provided under the assumption of a certain distribution shape. Furthermore, the accuracy of these measuring instruments significantly diminishes when the actual distribution shape deviates from the assumed one. Therefore, extinction measuring instruments yield less comprehensive information compared to other measurement techniques.

**Optical particle counters (OPCs)** utilize the light scattered by individual particles passing through a well define optical measuring volume to gather detailed information about their size and concentration. Monochromatic lasers are advantageous as light sources due to their high intensity but have limitations in classifying specific particle sizes unambiguously. On the other hand, broadband white light sources enable an accurate allocation of particle size and scattered light intensity but at the expense of lower intensity. OPCs have both high size and high temporal resolution, enabling real-time monitoring of size distribution and concentration changes. Measurements are typically obtained at the rate of one per second. However, the lower detection limit is constrained severely by the rapidly decreasing intensity of scattered light with particle size. Many commercial instruments have a lower size limit of about 0.2 to 0.5  $\mu\text{m}$ , which is sufficiently low to detect most particles in the blow-by in terms of mass concentration (Scheiber et al. 2021). Another issue with single-particle OPCs is the problem of coincidence, i.e., the presence of more than one particle at the time in the optical sensing volume. Coincidence imposes an upper limit to the inlet aerosol concentration, typically on the order

of  $10^5 \text{ cm}^{-3}$ . This has to do with its size and shape. There are strategies to extend this range by using additional information about the particles, such as their transit time through the sensing volume, to a maximum of about  $1 \times 10^6 \text{ cm}^{-3}$ . It is therefore necessary in general to dilute crankcase ventilation aerosols. The OPC from Palas® GmbH used in this study has a T-shaped optical measuring volume to correct for partially illuminated particles at the volume's edge (see Fig. 1-1). The effects and limitations of this correction procedure are discussed extensively in Chapter 2.

All optical devices are very sensitive to contamination by the sampled aerosol or vapor, and many can not tolerate elevated temperatures. Some commercial devices, such as the OPC from Palas® GmbH can deal with the elevated temperatures of exhaust gases pose because the sensor can be heated. More information is given in Chapter 2, where this device undergoes extensive validation to ensure its suitability for measuring blow-by aerosols.

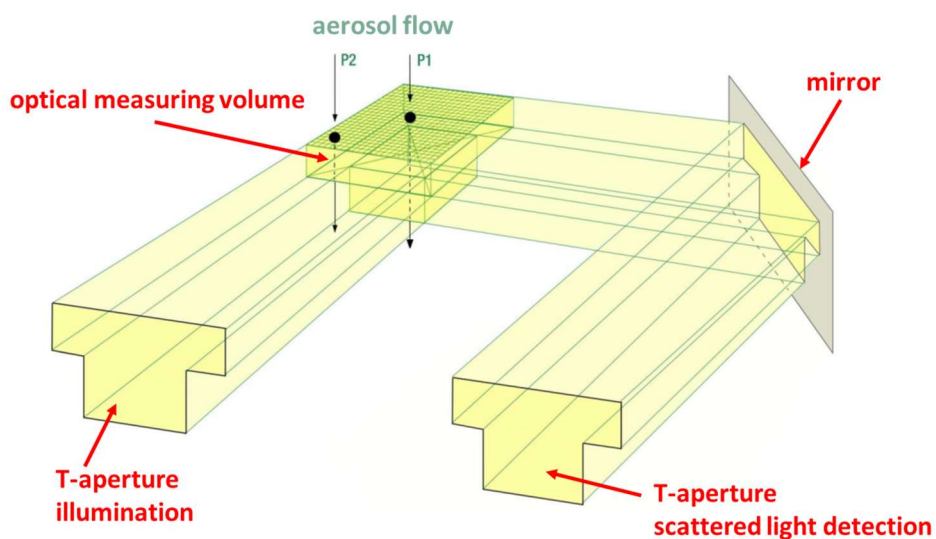


**Figure 1-1:** Schematic of a beam path in a Palas® OPC sensor with T-shaped aperture for correcting size detection of partially illuminated particles. (adapted from Palas® GmbH, 2011)

### 1.3 Formation mechanisms of blow-by aerosols

Potential aerosol sources in the crankcase environment require both liquid oil from which particles form, and a gas flow that transports these particles out of the engine. The latter is provided by the blow-by, which is the sum of all leakage flows that get past piston rings, turbocharger seals, and valve stems into the crankcase. The blow-by flow typically accounts for up to 2% of the intake combustion air mass flow, although its magnitude depends heavily on factors such as the combustion process, engine design, engine wear, and operating conditions (Meinig et al., 2004). Liquid oil is supplied by the lubricating circuit, which delivers fluid to bearings and cooling nozzles. These engine components are particularly prone to generating aerosols. Additionally, any surface in contact with oil can produce droplets when subjected to sufficient kinetic energy from rotational motion (e.g., camshaft, crankshaft, and gears) or quasi-linear motion (e.g., pistons and valves), or through intense shear (e.g., piston rings). Apart from the mechanical atomization, another significant pathway for the formation of fresh crankcase aerosols or the growth of existing particles is the re-condensation of supersaturated oil vapor. Both generation mechanisms typically occur simultaneously at various points within the engine. Due to the numerous parameters involved and their interdependencies, it is generally challenging to determine the specific contribution of a particular source to the overall size distribution of crankcase aerosol. In Fig. 1-2 Johnson (2012) provides an overview of blow-by aerosol sources that can be readily identified.

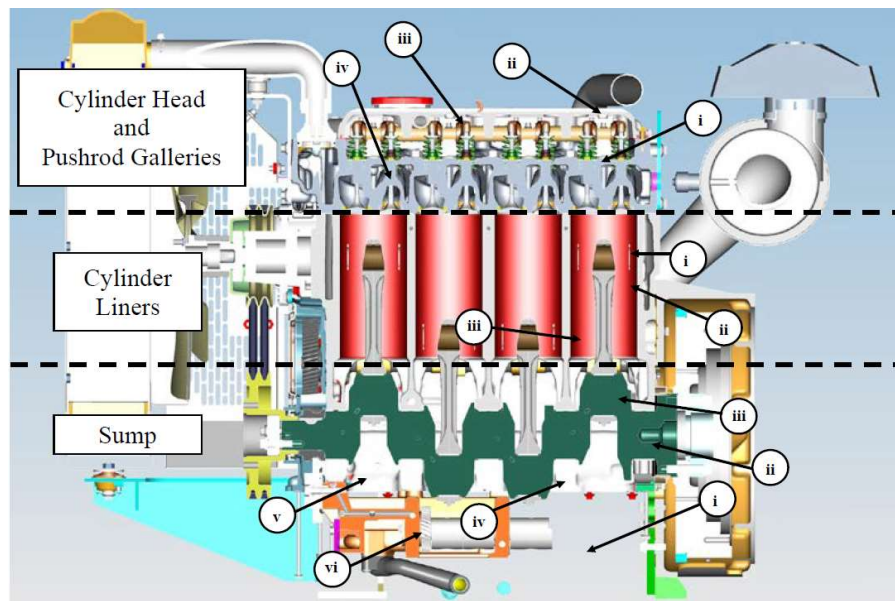


**Figure 1-2:** Potential aerosol sources in the crankcase of an internal combustion engine. (Johnson B.T., 2012)

In his thesis, Johnson (2012) links the individual sources to their respective aerosol formation/generation mechanisms:

### **Cylinder Head and Pushrod Galleries –Potential Aerosol Generation Mechanisms**

- (i) Pushrod galleries and cylinder head oil drainage pathways - Atomisation of oil films by high velocity blow-by gas.
- (ii) Cylinder head and pushrod galleries - Impaction and breakup of oil drops on static or dynamic surfaces.
- (iii) Valves, valve springs, rockers and pushrods - Atomisation of oil by the motion of the valve gear.
- (iv) Valve guides - Atomisation of oil by the blow-by.

### **Cylinder Liners – Potential Aerosol Generation Mechanisms**

- (i) Piston rings and cylinder liner - Atomisation of oil films due to high velocity gas from combustion.
- (ii) Piston cooling jets - Atomisation directly from the piston cooling jets.
- (iii) Piston and cylinder liners - Atomisation/vapour generation when oil from the piston cooling jets impacts on the high temperature surfaces with a high relative velocity.

**Sump – Potential Aerosol Generation Mechanisms**

- (i) Sump oil volume - Atomisation when trapped bubbles of gases rise to the surface of the oil and burst. The bubbles are generated in oil galleries and regions of high pressure drop, due to sharp changes in geometry.
- (ii) Crankshaft and camshaft - Atomisation at the side of journal bearings.
- (iii) Crankshaft and camshaft - Atomisation of oil films due to rotational forces.
- (iv) Engine block - Atomisation of oil films by high velocity blow-by gas.
- (v) Sump - Impaction and breakup of oil drops on static or dynamic surfaces.
- (vi) Journal bearings, oil pump vanes, oil cooler, oil filter - Cavitation and aeration within galleries and components.

Although there are many sources of oil atomization in the crankcase, this does not necessarily mean that this mechanism is the largest contributor to aerosol concentration. Instead, the re-condensation of oil vapor from the pistons and cylinder liners may be a significant factor. Consequently, this generation mechanism is extensively studied in Chapter 5 and will not be further discussed here. Here, the focus is on oil atomization, which has been shown also to be an important contributor in various experiments conducted in Chapters 3 and 4.

The term “atomization of oil by mechanical means” includes all processes in which kinetic and/or potential energy is partially transformed to surface energy of airborne particles. While certain processes predominantly form supermicron particles that are easier to separate, others contribute to the more challenging submicron size range. Submicron particles can originate from spray and rotary atomization, which occur at different locations within the crankcase of combustion engines. Single fluid oil atomization occurs at lubricant cooling nozzles, while two-fluid atomization of oil films by blow-by gases takes place at the gap between the piston rings and the cylinder liner. Rotary atomization of oil occurs at the crankshaft, camshaft, and gearwheels. Additionally, atomization by bubble bursting, where gas trapped by a liquid film exceeds the film's capillary pressure, leading to break-up, is a phenomenon frequently observed in the oil pan.

Given its potential significance as an aerosol formation mechanism in the crankcase, the atomization of sprays and jets is now discussed in greater detail. Extensive literature on jet break-up is available, including studies by Lasheras & Hopfinger (2000) and Marmottant & Villermaux (2004). It is known that several factors contribute to jet break-up, including the properties of the fluid, flow conditions, instabilities, and external influences:

- 1. Fluid Properties:** The physical properties of the fluid, such as its viscosity and surface tension, play a crucial role in jet break-up. A highly viscous fluid tends to resist break-up, whereas low viscosity facilitates break-up. Similarly, a high surface tension promotes jet stability, while low surface tension favors break-up.
- 2. Flow Conditions:** The flow conditions under which the jet operates greatly influence its break-up. Parameters such as jet velocity, flow rate, and nozzle geometry can impact the break-up process. High velocities and large flow rates tend to induce break-up due to the increased disruptive forces acting on the jet. Additionally, the shape and size of the nozzle orifice can affect the jet break-up by altering the fluid flow patterns.
- 3. Instabilities:** Jet break-up results from instabilities that arise within the jet flow. These instabilities can be categorized into two main types:
  - a. Kelvin-Helmholtz Instability:** This type of instability occurs when there is a velocity difference between the core of the jet and the surrounding fluid or ambient environment. The resulting shear forces at the interface lead to the formation of vortices, waves, and ultimately, the break-up of the jet into smaller fragments.
  - b. Rayleigh-Plateau Instability:** This instability arises due to the presence of surface tension within the jet. The reduction of the surface energy is the driving force of this process. It causes the formation of periodic variations or bulges along the length of the jet. As these bulges grow, they eventually pinch off into individual droplets or ligaments, resulting in jet break-up.

**4. External Influences:** Various external factors can influence jet break-up, including aerodynamic forces, acoustic perturbations, and interactions with solid surfaces. For example, aerodynamic forces such as turbulence or pressure gradients can promote jet break-up by increasing the disruptive forces acting on the jet. Acoustic perturbations, such as sound waves, can induce break-up through resonance effects. Interaction with solid surfaces can cause break-up by inducing splashing or secondary atomization.

During the break-up process filaments connecting larger droplets may disintegrate to form smaller particles referred to as satellite droplets. These droplets typically form a mass peak around 2  $\mu\text{m}$  as seen in re-entrainment spectra from oil mist filters (Wurster et al, 2017) as well as the output from oil mist nebulizers (Sagot et al., 2017).

Fig. 1-3 illustrates the characteristic patterns of cooling jet beams at various absolute oil pressures and oil temperatures. These photographs were captured from an operational cooling jet nozzle in a static piston setup of a diesel engine. As anticipated, higher temperatures (indicating lower viscosity) and higher pressures (resulting in increased velocity) enhance the break-up of the oil jet. Additionally, it is noteworthy that the stable length of the oil thread noticeably decreases from the image on the left to the one on the right. It is evident that there is a remarkable contrast in the rates of aerosol formation between these jets.

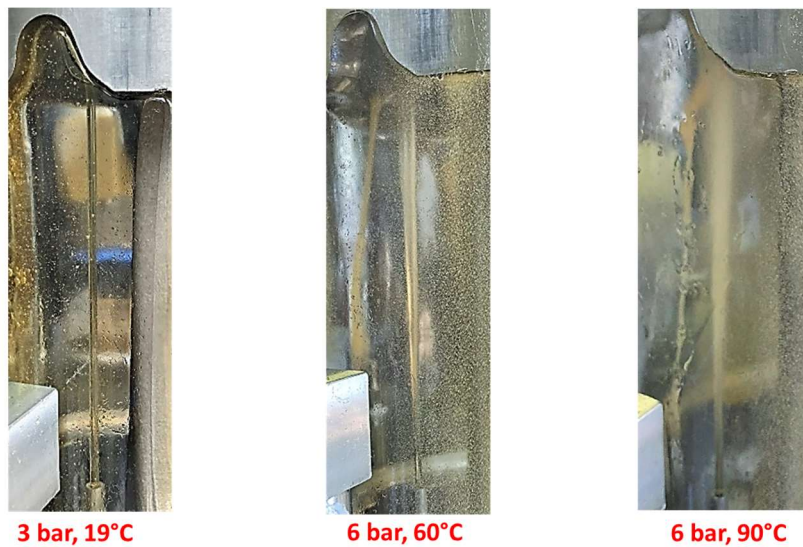


**Figure 1-3:** Liquid oil jet disintegration patterns at absolute oil pressures of 3 or 6 bar and oil temperatures of 19, 60, and 90 °C resulting in different oil viscosities and jet velocities. Photographs were captured from an actual cooling jet in a static piston environment.

The jet disintegration pattern can be predicted based on the Ohnesorge number (Eq. 1-1) and the Reynolds number (Eq. 1-2). The Ohnesorge number, denoted as  $Oh$ , is a dimensionless parameter that relates the viscous forces to inertial and surface tension forces. The formula for the Ohnesorge number is:

$$Oh = \frac{\mu}{\sqrt{\rho \cdot \sigma \cdot D}} \quad (1-1)$$

where:

- $\mu$  is the dynamic viscosity of the fluid,
- $\rho$  is the density of the fluid,
- $\sigma$  is the surface tension of the fluid,
- $D$  is the nozzle orifice diameter.

The Reynolds number, denoted as  $Re$ , is a dimensionless parameter used to describe the flow regime of a fluid. It represents the ratio of inertial to viscous forces:

$$Re = \frac{u \cdot \rho \cdot D}{\mu} \quad (1-2)$$

- where  $u$  is the jet velocity.

Plotting Oh against Re helps understand the transition from laminar to turbulent flow regimes and its influence on the behavior of the break-up of liquid jets or droplets.

Fig. 1-4 displays an Ohnesorge diagram featuring different regimes of jet break-up.

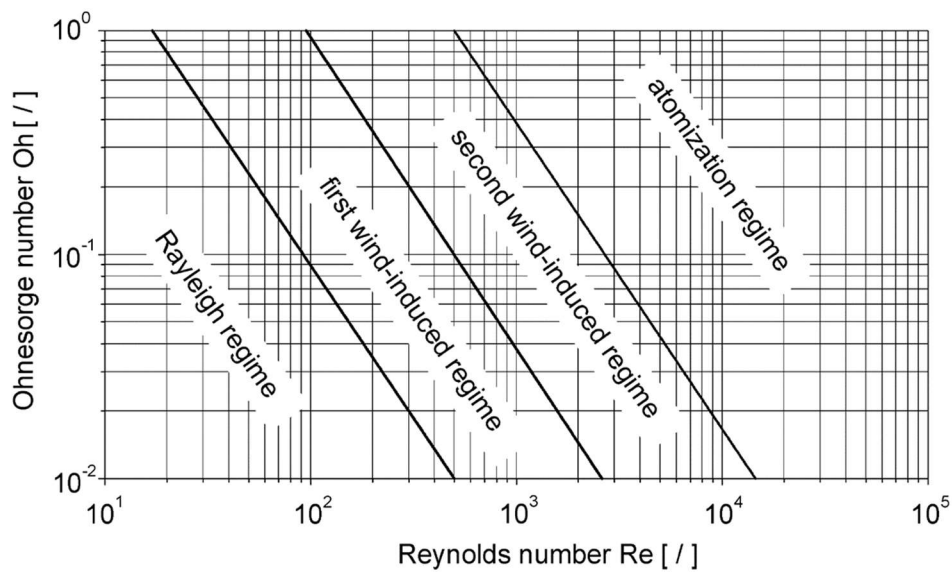


**Figure 1-4:** Ohnesorge diagram illustrating various jet break-up regimes, each labeled accordingly. Note that the exact location of the regimes is influenced by the gas-to-liquid density ratio. (Adapted from Baumgarten, 2006)

According to Baumgarten (2006), the Rayleigh regime and the first wind-induced regime generate droplets that are larger than or similar in size to the diameter of the nozzle orifice, respectively. As a result, these mechanisms are not considered significant contributors to the submicron aerosol in the crankcase. However, the second wind-induced break-up regime can lead to droplet sizes smaller than the nozzle diameter.

The atomization regime is the most crucial regime for generating submicron particles in the crankcase. This regime occurs when a conical spray is formed, and the spray begins to diverge immediately after exiting the nozzle. The theoretical understanding of jet

break-up in the atomization regime is more complex compared to other regimes because the disintegration process is strongly influenced by flow conditions inside the nozzle orifice, which are typically unknown and chaotic. Validating models in this regime is also challenging due to the complexities involved in conducting experiments with high velocities, small dimensions, and dense sprays.

### **1.4 Literature review on blow-by aerosol size distributions**

The existing literature on blow-by aerosols is concentrated mainly on the characterization of crankcase emissions in terms of size distributions and concentrations. A review of this literature encounters several challenges. One of these challenges is that the results depend heavily on the aerosol measurement device as well as the sampling and conditioning procedure. Additionally, some authors provide only cumulative instead of density distributions, which makes it harder to get a feeling of whether the measurement may have truncated a mode of the particle size distribution at the upper or lower boundary of the instrument's measuring range. This is especially interesting when analyzing multimodal distributions typical of the crankcase. Cumulative distributions provide limited insight into what is actually going on at the measurement boundaries if there are too few data points.

There are only a limited number of publications that specifically investigate droplet size distributions and number concentrations in crankcase ventilation. One of the first studies addressing these aerosols was carried out by Hare and Baines (1977). In their study, they utilized a multistage impactor and observed (for three engines) that the mass-weighted median oil droplet size ranged from 0.62 to 1.05  $\mu\text{m}$ . Although a median, and especially a mass based one, says little about multimodality, this means that a very significant amount of aerosol mass must be attributable to very fine particles.

Krause (1995) employed an optical particle counter and various cascade impactors to characterize the blow-by aerosol. However, the resolution of these measuring tech-

niques was limited. Krause's data correspond to findings from other authors and indicate that, depending on the engine type and operating conditions, the mass-weighted median of oil droplets range from 0.5 to 1.5  $\mu\text{m}$ , while the number-weighted median value is around 0.68  $\mu\text{m}$ . The total concentration is not provided by Krause, but based on the information shown it was likely less than  $5 \times 10^6 \text{ cm}^{-3}$ .

More extensive discussions on measurement results can be found in the publications of Sauter et al. (2000, 2003, 2004, 2012). In Fig. 1-5 (of 2000) Sauter presents mass-weighted cumulative distributions of crankcase ventilation aerosols for a gasoline engine at different speeds and loads, measured by a multistage impactor. The mass-weighted median of oil droplets is in a similar range from 0.6 to 1.0  $\mu\text{m}$ . The distributions indicate a possible bimodal nature with a main mode between 0.1 and 1  $\mu\text{m}$  and a secondary mode for larger droplets. However, the problem with a cumulative representation mentioned earlier arises here in particular. The steep slopes at the lower and upper limits of the instrument range, along with the absence of data points, suggest that the covered size range was too small to capture the true density distribution accurately. The cumulative distributions do not reach a value of 1 either. Sauter also provides additional cumulative distributions from crankcase ventilation measurements of a 4-cylinder common rail diesel engine, which resemble the curves mentioned earlier but with flatter distributions at the measurement limits. The dissertation of Sauter (2004) includes a cumulative distribution from the engine's idling operation, which clearly exhibits a bimodal shape.

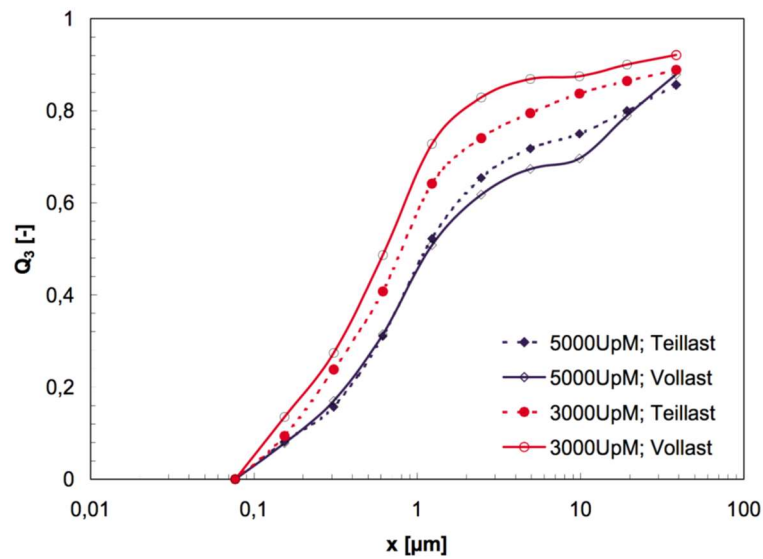


**Figure 1-5:** Mass-weighted cumulative distributions of blow-by aerosols sampled from a gasoline engine at different speeds and loads. (Sauter and Trautmann, 2000)

In Fig. 1-6 (Sauter, 2004) Sauter compares his measurements with other published results. Sauter's red-marked area summarizes findings from measurements on different gasoline and diesel car engines and truck engines at various load and speed conditions. Sauter's cumulative distribution range has reduced information compared to the earlier curves, limiting the ability to draw firm conclusions about the actual shape of density distributions. Among the results shown in that figure, the publication of Ahlborn et al. (1999) is the only one that was consulted for the current work, while the publications of Dürstein et al. (1998) and the lecture by Koch and Maasen (1998) were inaccessible. The blue region assigned by Sauter to the publication of Ahlborn et al. (1999) cannot be verified in the corresponding publication. Instead, Ahlborn et al. (1999) provide a narrow single cumulative distribution representing a monomodal aerosol between 0.3 and 6  $\mu\text{m}$ . The mass-weighted median is around 0.8  $\mu\text{m}$ , which is in concordance with other publications.

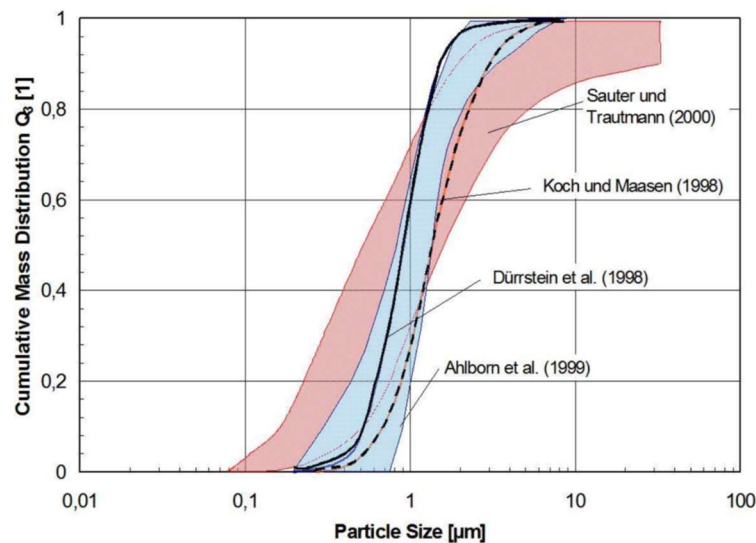


**Figure 1-6:** Mass-weighted cumulative distributions of blow-by aerosols sampled from a gasoline engine at different speeds and loads. (Sauter, 2004)

Sauter's findings do provide strong indications that crankcase ventilation aerosols may generally have a size distribution with multiple peaks, or at least with two distinct modes.

A study by Bischof and Tuomenoja (2003), employing an electrical low-pressure impactor (ELPI) capable of measuring particles within the range of 0.03 to 10.11  $\mu\text{m}$ , also suggests this possibility. The number of modes observed in that study varied depending on the engine's operating conditions. In contrast to Sauter's work, Bischof and Tuomenoja (2003) present results in the form of two density distributions. One of these distributions clearly exhibits a bimodal pattern, with the first mode at approximately 0.4  $\mu\text{m}$  and the second mode slightly above 1  $\mu\text{m}$ . On the other hand, the second distribution represents a distinctly monomodal pattern, with a mode at 1  $\mu\text{m}$ . These measurements were conducted under the same testing conditions but different engine operating conditions. Unfortunately, the authors do not provide further specific information on the variations, but the result is very relevant, nevertheless.

Other publications also report bimodal distributions in the vicinity of 1  $\mu\text{m}$ . Enderich et al. (2008) presents a bimodal density distribution that resembles the shape and positioning observed in Bischof and Tuomenoja's research. Similarly, Jaroszczyk et al. (2006) measured a bimodal distribution in the crankcase ventilation of two unspecified diesel engines. However, the significance of these measurements for the purpose of this study is questionable, since the measurement setup shows a filter situated between the engine outlet opening and the measurement point. Obviously, such a filter will influence the size distribution significantly.

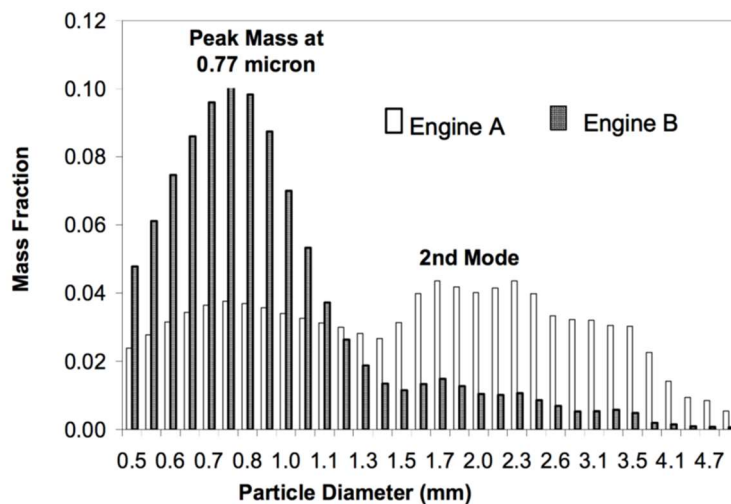


**Figure 1-7:** Mass fraction plotted against particle diameter of blow-by aerosols sampled from two diesel engines, downstream filter. (Jaroszczyk et al. (2006). The x-axis units appear to be mislabeled.

Tatli and Clark (2008) conducted a comprehensive investigation of particle size distributions and concentrations in the crankcase ventilation of various truck engines. They employed the DMS500 from Cambustion, which characterizes particles based on their electrical mobility. The DMS500 charges particles through a corona discharge and then classifies them electrostatically with highly sensitive electrometers providing information about the number distribution. The measuring range of the device is approximately 5 to 1000 nm, which includes particles significantly smaller than in previous measurements.

Measurements conducted by these authors at various operating conditions reveal that the number concentrations increase with higher engine speeds. Additionally, the density distributions of some engines undergo shape changes as the engine speed varies. When operated at 1000 rpm, all engines examined in the study exhibited a monomodal density distribution, with the mode falling between 10 and 100 nm. At higher speeds of 2000 rpm, the density distributions displayed a bimodal pattern, with a second mode ranging from 100 to 500 nm. While total concentrations are not provided, the diagrams suggest that number concentrations are significantly above  $1 \times 10^6 \text{ cm}^{-3}$ , and potentially even exceeding  $1 \times 10^7 \text{ cm}^{-3}$ .

However, in contrast to previous findings, the results of Tatli and Clark (2008) indicate that the blow-by aerosol may not be composed exclusively of oil droplets but may also contain solid particles that have potentially entered the crankcase along with the blow-by gas. An alternative explanation for these modes between 10 and 100 nm is condensation of oil vapor on pre-existing nuclei or in homogeneous form.

Johnson et al. (2011) also focused on a similar size range as Tatli and Clark (2008) but conducted measurements at various locations within the crankcase for a better understanding of aerosol formation. The investigations took place on a turbocharged 4-cylinder diesel engine with a displacement of 4.4 liters. A Cambustion DMS500 was used in the fired mode, while a scanning mobility particle sizer (SMPS) was used in the motored mode, giving a similar measurement range of about 5 to 1000 nm. In summary, it can be noted that individual parameters have a significant impact on the aerosol. For instance, even a slight increase in speed from 600 to 900 rpm during fired operation can shift the mode position by several hundred nm and increase the concentration by an order of magnitude, assuming all other conditions remain constant. The authors do not explicitly provide total number concentrations, but these are likely to be significantly above  $1 \times 10^7 \text{ cm}^{-3}$  in the fired mode.

Fig. 1-8 shows number density distributions during fired operation at 900 rpm. As the load increases, the distribution shape transitions from monomodal to bimodal. In the

no-load condition, the density distribution shows a slight shoulder on the left side, with the mode at approximately 130 nm. As the load increases, a second mode emerges around 30 nm, while the first mode gradually decreases in size.

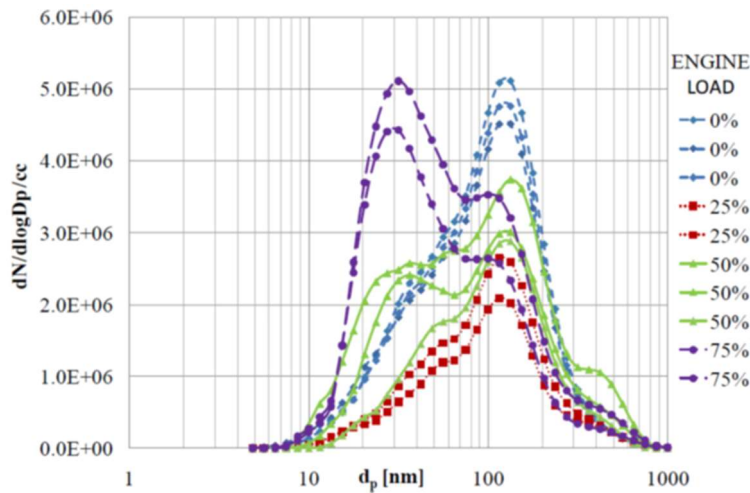


**Figure 1-8:** Number density distributions obtained from the push rod gallery with loads of 0%, 25%, 50%, and 75%. The diesel engine was operated with 900 rpm. (Johnson et al., 2011)

Fig. 1-9 compares measurement results from various sampling points at 50% load and 900 rpm. At all three sampling points, the number concentrations are of a similar magnitude, and the modes are located approximately at 30 nm and 130 nm. However, when sampling from the rocker cover, a possible location for crankcase ventilation, the mode at 130 nm appears more like a shoulder on the right side of the distribution.

Johnson also conducted measurements in motored engine operation. However, the informative value of the results is significantly limited due to the need for artificial adjustment of the venting flow during motored operation. This adjustment is necessary because the blow-by gases from the combustion chamber are mostly eliminated during this type of operation. The motored engine exhibits similar overall trends to the fired engine. At low vent gas flows, a single peak distribution is observed at 250 nm, but as the gas flow increases, the size distribution shifts to a bimodal pattern. The main peak is found between 10 and 100 nm, while the peak at 250 nm decreases in comparison.

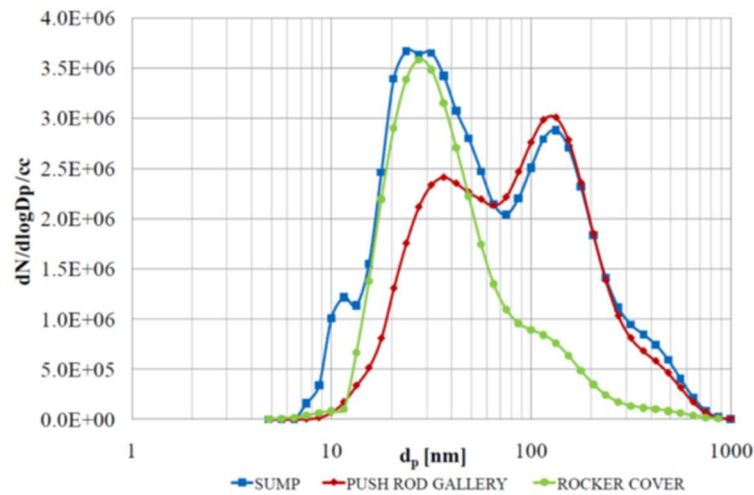


**Figure 1-9:** Number density distributions obtained from various aerosol sampling points at 50% load. The diesel engine was operated with 900 rpm. (Johnson et al., 2011)

In motored engine operation the number concentrations of oil droplets are generally one to two orders of magnitude smaller than in the fired mode.

In summary, the existing publications on blow-by aerosols indicate the presence of several modes in the micron and submicron range. Notably, in the submicron range the modes are predominantly located between 10 and 200 nm, while in the micron range, they range from 0.5 to 2  $\mu\text{m}$ . The studies provide only limited and mostly indirect insights into specific source strengths and spectral properties, but still provide valuable information on global system behavior. All studies agree that different engine operating conditions can lead to significantly different crankcase aerosol properties. Therefore, it is crucial to have knowledge of the engine specifications, load, and speed to interpret the results accurately. Explicit data on total number concentrations were not found but could be estimated from diagrams. It appears that a total concentration of more than  $1 \times 10^7 \text{ cm}^{-3}$  is likely in the combined micron and submicron ranges. It should be critically noted that none of the publications addressed condensation issues during aerosol sampling and cooling adequately. In addition, detailed information about the measurement setup including the transfer function of the dilution system is largely missing.

## 1.5 References

- Ahlborn, S., Blomerius, H., and Schumann, H. (1999). Neue Wege in der Reinigung von Kurbelgehäuseentlüftungsgasen. *MTZ - Motortechnische Zeitschrift*, 60, pp. 454–459.
- Basshuysen, R., Schäfer, F., (2015). *Handbuch Verbrennungsmotor Grundlagen, Komponenten, Systeme, Perspektiven*. Edition 7. Springer Vieweg Wiesbaden. 2628-104X.
- Baumgarten, C. (2006). *Mixture formation in internal combustion engines*. Springer ISSN-1860-4846.
- Bischof, O.F., Tuomenoja, H. (2003). Messung von Blow-by-Gaspartikeln. *MTZ - Motortechnische Zeitschrift*, 64, pp. 586–591.
- Bischof, O.F., Tuomenoja, H. (2003). Messung von Blow-by-Gaspartikeln. *MTZ - Motortechnische Zeitschrift*, 64, pp. 586–591.
- Burtscher, H. (2005). Physical characterization of particulate emissions from diesel engines. A review. *Journal of Aerosol Science*, 36, pp. 896–932.
- Dittler, A. (2012). Aschetransport in Diesel-Partikelfiltern. *Techn. Ber. Daimler AG*.
- Enderich, A., Kissner, G., Ruppel, S. et al. (2008). Hocheffiziente Ölabscheidesysteme für minimalen Ölaustrag. *MTZ Motortech Z* 69, 320–327.
- Hare, C. and Baines, T. (1977). Characterization of Diesel Crankcase Emissions. *SAE Technical Paper 770719*.
- Jaroszcyk, T. et al. (2006). New developments in diesel engine crankcase emission reduction - requirements, design and performance. *Journal of KONES* 13.2, pp. 155–168.
- Johnson, B.T. (2012). Experimental analysis of crankcase oil aerosol generation and control. B.T. Johnson.
- Johnson, B.T., Hargrave, G.K., Reid, B., and Page, V.J. (2011). Crankcase Sampling of PM from a Fired and Motored Compression Ignition Engine. *SAE International Journal of Engines*, 4, pp. 2498–2509.
- Krause W. (1995). Ölabscheidung in der Kurbelgehäuseentlüftung. *Diss. Universität Kaiserslautern*.

- Lakshmanan, M., Maddali, V., Natrajan, R., Muthyam, R., and Balasubramanian, N. (2019). Insight into Effect of Blow-By Oil Mist Deposits on Turbocharger Performance Deterioration in a Diesel Engine. SAE Technical Paper Series, 2019-26-0340.
- Lasheras, J. C., & Hopfinger, E. J. (2000). Liquid jet breakup. *Annual Review of Fluid Mechanics*, 32(1), 275-308.
- Marmottant, P., & Villermaux, E. (2004). On spray formation. *Journal of Fluid Mechanics*, 498, 73-111.
- Meinig, U., Pietschner, S. & May, T. (2004). Kurbelgehäuse-Entlüftung aktueller und zukünftiger Fahrzeugmotoren. *MTZ Motortech Z* 65, 910–915.
- Nigel N. Clark, David L. McKain, Derek R. Johnson, W. Scott Wayne, Hailin Li, Vyacheslav Akkerman, Cesar Sandoval, April N. Covington, Ronald A. Mongold, John T. Hailer, and Orlando J. (2017). Pump-to-Wheels Methane Emissions from the Heavy-Duty Transportation Sector. *Ugarte Environmental Science & Technology* 2017 51 (2), 968-976.
- Palas® GmbH (2011). *Brevier zur Aerosoltechnologie* (2nd ed.). Palas® GmbH: Karlsruhe.
- Pui, David Y. H., Romay-Novas, Francisco, Liu, Benjamin Y. H. (1987) Experimental Study of Particle Deposition in Bends of Circular Cross Section. *Aerosol Science and Technology*, 7:3, 301-315.
- Sagot, B., Forthomme A., Wojda M., De La Bourdonnaye G. (2014). Tuning of an oil mist generator for the performance evaluation of oil separators used in blow-by applications. *Proc. 1st European Conference on Fluid-Particle Separation*, Lyon, France.
- Sauter, H. (2004). *Analysen und Lösungsansätze für die Entwicklung von innovativen Kurbelgehäuseentlüftungen*.
- Sauter, H., Brodesser, K., und Brüggemann, D. (2003). Hocheffizientes Ölabscheidesystem für die Kurbelgehäuseentlüftung. *MTZ - Motortechnische Zeitschrift*, 64, pp. 180–184.
- Sauter, H., Mathiak, D., Müller, J., und List, S. (2012). Kurbelgehäuseentlüftung – direkte Messung von Ölaerosolen. *MTZ - Motortechnische Zeitschrift*, 73, pp. 140–145.
- Sauter, H.L., Trautmann, P. (2000). Messung und Abscheidung von Önebel aerosolen aus der Kurbelgehäuseentlüftung von Verbrennungsmotoren. *MTZ Motortech Z* 61, 874–878.

- Schaber, K., Schenkel, A., & Zahoransky, R.A. (1994). Drei-Wellenlängen-Extinktionsverfahren zur Charakterisierung von Aerosolen unter industriellen Bedingungen. *Technisches Messen* 61.7/8, pp. 295-300.
- Scheiber, K., Nowak, N., Pfeil, J., Koch, T., Kasper, G. (2021). Comparison of four diesel engines with regard to blow-by aerosol properties as a basis for reduction strategies based on engine design and operation, *AAET*, 6, 79–90.
- Tatli, E., and Clark, N. (2008). Crankcase Particulate Emissions from Diesel Engines. *SAE International Journal of Fuels and Lubricants*, 1, pp. 1334–1344.
- Uy, D., Pranis, G., Morelli, A., Gangopadhyay, A., Michlberger, A., Secue, N., Kinzel, M., Adams, T., Streck, K., Lance, M., and Wereszczak, A. (2017). Correlating Laboratory Oil Aerosol Coking Rig Tests to Diesel Engine Tests to Understand the Mechanisms Re-sponsible for Turbocharger Compressor Coking. *SAE Technical Paper Series*, 2017-01-0887.
- Wurster, S., Meyer, J., Kasper, G. (2017). On the relationship of drop entrainment with bubble formation rates in oil mist filters. *Journal of Separation and Purification Technology*, 179, 542-549.
- Yilmaz, E., Tian, T., Wong, V., and Heywood, J. (2002). An Experimental and Theoretical Study of the Contribution of Oil Evaporation to Oil Consumption. *SAE Technical Paper* 2002-01-2684.





## 2 Sampling and conditioning of engine blow-by aerosols for representative measurements by optical particle counters

The content of this chapter has been taken from:

Nowak, N., Scheiber, K., Pfeil, J., Meyer, J., Dittler, A., Koch, T., Kasper, G. (2020). *Sampling and conditioning of engine blow-by aerosols for representative measurements by optical particle counters*. *Journal of Aerosol Science*, 148, 105452. <https://doi.org/10.1016/j.jaerosci.2020.105612>

### 2.1 Abstract

Particle size distributions (PSDs) of engine blow-by aerosol are commonly obtained with an optical particle counter (OPC), but representative measurements are challenging due to high number concentrations, elevated temperatures, presence of saturated vapor, as well as unsteady flow conditions. A comprehensive study of blow-by aerosol sampling/conditioning and OPC performance in such an environment was therefore conducted, based on a commercial OPC (Palas Promo 2000).

Single (1:9) and double-stage (1:80) sampling/dilution/conditioning systems were devised and their transfer functions characterized in the OPC sensor range of 0.3 to 17  $\mu\text{m}$ . With (mostly inertial) particle losses >90% at 10  $\mu\text{m}$ , correcting for them was crucial for reliable PSD measurements. The effect of saturated oil vapor on droplet growth during cool-down and dilution of the sample flow was investigated between 80 and 120 °C, based on actual vapor concentration data. Without dilution, droplet growth became significant above 100 °C while diluting 1:20 with 20 °C air suppressed growth.

Tests of over-all sampling and dilution strategy with engine blow-by aerosol gave excellent reproducibility and good agreement (after loss corrections) with reference data regarding PSD in the 0.3-10  $\mu\text{m}$  range as well as total mass. The actual engine blow-by PSD was significantly broader though, exceeding the OPC range on both ends. Number-to-mass conversion of OPC data under-reported total mass by 10% to 20% (depending on sensor range) compared to weighed filter samples, provided OPC contamination with oil deposits was avoided. A re-calibration procedure is proposed to deal adequately also with pressure pulsations resulting from engine operation.

## 2.2 Introduction

The crankcase of combustion engines is a known source of aerosols consisting largely of oil droplets that have to be eliminated before the blow-by gas can be vented to the environment. In case of closed crankcase ventilation systems, returning these aerosols to the air intake would lead to deposits on critical components such as the turbo charger, valves or sensors and deteriorate their performance and operational life (Lakshmanan et al., 2019; Uy et al., 2017; Jaroszczyk et al., 2006). If sucked into the engine, the oil may further contribute to particulate matter emissions with negative impacts on the operation of the after-treatment system and on the environment (Sauter, 2004; Yilmaz et al., 2002). A key pre-requisite to any abatement strategy, be it by means of efficient aerosol separators (Golkarfard et al., 2019) or improved engine designs, is the characterization of aerosol sources at various points of the engine. This means obtaining reliable data on concentration and particle size distribution (PSD) in a relatively hostile environment characterized by elevated temperatures typically between about 90 °C and 120 °C in the presence of saturated vapor and pressure pulsations. Experimental challenges related to such measurements include dilution as well as the correct handling or at least quantification of potential condensation effects and particle losses when cooling down and sampling. Similar challenges are known from other applications such as sampling from combustion sources (e.g. Hildemann et al., 1989) or, more recently, from the exhaust train of combustion engines (Burtscher, 2005).

Various approaches to sampling and characterizing blow-by aerosols can be found in the literature. Many of these studies are focused on engine or filter performance, with a limited description of how the measurement train performs under engine conditions. A variety of measuring techniques have been used to determine the PSD of crankcase aerosols, including electrical low pressure impactors or multi-stage impactors followed by gravimetric analysis (Bischof & Tuomenoja, 2003), electrical-mobility based devices (Johnson et al., 2011; Tatli & Clark, 2008), aerodynamic particle sizers (Johnson, 2012; Uy et al., 2016), as well as optical methods based on extinction (Janßen et al., 2016; Sauter et al., 2012) or light scattering (Krause, 1995). In these studies, the aerosol is either extracted at different points of an engine or taken from external blow-by tubing if available. Generally, there is very limited information on the flow conditions at the sampling positions. Sampling lines are not heated in most measuring setups. Dilution – where required – is also treated very differently. Studies limited to submicron aerosols typically make use of diluters with a closed system of operation that isolates a sample of particles in an aerosol flow and reunites it with filtered gas from the original aerosol (e.g. rotating disc diluters). Studies that provide data in the super-micron range commonly use open diluter systems (e.g. ejector diluters) with an external source of particle free air.

A discussion of particle losses or other artefacts in these sampling trains is often missing. However, droplet size distributions within a crankcase environment are generally very broad and extend far into the sub-micron as well as the super-micron range, with ample opportunities for being captured. Having reliable quantitative information about how aerosol is transferred from the engine to the respective spectrometer is therefore as crucial as the performance of the latter.

Among the various measurement techniques mentioned above, optical particle counters (OPC) are of particular interest because they are capable of providing data with high resolution in time and particle size in a range of typically about 0.2  $\mu\text{m}$  to well over 10  $\mu\text{m}$ . Such features go a long way toward the objective of characterizing crankcase emissions and revealing emission sources. Some models, such as the Palas Promo 2000

used in this study, also come with a sensing capability up to 120 °C which helps to reduce condensation artifacts, and a calibration specifically for oil aerosol to improve the conversion accuracy from number to mass concentration.

Substantial challenges for the reliable application of OPCs to crankcase aerosols include the quantification of inertial losses of particles larger than a few micrometers in the sampling and dilution system, while the submicron range needs an understanding of droplet growth by vapor condensation. Unless the transfer function of the sampling system is available to correct the raw PSD data, one can not be certain of what one is actually measuring. As an example, claims that the volume weighted median diameter of the crankcase aerosol is about 1  $\mu\text{m}$  (Ahlborn et al., 1999; Bischof & Tuomenoja, 2003; Sauter et al., 2003) need to be substantiated by information about losses in the sampling and dilution system used to obtain these data.

The present paper has several objectives related to the practical application of OPCs for the accurate characterization of blow-by aerosols from a combustion engine.

For one, it investigates sampling geometries with regard to particle losses in the supermicron size range. Since a well characterized standard design was not available, two sampling systems were built for this purpose, with dilution factors of roughly one and two orders of magnitude, respectively. The systems were characterized in the laboratory with oil aerosols generated by a stable two-fluid spray nozzle. The goal here was to determine a loss correction function and hence a practical upper limit for the OPC measuring range. These two sampling systems were then tested with actual crankcase aerosols from a combustion engine.

Second, the paper investigates droplet growth effects below 1  $\mu\text{m}$  due to condensation of saturated oil vapor during cool-down. These measurements were done in a laboratory set-up at temperatures up to 120 °C using the same lab-generated oil aerosol. Since reliable vapor pressure data were not generally available for motor oil, a vapor pressure curve was actually measured for this purpose.

Also, the OPC itself is evaluated with respect to issues arising from blow-by measurements, including the impact of oil deposition on its optics, of flow pulsations due to engine operation on its measuring accuracy, and its accuracy in number-to-mass conversions for oil droplets. These latter data are understood to be device specific, but valuable nevertheless.

## 2.3 Experimental materials, methods, and procedures

This section provides the relevant characteristics of the OPC used in this study. It then describes two sampling and dilution systems for blow-by aerosol measurements with an OPC. Then, the laboratory setups and procedures are presented for generating test aerosols, to determine the transfer functions of the dilution systems, and to validate OPC accuracy by comparison with gravimetric data. Then follow setups and procedures to determine the possible influences of particle growth by oil vapor condensation during cool-down in the sampling system, and of the effects of flow pulsations on OPC calibration and accuracy. The section is concluded by a description on how blow-by aerosol was sampled from an actual diesel engine.

**OPC characteristics:** The Palas OPC used in this study is composed of a Promo 2000 H control unit, in combination with the Welas 2070 HP sensor that offers a choice of 3 measuring ranges of 0.2 to 10  $\mu\text{m}$ , 0.3 to 17  $\mu\text{m}$  or 0.6 to 40  $\mu\text{m}$ . The control unit provided a fixed sampling flow rate of 5 Liters/min controlled by MFC. All data shown in this work was obtained using a size resolution of 32 size channels per decade. The nominal upper limit of the inlet concentration is stated as  $10^6$  particles per cubic centimeter. The OPC sensor can be heated actively to temperatures of up to 120  $^{\circ}\text{C}$ , which permitted direct comparisons of sampling oil aerosol-vapor mixes at elevated temperature vs. cooling them down.

The proprietary OPC data processing software PDAalyze<sup>tm</sup> offers several calibration curves for converting the scattered light intensity to an optical equivalent particle size, including a choice of refractive indices for a more accurate correspondence of optical

and physical particle diameter. Among these pre-installed calibration curves, the one for paraffin oil closely matches the refractive index of the engine oil used for the present work (Total Quartz 7000; 10W-40), which was determined as 1.47 at STP.

Most experiments described in this paper were done in the lab using pure engine oil. In case of measurements on an actual diesel engine (as reported in results section 5), the soot content was kept sufficiently low by changing to fresh oil before each series of tests, to avoid an appreciable effect on the refractive index. The soot content in these engine oil droplets was too low to be determined by gravimetric means, but it was estimated for our case: Individual soot agglomerates entrapped in oil droplets were typically chain like with modest branching and average projected dimensions of 130 nm by 50 nm (La Rocca et al., 2013). On that basis the potential soot mass fraction can be expected to be rather low, even for the smallest 0.3  $\mu\text{m}$  drops of interest here, and the effect on the refractive index should be negligible for the present purposes. Also, with a monitored r.h. of typically <10 % in the dilution air, the water vapor concentration in our dilution system was sufficiently below condensable levels to not have an appreciable effect on the refractive index.

During operation in the field, the OPC sensor has to be cleaned and re-calibrated regularly by the user. This field re-calibration procedure must be performed also when changing the measuring range of the sensor. Cleaning can easily be done by removing the glass windows from the OPC cuvette and wiping off any residuals. Re-calibration involves a measurement of the time of flight (TOF) of particles through the sensing volume, using the actual blow-by aerosol. From the TOF spectrum displayed on a built-in display a representative value of the TOF is determined and entered into the OPC software. This information is used by the OPC software to correct for coincidence events and other error sources (Palas GmbH, 2011). As it turns out, the particle TOF is quite sensitive to non-steady flow conditions at the OPC inlet, such as pressure pulsations in an engine environment, an issue addressed later on.

***Design of the sampling and dilution systems:*** Aerosol concentrations emitted from the crankcase of a typical combustion engine frequently exceed the upper limit of an OPC. Dilution is therefore an integral part of any sampling arrangement. Another important consideration is to minimize the loss of large particles by inertia and other effects, in order to extend the upper measuring range as far as possible. Several approaches and geometries were considered and tested during the development process before settling on a compact design suited for tight engine environments that had to be easy to assemble and clean.

As seen schematically in Fig. 2-1, aerosol is sampled via a thin-walled isokinetic probe (inlet ID 8 mm, length 160 mm) and diluted either 1:9 (single-stage) or 1:80 (double-stage) with particle-free dry air (r.h. <10%), using readily purchased or slightly modified flow components. Dilution takes place in T-pieces and upstream the flow divider at Re of about 1000 and 700, respectively. Internal transitions between the individual components were made as smooth as possible. This was especially important for the very compact flow-divider used in double-stage dilution. The position of the pointed probe in the flow-divider (L 60 mm; ID 9 mm, probe ID 3 mm) was carefully aligned during reassembly to ensure representative and reproducible data. The flow-divider also served as a trap for deposited oil moving along the walls toward the OPC.

OPC sample flow and dilution flow were held constant by MFCs. Pressure pulsations in the range of 40 to 80 Hz stemming from the engine were damped by two HEPA filters installed between the OPC sensor and the OPC control unit that included the pump and the MFC. The dilution flow was regulated by a Brooks 5850E MFC and damped by using a 3 m tubing with an ID of 6 mm. The time-averaged MFC flows of both dilution and OPC were thus very constant regardless of what went on at the probe inlet due to any pulsations. In addition, the dilution factor was verified to be within 5 % before and after each measurement series by checking with a flowmeter.

After dilution, the aerosol was directed to the OPC via a flexible, electrically conductive polyurethane tube (L 150 mm) to decouple it from mechanical engine vibrations, followed by a 150 mm stainless-steel tube to provide further accommodation of the flow profile before entering the OPC. Both measures had proven necessary for reproducible and artifact-free measurements.

As noted in Fig. 2-1, the flow rate at the interface to the OPC was always 5 Liter/min; the other flow rates were determined by the desired dilution factor. The flow rate on the inlet side of the sampling system was typically 0.56 Liter/min.

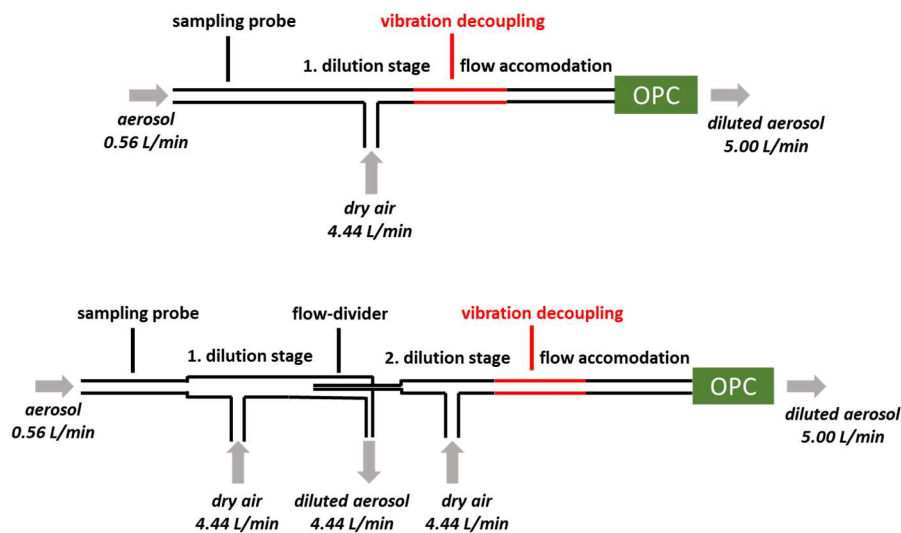


**Figure 2-1:** Schematics of the single-stage (top) and double-stage (bottom) dilution systems incl. vibration decoupling and flow profile accommodation.

**Laboratory test aerosol generation:** Oil aerosols were generated by a classical two-fluid nozzle (May, 1973) in which pre-heated dry compressed air was used to atomize engine oil (Total Quartz 7000; 10W-40) in a chamber maintained at temperatures between 30 °C and 120 °C. The temperature of the chamber and the  $\Delta p$  across the nebulizer were adjustable to vary the aerosol properties. By these means and by the use of dry air for dilution, aerosol mass concentrations at the generator exit could be varied between about 20 and 1300 mg/ m<sup>3</sup>.

As seen in Fig. 2-2 the aerosol had a multimodal size distribution with a number median diameter close to 2  $\mu\text{m}$  when nebulizing oil at room temperature, and about 0.8  $\mu\text{m}$  at 120  $^{\circ}\text{C}$ . The size distributions were highly stable and reproducible with regard to shape; the total concentration varied over time on the order of  $\pm 3\%$ .

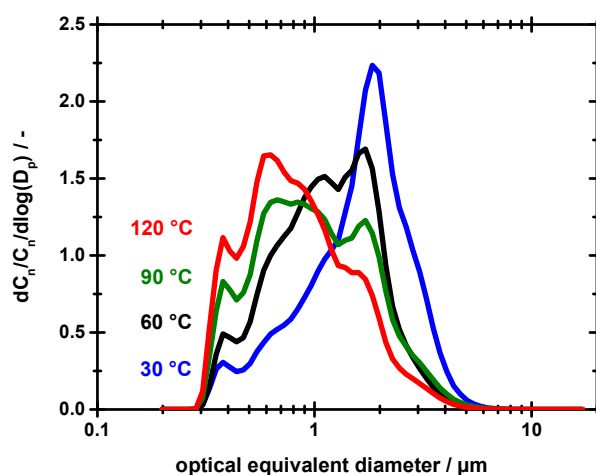


**Figure 2-2:** PSD of lab-generated oil aerosols at various heating chamber temperatures. The PSDs were measured at room temperature after diluting and cooling down with particle-free dry air.

**Particle growth by oil vapor condensation** during cool-down of a vapor laden aerosol flow was investigated in a set-up shown in Fig. 2-3. First, a particle-free stream of vapor-saturated air was generated by nebulizing oil (Total Quartz 7000; 10W-40) in a chamber heated to a temperature chosen between 80  $^{\circ}\text{C}$  and 140  $^{\circ}\text{C}$  and then removing the disperse phase by a highly efficient glass microfiber filter (GF-25-64-50CK). The filter was pre-saturated with oil to ensure not only a constant separation efficiency, but also a constant oil distribution inside the media and thus a constant saturation effect for the gas flow. Negligible particle penetration through the media and the absence of new aerosol formation by re-entrainment were verified by measurements with a heated OPC. The oil vapor concentration in the saturated stream (at 5 Liters/min) was determined by cooling it down to room temperature in a cold trap (path d in Fig. 2-3) and weighing the condensate mass deposited in the tube and on an absolute filter.

Separately, oil aerosol was generated using the same types of nebulizer and engine oil as described previously. This aerosol was mixed isothermally and diluted as needed with

the saturated but particle-free air, and then directed to the OPC in one of two ways. Either, the aerosol flow was introduced to the OPC sensor at the temperature of the heating box, i.e. with a heated sensor (path a in Fig. 2-3) or after cooling it down to room temperature (path b). Additionally, the aerosol was directly led to the exit of the heated chamber where it was cooled down and diluted with particle-free dry air at room temperature (path c). Condensation effects were studied by comparing OPC measurements at various temperatures between 80 °C and 120 °C with measurements of the same aerosol at ambient temperature, with or without dilution. The aerosol concentration was held to about  $10^4$  particles per cubic centimeter, to ensure conditions favoring condensation growth with a relatively large amount of vapor per droplet, and thus a greater experimental accuracy. Obviously, these experiments represent a worst-case scenario, since particle growth may be expected to be less at higher aerosol concentrations, but that can be estimated on the basis of the data.

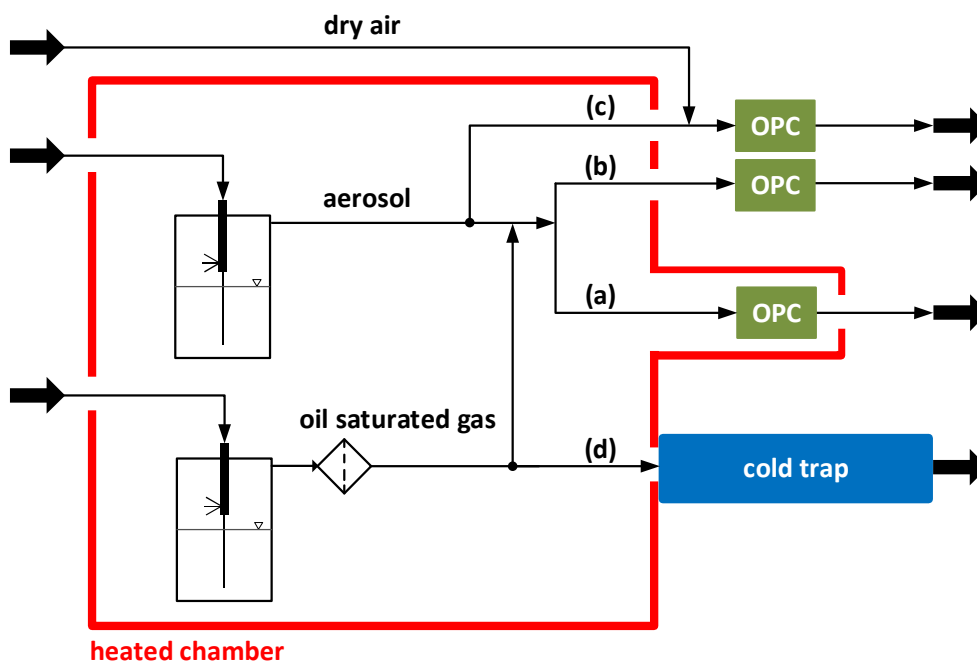


**Figure 2-3:** Set-up for measuring vapor condensation effects on the aerosol. Inside a heated chamber, vapor-saturated particle-free air is mixed with aerosol from a nebulizer and diluted as needed to maintain a concentration of  $10^4 \text{ cm}^{-3}$ . That flow is either maintained at temperature (path a) or cooled to ambient temperature (path b) before entering the OPC. In (path c) the aerosol was diluted and cooled down with particle-free dry air at room temperature. A cold trap is used to measure the vapor concentration (path d).

***Effect of flow pulsations on OPC accuracy.*** Pressure pulsations in the crankcase are the result of small variations in crankcase volume due to piston movement. The magnitude of these  $\Delta p$  variations depends on the engine, its operating point and the sampling position. On our 4-cylinder test engine and for a typical OPC sensor position, the variations were on the order of  $\pm 10$  mbar at 1200 rpm. Such pulsations influence the time of flight of a particle in the optical sensing volume, and thus also the OPC calibration as explained earlier. The effect was studied in a laboratory setup using the highly reproducible aerosols generated as described above. Pressure pulsations similar in frequency and intensity as from the engine were generated with a loudspeaker coupled to the aerosol stream. The acoustic frequency was set to 80 Hz, which corresponds to an operating point of 2400 rpm in our 4-cylinder test engine. The intensity of  $\Delta p$  fluctuations was adjusted in the range of interest via the amplitude.

***Sampling directly from the engine:*** A commercial 4-cylinder, 5.1-Liter diesel engine installed on an engine test stand was used for the purpose of testing our sampling and dilution system under true engine conditions. Aerosol was sampled via a thin-walled 8 mm ID sampling probe inserted in vertical downward orientation in the perforated valve cover, at a point just before it enters the crankcase ventilation system (see Fig. 2-4 for a schematic). The flow field in the region of the probe inlet as determined by particle image velocimetry measurements was aligned vertically, with a mean velocity in probe direction around 0.2 m/s, and momentary variations from nearly zero to about 0.4 m/s. The value of 0.2 m/s was used to set the sampling inlet velocity, understanding of course that this does not represent exactly isokinetic conditions.

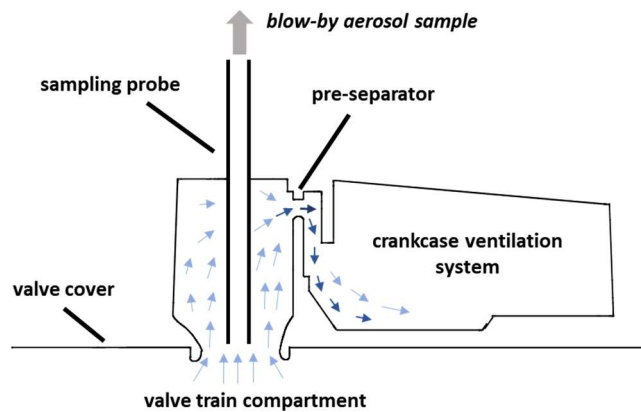


**Figure 2-4:** Schematic of the blow-by aerosol sampling location and flow field. The sample was extracted before the entry into the crankcase ventilation system.

It should be emphasized here that the primary purpose of this part of the study was not to study engine emissions but to validate the combination of OPC and sampling systems in the field, especially with regard to their transfer functions as determined previously in the lab. This was done in a first step by comparing PSD of engine blow-by aerosol obtained with and without the sampling and dilution system. Using undiluted blow-by aerosol for a reference size distribution necessitated engine operation at low power where concentrations remain below the specified maximum number concentration. Thus, the engine was fired at 1200 rpm and zero load with a coolant inlet temperature of 90 °C that resulted in an oil sump temperature of 92 °C and a blow-by of 26 Liter/min.

In a second step, the OPC number size distributions were converted to volume size distributions, summed up to total aerosol volume and converted to total mass using the actual oil density of 0.85 g/cm<sup>3</sup>. The total aerosol mass was compared to filter samples obtained directly at the outlet of the OPC. The aerosol mass on the filters was determined by weighing.

## 2.4 Results and discussion

### *Results (1) - Transfer functions of the two sampling and dilution systems*

Fig. 2-5 shows transfer functions for the single-stage (1:9) and the double-stage (1:80) dilution systems, expressed as penetration vs. particle size. Penetration data were obtained in a straightforward lab set-up with the oil aerosol described earlier, by alternating PSD measurements with and without the interposed sampling and dilutions system. These experiments were conducted at a chamber temperature of 40 °C and repeated twice, with at least 900 sampled particle spectra each. The undiluted reference aerosol was sampled with the OPC flow rate of 5 Liter/min. Downstream number concentrations became rather low due to dilution, especially at the edges of the PSD. This caused statistical fluctuation in the counts of individual size channels and made penetration data noisy. An unweighted moving 7-point average algorithm was therefore used to smooth the data and produce the plots shown in Fig. 2-5. The reciprocals of these plots were subsequently used to correct the OPC data for losses above 2  $\mu\text{m}$ . This can be done with reasonable accuracy up to about 8  $\mu\text{m}$ . Beyond that, statistical errors become too large for a meaningful correction.

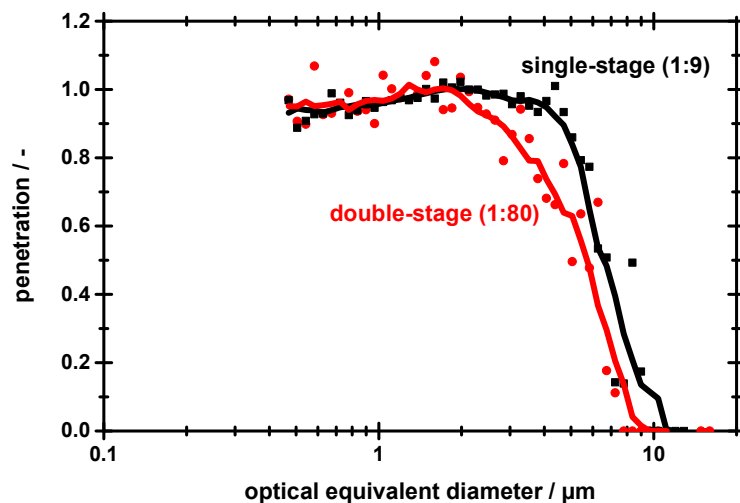


**Figure 2-5:** Transfer functions for the single-stage and the double-stage dilution system plotted against the optical equivalent particle diameter.

According to Fig. 2-5, the transfer functions below about 2  $\mu\text{m}$  are near unity as expected. Some oscillation of penetration values around unity is noticeable especially for the 1:80 dilution, due to low downstream particle counts. Above 2  $\mu\text{m}$  the penetration drops off rapidly with increasing particle losses. The 50 % cut points on the upper end of the size spectrum are reached at particle diameters of about 7  $\mu\text{m}$  and 6  $\mu\text{m}$  for the single and double-stage system, respectively. For other designs of the dilution stage(s) tested but not shown here, the losses were not substantially different. Cut points on that order are rather typical for many sampling situations, with loss rates of over 90 % around 10  $\mu\text{m}$ .

Evidently, droplets smaller than a couple of micrometers in diameter pass these dilution systems almost unhindered. This is mainly due to their short residence time of under 1 second and consistent with estimates for diffusion losses. Using elementary expressions for diffusion in laminar pipe flow (e.g. Hinds, 1999) yields losses of about 0.2 % for 0.3  $\mu\text{m}$  particles. Thermophoresis can be excluded as a significant loss mechanism for sampling and diluting actual engine blow-by aerosol. The blow-by temperature at the entrance to the sampling system was no more than 50  $^{\circ}\text{C}$  above ambient and this difference was evened out completely about 50 mm downstream by dilution with air at ambient temperature. Assuming a temperature gradient of 20  $^{\circ}\text{C}/\text{mm}$  along that 50 mm section of tubing and using standard formulae (Hinds, 1999) yields losses of under 5 % for 0.3  $\mu\text{m}$  particles, and even less for larger particles. Thermophoresis losses were thus negligible during blow-by sampling from the engine. During lab transfer function experiments, the temperature differences were even smaller not exceeding 15  $^{\circ}\text{C}$ .

The laboratory tests were performed with the system in horizontal position. In that case, gravitational particle losses for oil droplets with near unit density amount to about 5 % at 8  $\mu\text{m}$  and 10 % at 10  $\mu\text{m}$  for our geometry (Hinds, 1999). During actual engine experiments the sampling and dilution system was operated in vertical position. Losses toward larger droplets are thus driven mostly by inertial effects, despite modest Re numbers in the mixing regions of the dilution system, avoidance of steps etc. Further reaching calculations would require extensive simulations and were not pursued here.

### **Results (2) – Impact of a high oil vapor concentration on the aerosol after cooldown**

Droplet growth by condensation is a potential problem when sampling a mix of oil vapor and particles. At the very least it needs to be quantified, better yet avoided. As a first step, the saturation vapor concentration of engine oil had to be determined, since data of this kind are generally unavailable in the literature or from suppliers. The data were obtained by experiments with a cold trap as described in the materials and methods section. Fig. 2-6 shows mass concentrations for fresh oil (Total Quartz 7000 10W-40) in 10 °C increments. In the range between 110 °C and 140 °C the concentration of saturated oil vapor varies between about 50 and 400 mg/m<sup>3</sup>.

The experimental data shown in Fig. 2-6 were smoothed with an exponential fit function to facilitate further calculations. The assumption of an overall exponential dependence is reasonable even though engine oil is a complex mixture mainly of hydrocarbons from under C18 to about C40, each with its own exponential dependence, of which the lightest fractions may actually boil off with time. Extrapolation toward the lower end of the temperature range of interest predicts a value of 9 mg/m<sup>3</sup> at 80 °C. At ambient temperature, the vapor mass becomes comparatively negligible.

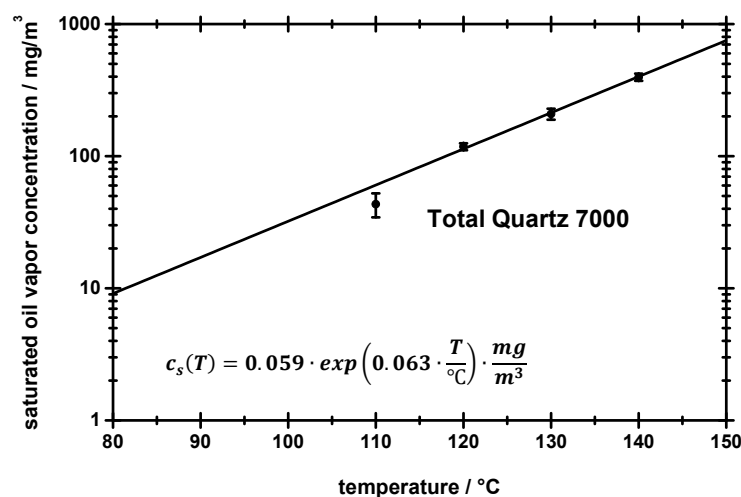


**Figure 2-6:** Concentration of saturated oil vapor vs. temperature for a typical engine oil.

One can therefore conclude that cooling down an aerosol-vapor mix to temperatures on the order of 80 °C or less will cause practically all the oil vapor to condense, either on the particles or on the tubing. Fig. 6 provides the basis for worst-case estimates of the growth potential of aerosol droplets by vapor condensation based on a simple mass balance equation:

$$d_{p,1} = \sqrt[3]{d_{p,0}^3 + \frac{6 \cdot c_{m,v}}{\pi \cdot c_{n,p} \cdot \rho_p}} \quad (2-1)$$

Eq. 2-1 distributes the saturated oil vapor mass concentration  $c_{m,v}$  evenly onto monodisperse droplets of a given initial diameter  $d_{p,0}$  and a given number concentration  $c_{n,p}$ . The particle diameter after growth becomes  $d_{p,1}$ . The oil density  $\rho_p$  is 0.85 g/cm<sup>3</sup>. It is further assumed that the vapor condenses only onto droplets.

Assuming an aerosol of monodisperse 0.5 µm droplets at a concentration of 10<sup>4</sup> per cubic centimeter which corresponds to an aerosol mass of about 0.6 mg/m<sup>3</sup>, these droplets will grow to 1.8 µm when cooling down from 100 °C, and to 3.6 µm from 130 °C. If the number concentration increases by one order of magnitude, the respective diameters after condensation will still be 0.9 and 1.7 µm, which amounts to growth factors of roughly 2 and 3.

Actual changes in droplet PSD during cool-down were measured with a set-up described in the section on experimental materials, methods and procedures (Fig. 2-3). Fig. 2-7 compares droplet spectra obtained without cooling down the mix of aerosol and saturated vapor, i.e. isothermally (red lines; path a in Fig. 2-3) with those obtained after cooling down to 25 °C from temperatures between 80 °C and 120 °C (gray and black lines; paths b and c in Fig. 2-3). Since the isothermal plots were almost identical, only one is shown per graph to avoid clutter. The left-hand graph shows experiments where the cooling down occurred without diluting the aerosol-vapor mix (path b in Fig. 2-3), the right-hand graph with dilution using dry air at ambient-temperature (path c in Fig.

2-3). Number concentrations were maintained within 10 % of  $10^4$  per  $\text{cm}^3$  for all measurements. PSDs were nevertheless normalized with regard to total concentration, to ensure accurate comparisons between size distributions.

According to Fig. 2-7 (left-hand graph), cooling down the mixture without dilution from 80 °C or 100 °C to ambient did not lead to significant changes in the original PSD. Despite a roughly 4-fold increase in saturation vapor concentration from 80 °C to 100 °C, the prevailing cooling rate (about 0.1 s to reach 60 °C) was not sufficient to induce measurable droplet growth in that temperature range, because the excess vapor condensed mostly on the system walls.

Upward of 105 °C however, the changes to the PSD became significant, in that the lower submicron size mode situated around 0.35  $\mu\text{m}$  began to decrease in favor of growth in the second mode located initially around 0.7  $\mu\text{m}$ . At 120 °C the lower mode had almost vanished while the second mode nearly doubled in height. For the third mode at 1.8  $\mu\text{m}$  and beyond there was no noticeable change in PSD.

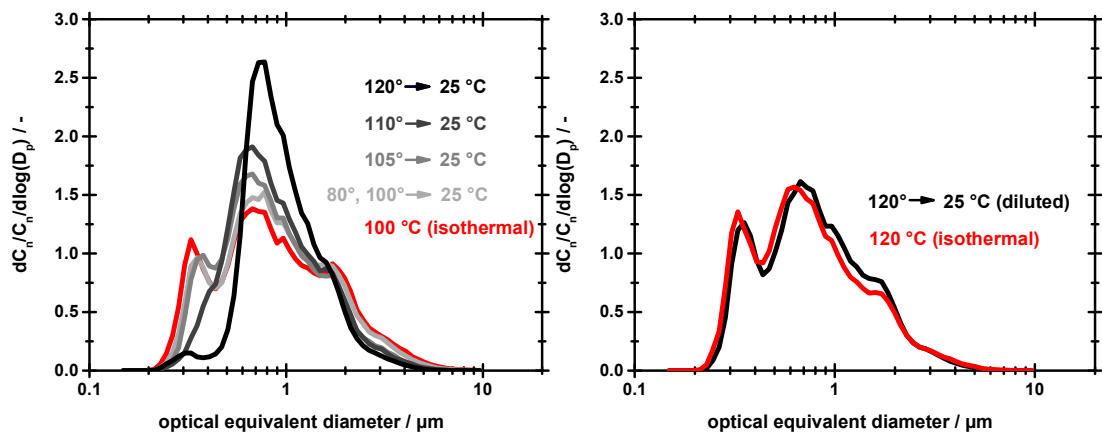


**Figure 2-7:** Comparison of droplet PSD obtained isothermally (red lines) with those obtained after cooling down the aerosol-vapor mix to 25 °C (gray and black lines), either without dilution (left-hand graph) or diluted 1:20 with dry air at ambient-temperature (right-hand graph). Only one isothermal plot is shown per graph because these plots were almost identical for different temperatures.

Dilution with dry room-temperature air in a ratio of about 1:20 (Fig. 2-7, right-hand graph), did not affect the PSD, even at the highest oil vapor temperatures. From the

practical perspective of this paper, i.e. the avoidance of artifacts during aerosol sampling, one may conclude that diluting a mixture of saturated oil vapor and submicron crankcase aerosol with dry air at room temperature in a ratio of about 1:20 suffices to suppress noticeable changes in PSD up to 120 °C.

### ***Results (3) – Impact of oil contamination on OPC optics; comparisons with gravimetric data***

The optics of any OPC are quite sensitive to contamination because this will diminish the intensity of the scattered light signal, reduce apparent particle sizes and thus lead to apparently lower mass concentrations. Oil aerosols are particularly noxious in this regard.

The extent to which such oil deposits affected the OPC measurements was determined by comparing the OPC derived total aerosol mass with gravimetric data obtained with a high efficiency glass fiber filter (GF-25-64-50CK) that was installed immediately behind the unheated OPC sensor. The comparisons were carried out with the same lab-generated test aerosols described in the experimental section. The aerosol was transferred to the OPC via an unheated 50 cm stainless steel tubing. OPC measurements and filter samples were taken in parallel over a period of several hours as seen in Fig. 2-8. The corresponding filter data are of course time-averaged and the length of the respective black horizontal line represents the averaging interval.

The left-hand figure compares OPC and filter data at two different aerosol concentrations of about 50 and 1300 g/m<sup>3</sup>. The right-hand figure compares them on a longer time scale. Soiling is dramatic at the very high concentration. It causes the OPC recorded mass concentration to drop rapidly and visibly from the beginning of the run by over 50 % per hour, while at under 50 mg/m<sup>3</sup> inlet concentration it appears to remain relatively constant on the time scale of the measurement (150 min). When observed over a longer period of time however (right-hand graph) one sees that the OPC concentration is not

really constant even at low inlet concentrations but drops at the rate of about 3 to 4 % per hour.

Evidently, the rate of sensor contamination by oil decreases with aerosol concentration and this helps to extend the cleaning interval. Nevertheless, long sampling times will reduce OPC accuracy significantly even at low concentrations. Aside from operating the OPC at low inlet oil concentrations (i.e. diluting) and building a wall-flow trap into the sampling system to capture oil before it reaches the OPC, another practical strategy to extend cleaning intervals is the use of purge air between short measurements to reduce the pollution rate of the lenses.

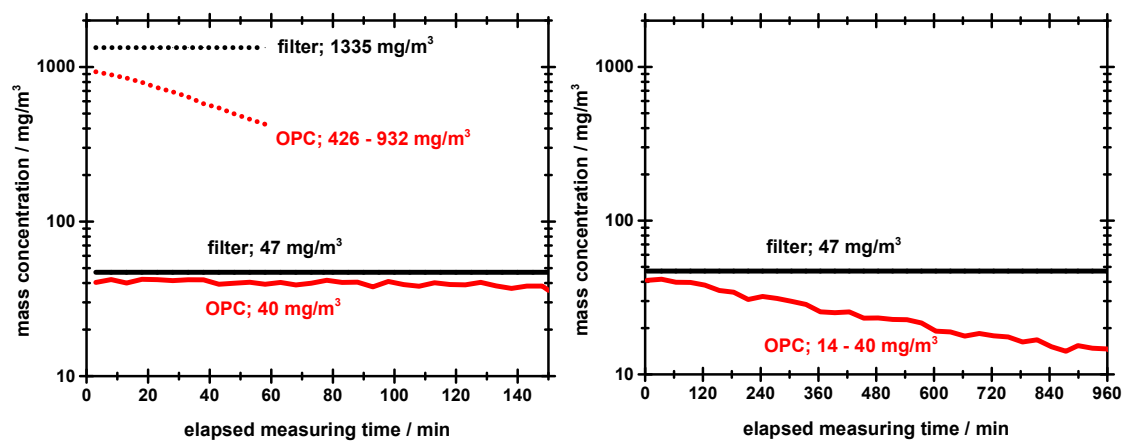


**Figure 2-8:** Mass concentration vs. time as obtained by OPC (with 0.3 - 17  $\mu\text{m}$  sensor range) compared to average mass concentration by gravimetric analysis (filter). The left-hand graph shows measurements at two very different aerosol concentrations (note the log. concentration axis); the right-hand graph shows low-concentration data for a longer measurement interval.

Fig. 2-8 makes use of the built-in OPC software to convert number size distributions to volume, and then to total aerosol mass concentrations. The density used for the conversion was 0.85  $\text{g}/\text{cm}^3$ . The conversion is based on ideally spherical particles, a condition most likely fulfilled for small oil droplets, as well as an exact correspondence of optical equivalent and physical droplet diameters. The latter condition is probably also fulfilled reasonably well due to the use of a refractive index that matched the oil aerosol closely. Additional information on this topic can be found in e.g. (Chien et al., 2016; Sang-Nourpour & Olfert, 2019).

The accuracy of this conversion will now be investigated in more detail for our type of aerosol, based on measurements in the concentration range below 50 mg/m<sup>3</sup> where soling of OPC optics is not a severe problem. The nominal OPC sensor ranges investigated were 0.2 to 10 μm and 0.3 to 17 μm. The aerosol PSD was varied via the nebulizer temperature during these tests, to obtain some variation of the mean particle size. Comparisons between OPC and filter samples on the basis of total mass are shown in Tab. 2-1.

**Table 2-1** – Comparison of OPC based and gravimetric total mass concentrations for two of the OPC sensor ranges. The number mean diameter of the PSD was varied via the nebulizer temperature:

Sensor range 0.2 to 10 μm					Sensor range 0.3 to 17 μm				
T <sub>neb</sub>	d <sub>50,0</sub> μm	C <sub>OPC</sub> mg/m <sup>3</sup>	C <sub>filter</sub> mg/m <sup>3</sup>	C <sub>filter</sub> /C <sub>OPC</sub> -	T <sub>neb</sub>	d <sub>50,0</sub> μm	C <sub>OPC</sub> mg/m <sup>3</sup>	C <sub>filter</sub> mg/m <sup>3</sup>	C <sub>filter</sub> /C <sub>OPC</sub> -
30 °C	1.5	34	34	±0 %	30 °C	1.7	29	36	+24 %
60 °C	1.1	31	33	+6 %	60 °C	1.2	39	46	+18 %
90 °C	0.8	28	30	+7 %	90 °C	1.0	31	39	+26 %
120 °C	0.7	30	36	+20 %	120 °C	0.8	31	44	+42 %

According to Tab. 2-1 the agreement for the 0.2-to-10 μm range is generally very good, with differences of under 10 percent; for the wider measuring range it is on the order of 20 %, thus larger but still acceptable. Note also that the OPC generally tends to give lower readings than the filter. The difference between the two OPC sensor ranges is related to the inner workings of the OPC and cannot be analyzed here without additional information not available to us. One can simply say, that the 0.2 - 10 μm range of this particular OPC is more accurate when it comes to mass conversions.

For both sensor ranges, the values at the bottom line of the table stand out as particularly high. Given that these measurements were made at a nebulizer temperature of 120 °C, we must interpret these deviations as being due to the high vapor content in the

aerosol. Regardless of the measuring range used, this points to oil vapor as an additional cause for soiling of the OPC optics.

***Results (4) – Impact of pulsating flow on OPC accuracy:***

Pressure pulsations in the crankcase ventilation duct of a combustion engine are a normal side effect of engine operation. They occur at the frequency of crankcase volume variations resulting from piston movement and range in amplitude from typically a few mbar to a few tens of mbar (Randall et al., 2017). When these pressure pulses are transmitted to the optical sensing volume of the OPC, they appear to affect the TOF spectrum, which is critical for an accurate representation of PSDs as indicated earlier in the “OPC characteristics” section. In the context of this paper, the issue reduces to the best way of performing the time of flight calibration. Would a calibration under steady flow conditions still be adequate, or would it give erroneous PSD readings when measuring on an engine in operation?

This was tested in a laboratory experiment under well-defined conditions with the usual nebulizer generated aerosol. At first a PSD was obtained in the conventional way, under steady flow conditions for both the measurement and the OPC calibration. This PSD, shown in blue in Fig. 2-9, is considered the reference PSD.

The same aerosol was then sampled twice under pulsating flow conditions to obtain PSDs, once using the TOF calibration under steady-flow (Fig. 2-9, red continuous line), and then with a new TOF calibration under pulsating flow conditions (Fig. 2-9, red dashed line). Evidently, the continuous red and blue plots are virtually indistinguishable, indicating that an OPC calibration under steady flow conditions gave satisfactory results also when the sampling flow was not steady with pulsations not exceeding  $\pm 10$  mbar. Conversely, with the new calibration under pulsating flow, the OPC was not able to reproduce the reference PSD. This conclusion is obviously not based on an exhaustive in-

investigation, but sufficient for the present purposes. As a practical consequence for engine crankcase measurements, an OPC residence time calibration should not be performed with aerosol from the engine in operation, but instead after shutdown using the remaining blow-by aerosol still present in the crankcase.

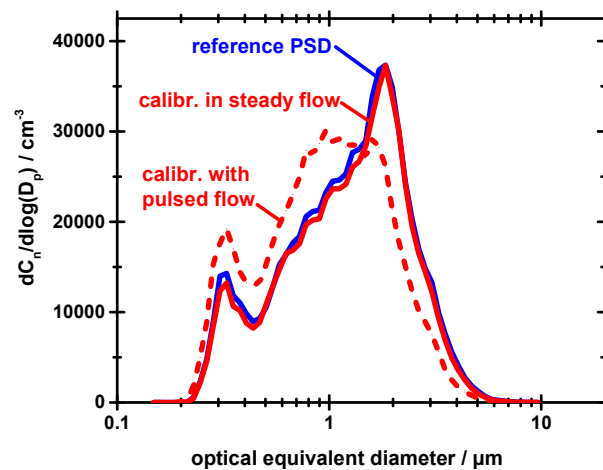


**Figure 2-9:** Influence of OPC calibration under steady flow (solid red line) and pulsating flow (dashed red line) on a PSD obtained under pulsating flow conditions (80 Hz,  $\pm 10$  mbar) for the same aerosol. The reference PSD and was obtained when measuring and calibrating under steady flow.

### ***Results (5) – Test of the sampling systems with actual engine aerosol***

Finally, tests were performed on a combustion engine in operation, to evaluate the usefulness of the loss correction functions shown earlier for the respective sampling and dilution systems (Fig. 2-5) for field measurements. In order to do this, the engine was run under conditions where the crankcase aerosol concentration was sufficiently low to be able to obtain OPC data without dilution. These undiluted OPC measurements served as a reference for measurements with the sampling and dilution systems. The results are shown in Fig. 2-10, with concentrations given in terms of particle mass. The left-hand graph shows the data without correction for particle losses, the right-hand graphs after correction in the size range  $\leq 8 \mu\text{m}$ . The OPC sensor with the widest measuring range was used for the undiluted reference data (in black).

One sees first of all, that the undiluted crankcase aerosol (black plot; sensor range of 0.6 to 40  $\mu\text{m}$ ) exhibits two major modes, a first mode around 2 to 4  $\mu\text{m}$ , and a second mode above 10  $\mu\text{m}$  which is evidently cut off beyond about 15  $\mu\text{m}$  because such large particles are impossible to get into the sensor. The two modes contain roughly equal amounts of mass. The mass mean diameter corresponding to the black plot is 4.4  $\mu\text{m}$ . With either of the two dilution systems in place, the finer mode is very well represented even without correction, while the second mode would disappear without a loss correction. Evidently, the losses become so substantial toward larger particles that an uncritical appraisal of the data would suggest a quasi-monomodal PSD centered around 2  $\mu\text{m}$ . After correcting the red and blue PSDs for losses they agree much more closely with the “actual” undiluted PSD. The value of the loss correction becomes apparent also when comparing total aerosol mass. Without correction one misses about 17 % of the aerosol mass below 8  $\mu\text{m}$ , according to Fig. 2-10. The dilution accuracy was always within 5 %. The remaining differences in the right-hand graph after correction for sampling and dilution losses must therefore be associated with variations over time in the aerosol spectra coming from the engine. Note that switching between sensor ranges required stopping the engine, re-calibrating the OPC and restarting.

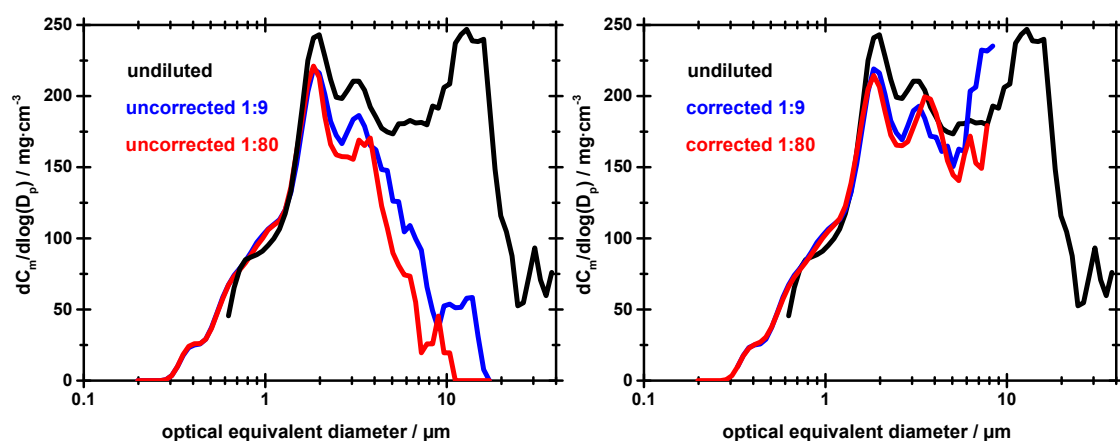


**Figure 2-10:** PSD of crankcase aerosol obtained without dilution (black; sensor range 0.6 to 40  $\mu\text{m}$ ), and with the respective dilution systems (red, blue; sensor range 0.3 to 17  $\mu\text{m}$ ). Left-hand graph shows PSD before applying the correction for losses in the dilution system, the right-hand side with loss correction. The engine was fired at 1200 rpm and 0 Nm.

These measurements provide an opportunity also to evaluate the OPC's ability to reproduce the total mass concentration within its measuring range for an actual engine blow-by aerosol. For this purpose, the same comparison between optical and gravimetric data was performed as described in results Section 2.3. The filter was again installed immediately behind the OPC sensor; the OPC data in the 0.3 to 17  $\mu\text{m}$  size range were taken for the 1:9 dilution shown also in Fig. 2-9. Note that this comparison requires the use of the OPC PSD without the loss correction but with the correction for the dilution factor, because that corresponds to the aerosol arriving also at the filter. The aerosol mass on the filter (mean of 2 measurements) was 300  $\text{mg}/\text{m}^3$ , while the OPC gave 240  $\text{mg}/\text{m}^3$ . The OPC thus measures about 80% of what the filter sees. This corresponds very well with the comparison presented earlier for laboratory aerosols and shows that the OPC is consistent and reliable also for engine measurements.

## 2.5 Summary and conclusions

A comprehensive study of aerosol sampling and conditioning was conducted with regard to the reliability of OPC based size and concentration measurements in a typical engine blow-by environment characterized by a mixture of oil aerosol and saturated oil vapor at temperatures of up to 120 °C. The study is based on an OPC Promo 2000 H by Palas GmbH, a device often used in practice for such measurements.

A single-stage (1:9) and a double-stage (1:80) *sampling and dilution system* were devised. Their transfer functions were measured by OPC in the size range of 0.3 to over 10  $\mu\text{m}$ . Losses below 2  $\mu\text{m}$  were found to range between negligible and 10 %; losses above that size range increased progressively and reached values of over 90 % around 10  $\mu\text{m}$ ; the  $d_{50}$  cut-points were on the order of 7 and 6  $\mu\text{m}$ , respectively. From these transfer functions, a *correction function* was derived for particle sizes up to 8  $\mu\text{m}$ , to account for particle losses.

*Droplet growth by condensation during cool-down* of a mixture of aerosol and saturated oil vapor was investigated for temperatures between 80 °C and 120 °C, a range where

saturation vapor concentrations increase from 9 mg/m<sup>3</sup> to about 110 mg/m<sup>3</sup>. Theoretically this could lead to substantial growth because the vapor mass far exceeds the aerosol mass. Measurements of actual droplet growth during cool-down of an undiluted mixture of vapor and aerosol showed, however, that growth was negligible below about 100 °C, presumably because all the vapor condensed on the system walls. Above that, cool-down generated sufficient supersaturation to activate growth and cause substantial changes in PSD, mainly in the size range from the lower OPC detection limit to about 2 µm. Even at a temperature of 120 °C, condensation to the walls exceeded 95 % of total vapor mass. Dilution of 1:20 during sampling suppressed condensational growth at all starting temperatures. A heated OPC sensor is thus not necessarily required for blow-by aerosol measurements.

The *conversion accuracy of OPC* based number distributions to total aerosol mass was investigated for two of the available sensor ranges (0.2 to 10 µm and 0.3 to 17 µm), by comparison with filter samples. The 0.2 to 10 µm range was found to be more accurate and agreed to generally better than -10 %; the 0.3 to 17 µm range agreed to within -20 %.

*Contamination of the OPC sensor optics* was a problem for the device used (Welas 2070 HP by Palas GmbH) due to deposition of oil droplets and/or oil vapor. When left uncontrolled, this resulted in a massive decrease in effectively recorded mass. There are different strategies for avoiding this problem. For example, one can clean the optics regularly, or one must shorten the sampling time intervals drastically.

The OPC calibration was found to be sensitive to *pulsations in the sampling flow*. Such problems are best circumvented by calibrating with an aerosol in steady flow. The exact nature of these issues has not been fully understood, however.

Tests were performed with *crankcase aerosol from a modern 4-cylinder 5.1-Liter combustion engine*, in order to evaluate the entire train of sampling, diluting and conditioning plus OPC sensor, together with the various loss corrections and experimental precautions derived in the laboratory under field conditions. The aerosol was sampled from

a port installed in the valve cover, before it enters the crankcase ventilation system. In parallel, OPC measurements were obtained with undiluted aerosol that required running the engine in a low-torque mode with rather low aerosol concentrations in order to obtain a reference PSD for comparison.

In the size range for which a loss correction function had been applied ( $\leq 8 \mu\text{m}$ ), it was found that the total aerosol mass would have been underestimated without correction by about 17 % for the engine aerosol. Measurements of the undiluted blow-by aerosol in the OPC sensor range 0.6 to 40  $\mu\text{m}$  showed that the PSD was actually much wider and exceeded the sensor size range on both ends. Two major modes were detected in the volume-based PSD visible to the OPC, one in the range of 2 to 4  $\mu\text{m}$ , and another one around 20  $\mu\text{m}$ .

In summary, representative sampling from the crankcase of a combustion engine is possible within a well-defined range of particle sizes, provided significant precautions are taken above and beyond those customarily applied to aerosol measurements. Depending on the specific sampling and dilution strategy, data in the size range of typical OPCs can be affected by losses as well as condensational growth, sensor contamination and other effects. This makes it difficult to compare published crankcase emission data – especially those limited to reporting a mass mean diameter or total mass concentration – unless such data are accompanied by supporting information of the sampling systems to judge their range of validity.

## 2.6 References

- Ahlborn, S., Blomerius, H., and Schumann, H. (1999). Neue Wege in der Reinigung von Kurbelgehäuseentlüftungsgasen. *MTZ - Motortechnische Zeitschrift*, 60, pp. 454–459.
- Bischof, O.F., and Tuomenoja, H. (2003). Messung von Blow-by-Gaspartikeln. *MTZ - Motortechnische Zeitschrift*, 64, pp. 586–591.
- Burtscher, H. (2005). Physical characterization of particulate emissions from diesel engines. A review. *Journal of Aerosol Science*, 36, pp. 896–932.
- Chien, C.-H., Theodore, A., Wu, C.-Y., Hsu, Y.-M., and Birky, B. (2016). Upon correlating diameters measured by optical particle counters and aerodynamic particle sizers. *Journal of Aerosol Science*, 101, pp. 77–85.
- Golkarfard, V., Subramaniam, R., Broughton, J., King, A., and Mullins, B. (2019). Comparative Performance of 12 Crankcase Oil Mist Separators. *SAE International Journal of Engines*, 12, pp. 5–14.
- Hildemann, L.M., Cass, G.R., and Markowski, G.R. (1989). A Dilution Stack Sampler for Collection of Organic Aerosol Emissions. Design, Characterization and Field Tests. *Aerosol Science and Technology*, 10, pp. 193–204.
- Hinds, W.C. (1999). *Aerosol Technology. Properties, Behavior, and Measurement of Airborne Particles* (2nd ed.). Wiley-Interscience: s.l.
- Janßen, M., Ruppel, S., and T. Fukusen, A.N. (2016). Systematische Optimierung der Kurbelgehäuseentlüftung in turbogeladenen Benzin- und Dieselmotoren. *MTZ - Motortechnische Zeitschrift*.
- Johnson, B.T. (2012). Experimental analysis of crankcase oil aerosol generation and control. B.T. Johnson.
- Johnson, B.T., Hargrave, G.K., Reid, B., and Page, V.J. (2011). Crankcase Sampling of PM from a Fired and Motored Compression Ignition Engine. *SAE International Journal of Engines*, 4, pp. 2498–2509.
- Lakshmanan, M., Maddali, V., Natrajan, R., Muthyam, R., and Balasubramanian, N. (2019). Insight into Effect of Blow-By Oil Mist Deposits on Turbocharger Performance Deterioration in a Diesel Engine. *SAE Technical Paper Series*, 2019-26-0340.
- La Rocca, A., Di Liberto, G., Shayler, P.J., and Fay, M.W. (2013). The nanostructure of soot-in-oil particles and agglomerates from an automotive diesel engine. *Tribology International*, 61, pp. 80–87.

- May, K., (1973). The collision nebulizer: description, performance and application. *Journal of Aerosol Science*. 4, 235-243.
- Palas® GmbH (2011). *Brevier zur Aerosoltechnologie* (2nd ed.). Palas® GmbH: Karlsruhe.
- Randall, K., Bradford, C., Ross, J., Church, J., Dickey, N., Christian, A., and Dunn, M. (2017). Characterization of Crankcase Pressure Variation during the Engine Cycle of an Internal Combustion Engine. In: SAE International 400 Commonwealth Drive, Warren-dale, PA, United States.
- Sang-Nourpour, N., and Olfert, J.S. (2019). Calibration of optical particle counters with an aerodynamic aerosol classifier. *Journal of Aerosol Science*, 138, p. 105452.
- Sauter, H. (2004). *Analysen und Lösungsansätze für die Entwicklung von innovativen Kurbelgehäuseentlüftungen*.
- Sauter, H., Brodesser, K., und Brüggemann, D. (2003). Hocheffizientes Ölabscheidesystem für die Kurbelgehäuseentlüftung. *MTZ - Motortechnische Zeitschrift*, 64, pp. 180–184.
- Sauter, H., Mathiak, D., Müller, J., und List, S. (2012). Kurbelgehäuseentlüftung – direkte Messung von Ölaerosolen. *MTZ - Motortechnische Zeitschrift*, 73, pp. 140–145.
- Uy, D., Storey, J., Sluder, C.S., Barone, T., Lewis, S., and Jagner, M. (2016). Effects of Oil Formulation, Oil Separator, and Engine Speed and Load on the Particle Size, Chemistry, and Morphology of Diesel Crankcase Aerosols. *SAE International Journal of Fuels and Lubricants*, 9, pp. 224–238.
- Uy, D., Pranis, G., Morelli, A., Gangopadhyay, A., Michlberger, A., Secue, N., Kinzel, M., Adams, T., Streck, K., Lance, M., and Wereszczak, A. (2017). Correlating Laboratory Oil Aerosol Coking Rig Tests to Diesel Engine Tests to Understand the Mechanisms Responsible for Turbocharger Compressor Coking. *SAE Technical Paper Series*, 2017-01-0887.
- Jaroszcyk, T. et al. (2006). New developments in diesel engine crankcase emission reduction - requirements, design and performance. *Journal of KONES* 13.2, pp. 155–168.
- Tatli, E., and Clark, N. (2008). Crankcase Particulate Emissions from Diesel Engines. *SAE International Journal of Fuels and Lubricants*, 1, pp. 1334–1344.
- Krause, W. (1995). *Ölabscheidung in der Kurbelgehäuseentlüftung*.





# 3 Blow-by aerosol spectra from a 4-cylinder 5.1-liter diesel engine

Parts of this chapter have been published in:

Scheiber, K., Nowak, N., Pfeil, J., Koch, T., Kasper, G. (2021). Comparison of four diesel engines with regard to blow-by aerosol properties as a basis for reduction strategies based on engine design and operation, AAET, 6, 79–90.

## 3.1 Introduction

Size and concentration of blow-by aerosols depend critically on source properties and on particle interactions in the crankcase environment. Interactions that affect the aerosol size spectrum include particle-particle, particle-wall, and particle-gas interactions. While the extent of these interactions and the contribution of single sources may vary depending on the specific engine considered, the underlying aerosol formation mechanisms apply to a wide spectrum of combustion engines. To identify these basic mechanisms, size distribution measurements were conducted with an OPC under well-controlled conditions on a medium duty 4-cylinder 5.1-liter diesel engine installed on a test stand. The influence of oil temperature, engine load, and engine speed on aerosol properties was assessed in the context of blow-by aerosol formation mechanisms. The location of blow-by aerosol sources within the engine was determined by varying OPC sampling points as well as the addition of dilution air to either the upper or the lower compartment of the crankcase. In this context, the transfer functions of two riser pipes were determined to estimate aerosol transport losses due to particle-wall interactions. Additionally, the aerosol contribution of the turbocharger was determined at various engine operating points. Separately, the particle measuring range was extended by means of both an electrical mobility spectrometer and filter samples to obtain information on aerosol sources beyond the OPC range.

### 3.2 Engine characteristics and test stand

The engine used for the investigations is a commercial medium-duty 4-cylinder 5.1-liter diesel engine (Daimler OM 934). This engine has a 2-stage charging concept, provides a nominal power of 170 kW at 2200 rpm, and has a nominal torque of 900 Nm in the range of 1200 to 1600 rpm. Fig. 3-1 gives more details on the engine power and torque characteristics in the speed range of 1000 to 2400 rpm.

Engine characteristics that are essential in the context of blow-by aerosols include the actual blow-by flow rate and the sump oil temperature at various operating points. As described in Section 1.3, the blow-by gases arise mainly from leakage between the piston rings and the cylinder liner as well as from the turbocharger bearing and, therefore, affect particle generation at these specific locations directly. Simultaneously, these gases dilute any aerosols from other sources and affect particle transport speeds and dwell times in the crankcase, all of which have an effect on particle interactions and ultimately, on the aerosol size spectrum. On the other hand, the oil temperature directly affects oil viscosity and oil vapor concentrations, thereby impacting the generation of aerosols by mechanical means and by condensation.

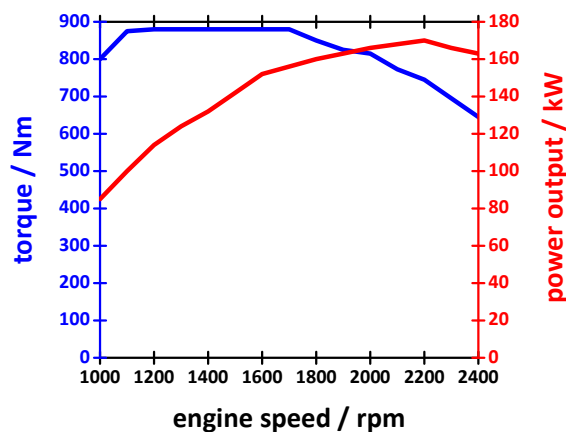


**Figure 3-1:** Engine torque and power at full load in the speed range of 1000 to 2400 rpm for the Daimler OM 934 engine.

The graph on the left-hand side of Fig. 3-2 shows blow-by flows, while the graph on the right displays oil sump temperatures at a constant cooling water temperature of 90 °C.

The data shown in this figure was interpolated from measurements of 23 engine-operating points.

Blow-by gas flows were in the range of 22 to 81 L/min (referring to uncorrected AVL data at 1013 mbar and approximately 30 °C). Generally, blow-by flows increase with rising engine speed due to more pressurizing cycles per unit time, and with load due to more leakage caused by higher pressure levels in combustion chamber and turbo charger. When cooling water was actively kept at 90 °C, the oil temperature in the sump ranged from 91 °C (in idle) to 121 °C (at nominal power). The oil temperature rises monotonously with engine speed and load due to increased heat dissipation into the oil. This rise in oil temperature corresponds to a reduction in oil viscosity by approximately 50 %, and to an increase in saturated vapor concentration from about 12 mg m<sup>-3</sup> to 140 mg m<sup>-3</sup>.

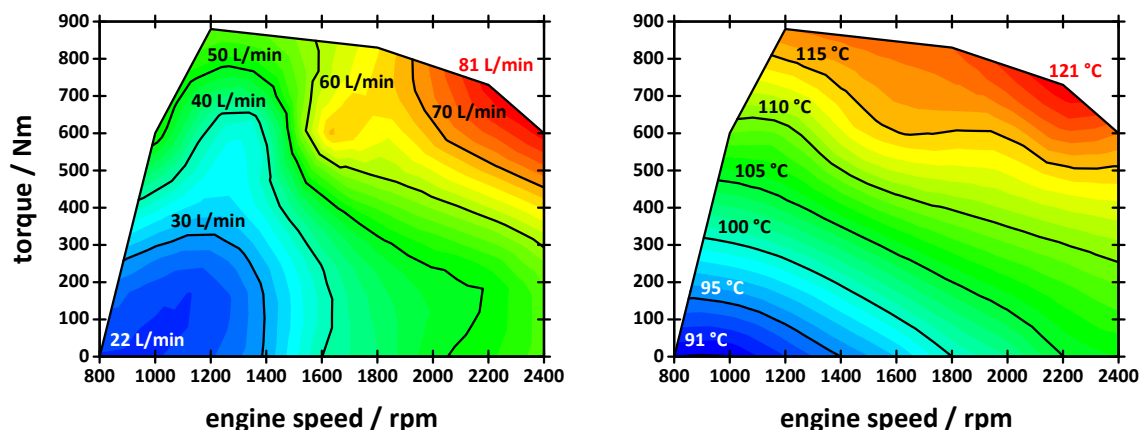


**Figure 3-2:** Daimler OM 934 – Blow-by flows (left) and sump oil temperatures (right) at various engine-operating points. Data from 23 operating points was interpolated to generate these graphs. Engine cooling water temperature was kept at 90 °C.

A synthetic lubricant oil from Shell named Rimula R6 LME (5W-30) was used for all experiments with the Daimler OM 934 engine. To avoid the influence of aging on oil properties, the oil was pre-aged in the engine (24h at medium to high power output) and changed on a regularly basis. The oil level was kept constant for all experiments. This procedure is necessary to prevent a potential effect of changing lubricant oil properties on the blow-by aerosol spectra.

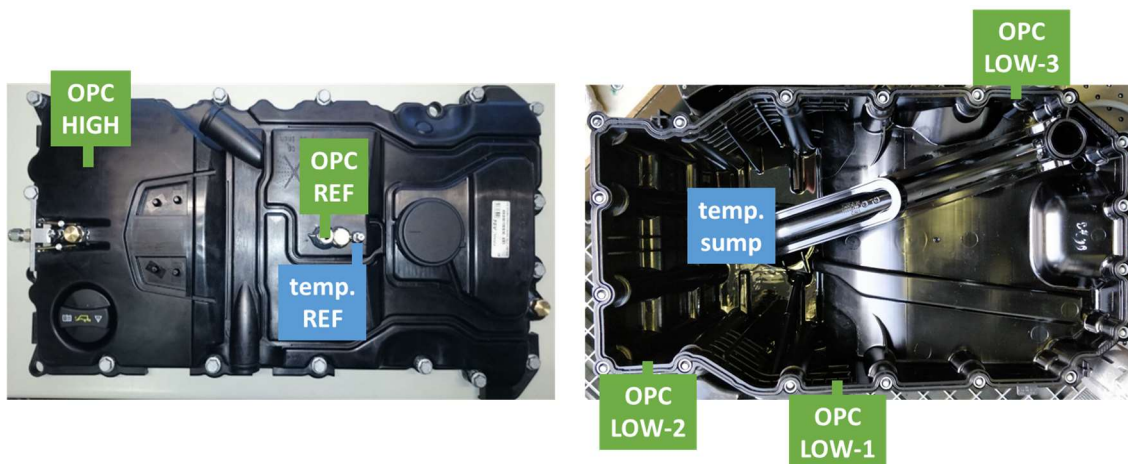


**Figure 3-3:** Daimler OM 934 – Temperature sensors and aerosol sampling points for OPC measurements located in the valve cover (left) and in the oil pan, above oil level (right).

The experimental engine was equipped with temperature sensors and several aerosol sampling points suitable for OPC measurements. The location of these sensors and sampling points is shown in Fig. 3-3. Otherwise, the engine design corresponds to that of a production model.

Operating an experimental engine under well-controlled conditions requires an elaborate test stand infrastructure. The test stand must meet the mechanical, electrical, and thermodynamic requirements of the engine and provide monitoring options for temperatures, pressures, and flows. The correct mechanical dimensioning of the engine mounting system and the implementation of vibration decoupling are two essential aspects that were considered. To operate the engine safely in the entire engine operating map, an adequate electrical break (INDY 44/8p) was implemented. No gearbox was used in the power transmission train. Instead, the engine and the electrical brake were directly connected via a clutch and a main shaft. The engine control unit was provided with signals of a virtual car generated by a dedicated device (ETHER-CAT Haußmann) and controlled by commercial software (Morphee 2.8). To meet the thermodynamic requirements, the engine intake air was sucked from the test stand environment and conditioned by the standard engine turbo charger and air intercooler. The cooling water was actively kept at 90 °C and the engine lubricant / cooling oil was circulated in a loop corresponding to the production model with the only exception being an additional heat

exchanger installed in the oil pan. The core elements of the engine test stand infrastructure are shown schematically in Fig. 3-4.

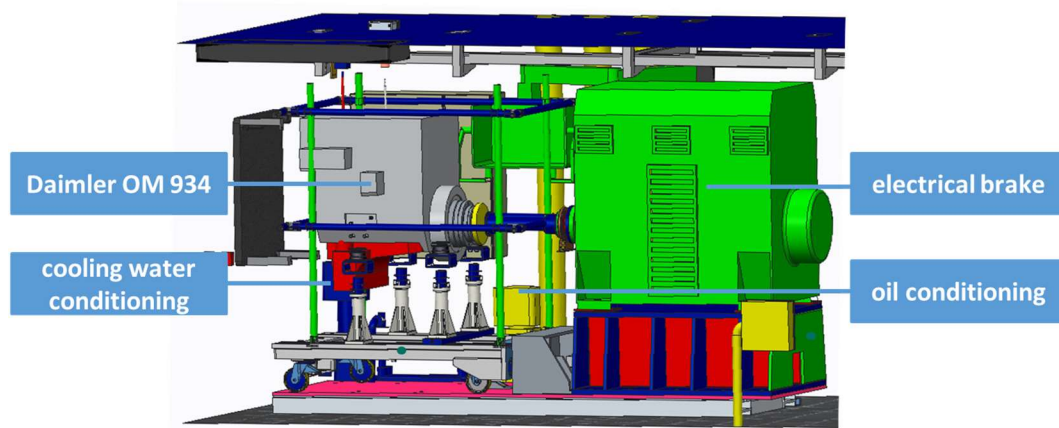


**Figure 3-4:** Schematic illustration of the core elements of the engine test stand infrastructure.

The experiments to determine the contribution of the turbocharger to the blow-by aerosol made it necessary to decouple the device from the engine oil circuit and the air flow path. This was done via an external oil circuit that also vented the blow-by from the turbo charger. Oil temperature and pressure in this external circuit were conditioned to match the conditions of the oil in the engine. To maintain similar flow conditions in the crankcase during decoupled operation, dry make-up air at room temperature was added into the return pipe of the turbocharger.

Certain experiments to localize aerosol sources within the engine required the addition of dry dilution air to either the sampling point LOW-1 in the lower region of the engine or the sampling point HIGH, between the crankcase and the valve cover. Simultaneously, OPC measurements were conducted during engine operation at the reference sampling point (REF). This procedure allowed identifying blow-by aerosol sources and transportation effects.

To characterize blow-by aerosols, the test stand was equipped with an AVL blow-by meter (AVL 442.D/300) and an OPC (the reference Palas<sup>®</sup> OPC introduced in Section 2.3)

connected to the engine by the single-stage (1:9) sampling and dilution system described and characterized in Section 2.4. The OPC sampling flow rate was set to 0,56 L/min for all experiments. When sampling from the reference sampling position (REF), the OPC sensor was located directly above the port to reduce particle losses by minimizing the sampling length and avoiding any bend in the sampling line. Aerosol sampling positions in the lower region of the crankcase were connected to the OPC sensor via a 2 m electrically conductive polyurethane tube.

All data shown in this chapter were obtained with the reference Palas® OPC operated in the size range of 0.3 to 17  $\mu\text{m}$  with a resolution of 32 channels per decade. The remaining OPC settings correspond to those listed in Section 2.3. All PSD graphs shown in this chapter are based on a moving average (3 values) with each data point representing the average of a measuring interval of 300 seconds, which corresponds to 300 spectra at a 1-Hz sampling frequency. The OPC data shown here are generally not corrected for particle losses in the aerosol dilution system (unless noted otherwise), because the focus here was on relative changes with engine parameters etc. rather than on absolute levels.

### **3.3 Influence of oil temperature, engine load, and speed on aerosol**

Oil temperature and engine operating point are expected to have a significant effect on all blow-by aerosol sources within a combustion engine. The following investigations do not aim to identify the contribution of individual sources within the engine; they focus on a better understanding of how oil temperature and engine operating point (i.e., engine load and speed) affect the overall aerosol concentration and size. The data are also used to discuss and distinguish between aerosol formation by mechanical means vs. condensation. For all experiments in this section, the turbocharger was coupled to the engine (standard operation).

Experiments were conducted at 1200 rpm and workloads of 0, 200, 600, and 880 Nm, and at 2200 rpm with loads of 0, and 600 Nm to show the effect of engine load on the

blow-by aerosol spectrum. In one set of experiments (Fig. 3-5) the sump oil temperature was left to adjust itself freely according to engine conditions; in another set (Fig. 3-6) the sump oil temperature was held constant by conditioning the cooling water temperature and by activating the oil pan heat exchanger. The results of these OPC measurements at the REF position are represented by aerosol mass concentrations.

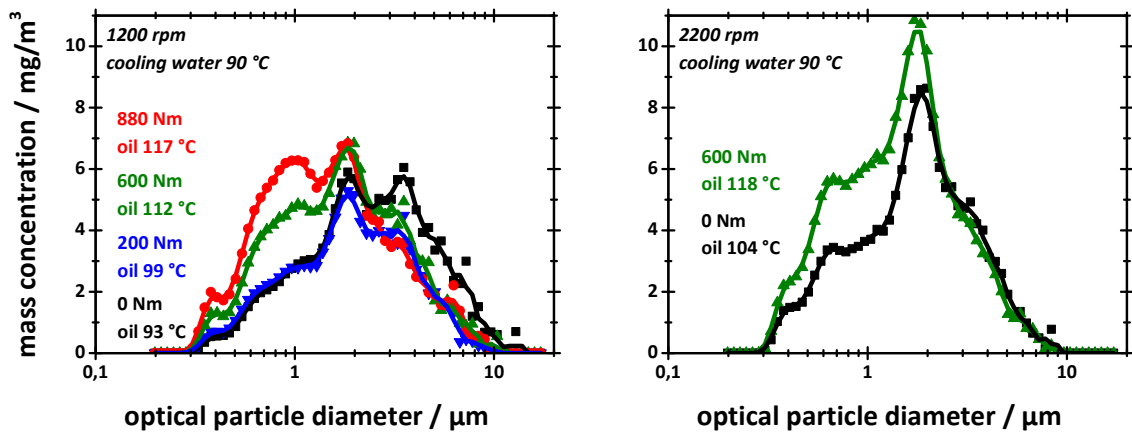


**Figure 3-5:** Blow-by aerosol spectra at 1200 rpm (left) and at 2200 rpm (right) and various engine loads. Sump oil temperatures were left to adjust freely according to engine operation. The cooling water temperature remained constant at 90 °C and the oil pan heat exchanger was deactivated. Aerosol was sampled from the reference point (REF).

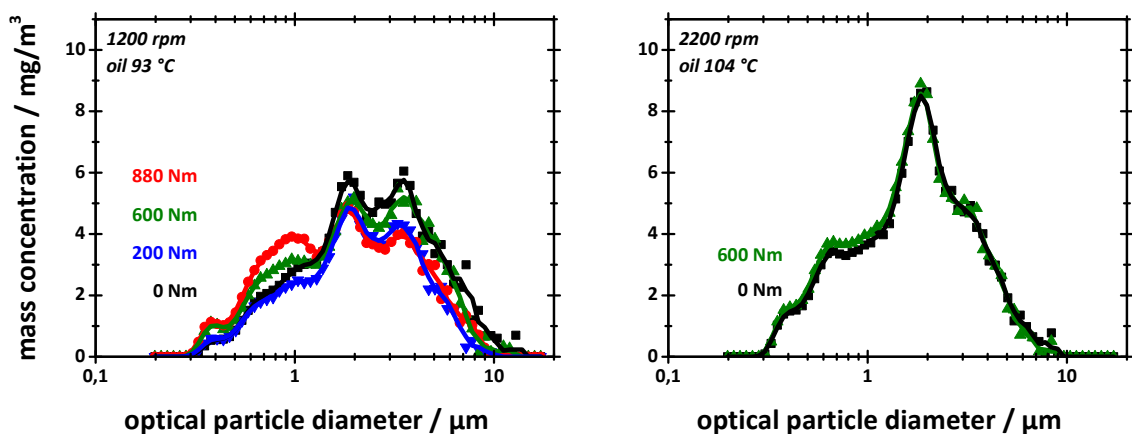


**Figure 3-6:** Blow-by aerosol spectra at 1200 rpm (left) and at 2200 rpm (right) and various engine loads. The sump oil temperature was held constant at 93 and 104 °C respectively, via an oil pan heat exchanger and by adjusting the cooling water temperature. Aerosol was sampled from the reference point (REF).

Fig. 3-5 shows that the oil temperature has a strong influence on the aerosol production. Concentrations below about  $2\ \mu\text{m}$  and in the submicron range change systematically with oil temperature. For the experiments at 1200 rpm the temperature difference between the lowest and the highest engine load was  $24\ ^\circ\text{C}$ , and this increase led to 64 % higher mass concentrations for particles smaller than  $1.2\ \mu\text{m}$ , compared to only 13 % more mass for particles larger than  $1.2\ \mu\text{m}$ . At 2200 rpm the blow-by aerosol concentration also rose notably with the sump oil temperature. Generally, one expects that higher oil temperatures promote the mechanical formation of blow-by aerosols by lowering the oil viscosity. Further, oil vapor generation at hot-spots that leads to particle growth or potentially even to the formation of new aerosols is also promoted by higher sump oil temperatures.

Figure 3-6 shows that keeping the oil temperature constant reduced but did not completely eliminate the influence of the engine load. At 1200 rpm the concentration of particles smaller  $1.2\ \mu\text{m}$  rose by about 50 % from 0 to 880 Nm. At higher rpm, the effect was negligible. The role of the engine load on blow-by aerosol formation can therefore not be attributed entirely to an effect of bulk oil temperature. Other factors are higher pressures in the combustion chamber, higher hot-spot temperatures, and an increased load on the main bearings. In order to gain more insight into the relevance of these factors, further experiments are described in Chapters 4 and 5.

In further pursuit of the influence of the oil temperature, more experiments were conducted at 1200 rpm with loads of either 0 or 600 Nm (where the effects seem greatest), in which the sump oil temperature was reduced significantly below typical levels, by applying the same means as described before. As shown in Fig. 3-7, respective sump oil temperatures of  $69$  and  $48\ ^\circ\text{C}$  resulted in even lower aerosol concentrations than seen in the preceding figures, and again predominantly in the submicron size range. Of course, such drastic reductions in oil temperature would not be feasible during normal engine operation for a variety of reasons. Nevertheless, these results underline the central role of oil temperature in the context of blow-by aerosol generation.

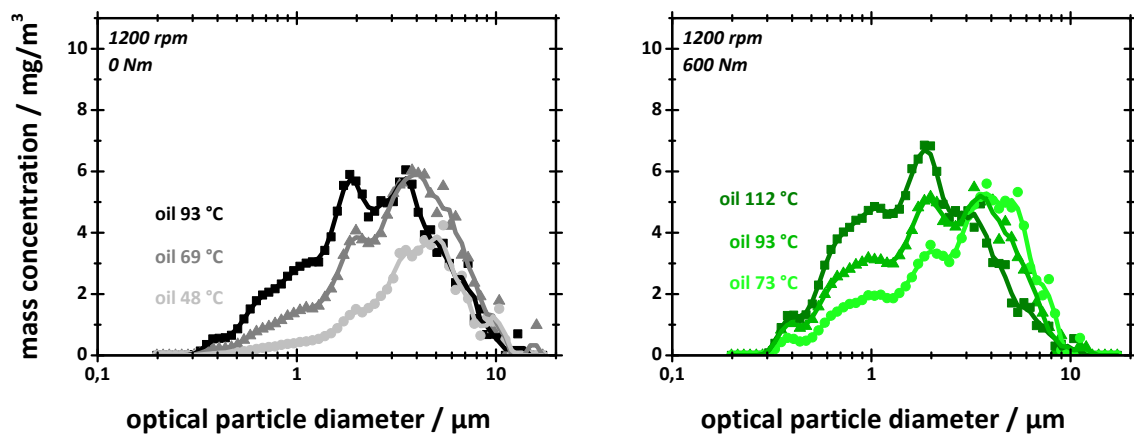


**Figure 3-7:** Blow-by aerosol spectra at 1200 rpm and workloads of 0 Nm (left) and 600 Nm (right) with reduced sump oil temperatures. Aerosol was sampled from the reference point (REF).

In the following, the influence of oil temperature will be analyzed for different particle size ranges, by replotting the data shown in the preceding figures. To make the respective trends more transparent, concentrations have been grouped into three size ranges defined as 0.3 to 1.2  $\mu\text{m}$  (small), 1.2 to 2.7  $\mu\text{m}$  (intermediate), and 2.7 to 10  $\mu\text{m}$  (coarse). These ranges were chosen according to typical peak positions in the blow-by aerosol spectra as shown in the example of Fig. 3-8 (left). The total mass in each size range was determined by converting the respective OPC number data to mass as seen in the right-hand graph. It is understood that mass concentrations in the size range of 2.7 to 10  $\mu\text{m}$  are affected by losses in the sampling and dilution system as well as by non-isokinetic sampling conditions. However, the data are not corrected for such losses, because the trends were of more interest than absolute values.

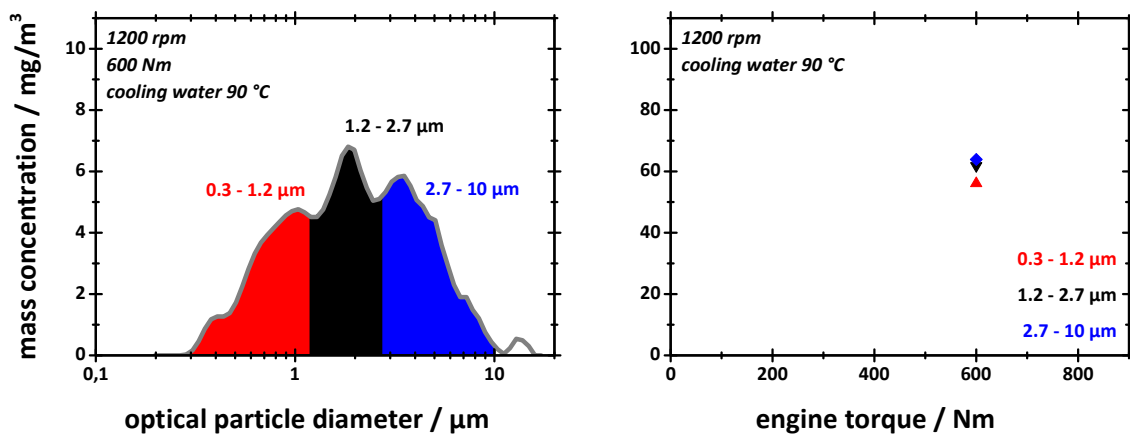


**Figure 3-8:** Data from a typical blow-by aerosol PSD (left) converted to total aerosol mass in the respective size ranges (right). Aerosol was sampled from the reference point (REF).

This technique was applied to all PSD for engine speeds in the range of 800 to 2400 rpm. The data in 200 rpm increments are plotted in Fig. 3-9. The cooling water temperature was kept constant at 90 °C (as in standard operation), resulting in a modest increase of oil temperature with speed from 91 to 106 °C at 0 Nm, and from 109 to 118 °C at 600 Nm; the variation between 1400 and 2200 rpm was even less. Engine operation at 0 Nm (fired operation equaling frictional losses) was of interest because oil vapor generation is minimal under such conditions and the aerosol formation is predominantly by mechanical means. The engine load of 600 Nm was used because it is typical for many driving situations.

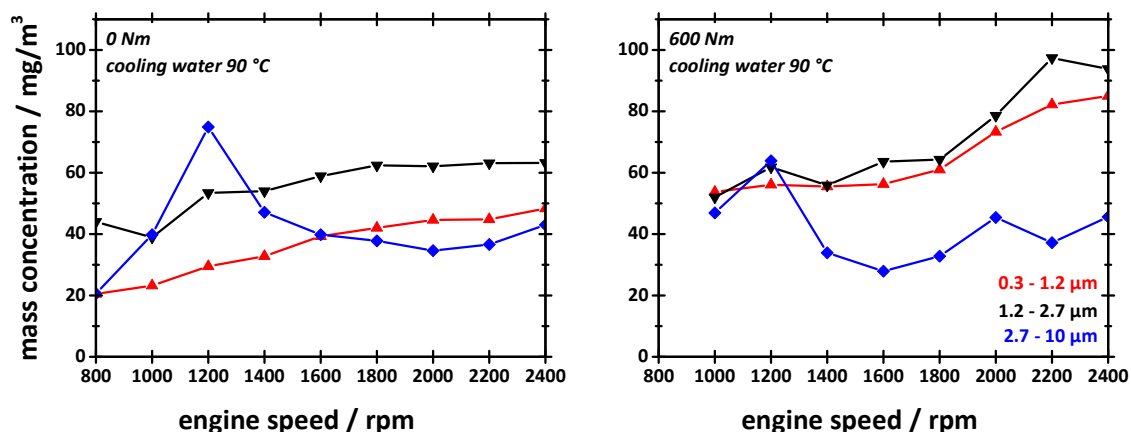


**Figure 3-9:** Blow-by aerosol concentration vs. engine speed in the three size ranges of 0.3 to 1.2 μm (red), 1.2 to 2.7 μm (black), and 2.7 to 10 μm (blue) at engine loads of 0 (left) and 600 Nm (right). Aerosol sampled from the reference point (REF).

According to Fig. 3-9, aerosol concentrations in the small and intermediate size ranges increased with engine speed and oil temperature to a combined value of up to  $180 \text{ mg/m}^3$  at 2200 rpm and 600 Nm. When comparing aerosol properties at the highest with those at the lowest engine speed, the respective concentrations rose by 80 % (at 0 Nm) and by 70 % (at 600 Nm). Since oil temperatures at 600 Nm are fairly independent of engine speed ( $115 \pm 2 \text{ }^\circ\text{C}$  in the range of 1400 to 2400 rpm) the observed, significant increase in particle concentration below  $2.7 \text{ }\mu\text{m}$  must essentially be an engine speed effect. Mechanical aerosol sources are promoted by engine speed due to increased kinetic energy of moving components such as valves, pistons, shafts and gear wheels, which enhance oil atomization. Further, increasing engine speeds leads to more pressurizing cycles per unit time and to higher gas leakage rates past the piston rings, thereby increasing not only the blow-by flow, but also particle generation at this specific location. In addition to more primary aerosol production, this extra blow-by gas flow can lead to more aerosol transport out of the crankcase and up to the probe inlet, which is installed at the entry of the crankcase ventilation system. Apparently, these combined processes more than compensate both the dilution effect by the additional blow-by gas and transport losses due to higher particle inertia.

As opposed to the trend seen for the intermediate and fine particles, the concentration of coarse particles in Fig. 4-9 appears relatively flat for all workloads and engine speeds. Only the data point at 1200 rpm is out of line with the neighboring measurements. As experimental errors or inconsistencies can be excluded because these measurements were re-analyzed carefully, the explanation for such a “local singularity” must be sought elsewhere. If the deviation was due to a change in flow conditions in the immediate vicinity of the sampling probe, this might for example have affected the transport of coarser particles from their local (mechanical) source to the OPC sensor. To investigate this effect in more detail, the sampling point was moved from REF to HIGH, a point located just below the valve cover near the oil refill cap. The OPC sensor was again positioned immediately above this sampling position to avoid any curvature in the sampling line. The engine was operated at 0 Nm torque, various speeds, and at a cooling water

temperature of 90 °C. The total aerosol concentrations at the measuring positions REF and HIGH are shown in Fig. 3-10 for the fine, intermediate, and coarse size range.

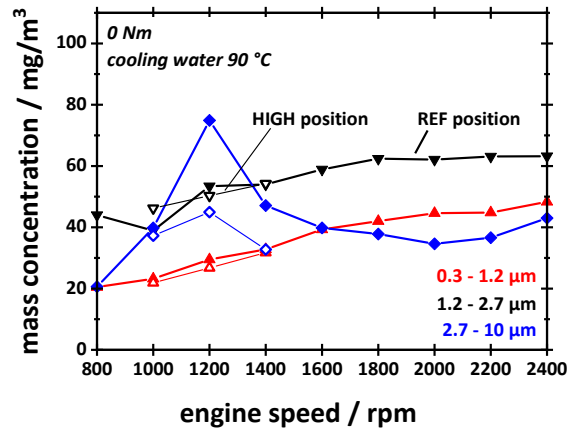


**Figure 3-10:** Blow-by aerosol concentration vs. engine speed in the size ranges 0.3 to 1.2 μm (red), 1.2 to 2.7 μm (black), and 2.7 to 10 μm (blue) at an engine load of 0 Nm. Cooling water temperature was kept at 90 °C. Aerosol was sampled from the reference point REF and an additional position HIGH located immediately below the valve cover.

From Fig. 3-10 it is apparent that fine and intermediate particle concentrations are hardly affected by the sampling position. Presumably these particles are distributed uniformly in the compartment below the valve cover, resulting in similar concentrations at different measuring points. However, concentrations in the coarse size range at 1200 rpm are clearly different between REF and HIGH. This suggests that the reference measuring point may be located near a source of coarse, mechanically generated particles that is affected by engine speed. Also, transport losses of coarse particles may be different between the two sampling points. While this does not entirely explain the reasons for the variability at 1200 rpm, one can now conclude with certainty that the trend in coarse particle concentrations in Fig. 3-9 is indeed flat, and different from those of the finer aerosols.

Along with the concentration, the total mass flow at the entry of the crankcase ventilation system is an important parameter for blow-by aerosol management. This mass flow is calculated by multiplying the aerosol concentrations with the corresponding blow-by

gas flows. Fig. 3-11 contains blow-by aerosol mass flows data of engine speed sweeps at 0 Nm (left) and 600 Nm (right).

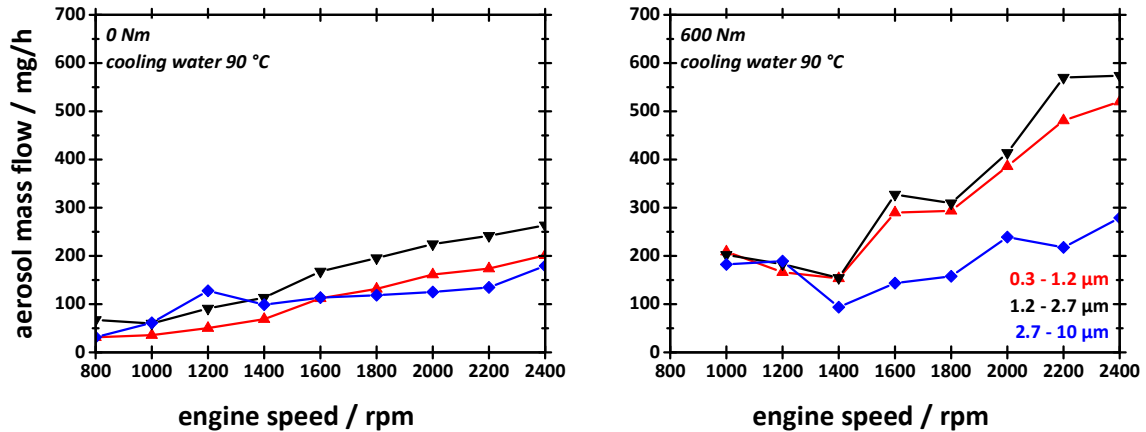


**Figure 3-11:** Blow-by aerosol mass flow vs. engine speed in the three size ranges 0.3 to 1.2 μm (red), 1.2 to 2.7 μm (black), and 2.7 to 10 μm (blue) at engine loads of 0 (left) and 600 Nm (right). Cooling water temperature kept at 90 °C; aerosol sampled from the reference point (REF).

The simultaneous increase with engine speed of blow-by flow and aerosol concentration leads to a steeper rise in aerosol mass flow curves compared to the aerosol concentration. When the engine is operated at 0 Nm, the absolute aerosol mass flows in the combined small and intermediate size range increase by 370 % with engine speed, up to 465 mg/h. When operated at 600 Nm, the aerosol mass flows rise by 160 %, to a maximum of 1094 mg/h. These data show that aerosol mass concentration and blow-by mass flow are equally important criteria in assessing the value of reduction strategies. Such strategies will be discussed later in this thesis.

The effect of engine torque on the aerosol concentration was assessed at workloads of 0, 200, 600 and 880 or 740 Nm for engine speeds of 1200 rpm and 2200 rpm. Although the cooling water temperature was kept at 90 °C, there was a noticeable increase in oil temperature with workload, from 93 to 117 °C at 1200 rpm and from 105 to 121 °C at 2200 rpm. The resulting total aerosol concentrations for each aerosol size range are shown in Fig. 3-12.

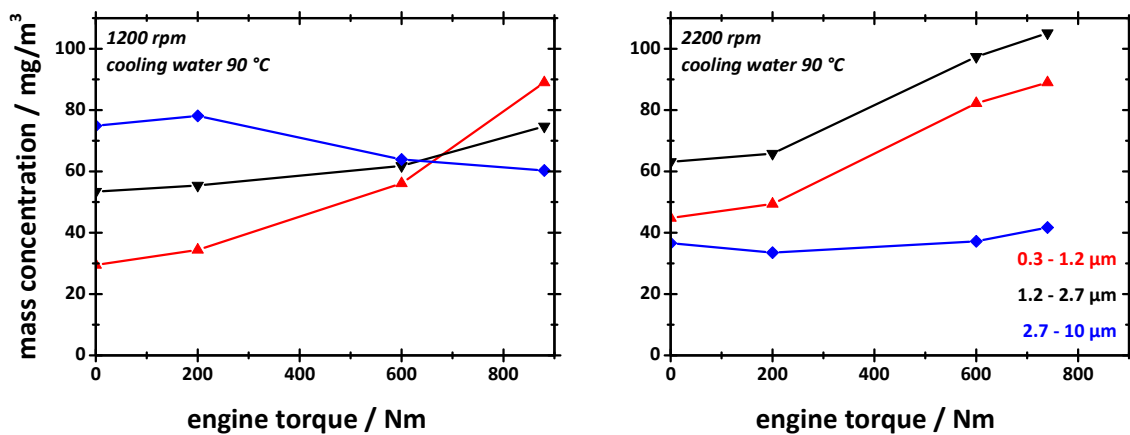


**Figure 3-12:** Blow-by aerosol concentration vs. engine load in the size the three size ranges 0.3 to 1.2  $\mu\text{m}$  (red), 1.2 to 2.7  $\mu\text{m}$  (black), and 2.7 to 10  $\mu\text{m}$  (blue) at engine speeds of 1200 (left) and 2200 rpm (right). Cooling water temperature was kept at 90  $^{\circ}\text{C}$ , aerosol was sampled from the reference point (REF).

Both graphs clearly show an increase in aerosol concentration with engine workload for the intermediate and especially for the small particle size range (by up to a factor of 3). This very significant increase in submicron aerosol production can also be observed in other engines (Scheiber et al., 2021). On the other hand, the concentration of coarse particles is – again – hardly affected by the engine load with flat or even decreasing concentration curves.

The bulk oil temperature in the crankcase increases considerably also with engine load. The reduction of oil viscosity associated with this temperature increase is likely to promote aerosol formation by mechanical means in the size range below about 3  $\mu\text{m}$ . Additionally, the engine operation near nominal power results in local hot spots which act as oil vapor sources for condensation. (More detail on the role of oil vapor condensation on the formation and growth of aerosols is given in Chapter 5). On the other hand these temperature related effects do not seem to contribute to larger droplets > 2.7  $\mu\text{m}$ . Instead, the engine speed has an impact on aerosol transport and generation near the OPC sampling probe leading to almost twice the concentration at 1200 rpm than at 2200 rpm.

Along with the rise of blow-by aerosol concentrations, the mass flow increases even more substantially with engine load, as shown in Fig. 3-13.

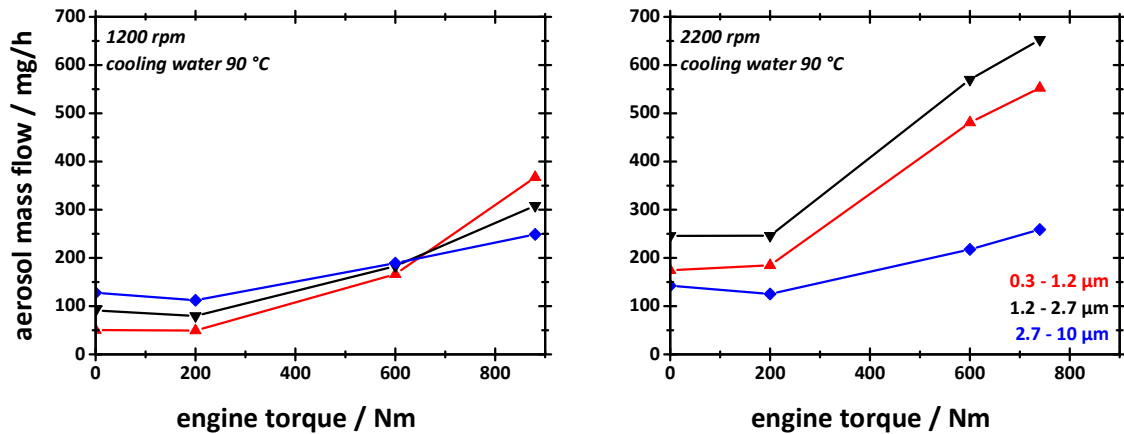


**Figure 3-13:** Blow-by aerosol mass flow vs. engine load in the size ranges 0.3 to 1.2  $\mu\text{m}$  (red), 1.2 to 2.7  $\mu\text{m}$  (black), and 2.7 to 10  $\mu\text{m}$  (blue) at engine speeds of 1200 (left) and 2200 rpm (right). Cooling water temperature was kept at 90  $^{\circ}\text{C}$ , the aerosol was sampled from the reference point (REF).

Aerosol mass flows in the combined small and intermediate particle size spectrum increased by an order of magnitude, from 129 mg/h (at 1200 rpm; 200 Nm) to 1205 mg/h at nominal power. Blow-by flows at these two operating points were 22 and 81 L/min respectively, which covers the entire spectrum of the engine. Again, it becomes clear that one key aspect in trying to reduce crankcase aerosol emissions is to minimize the blow-by gas flow.

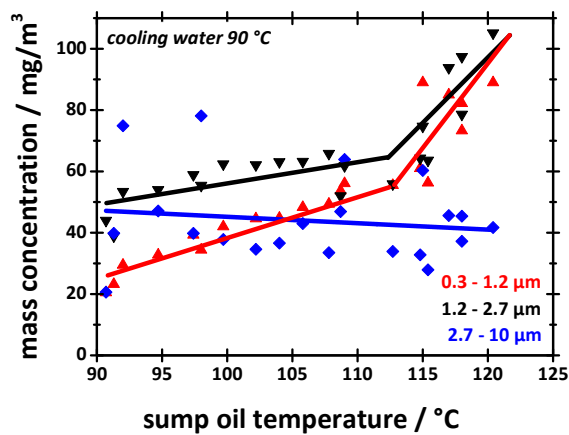


**Figure 3-14:** Blow-by aerosol mass concentration vs. sump oil temperature (obtained at various engine-operating points) in the three size ranges of 0.3 to 1.2  $\mu\text{m}$  (red), 1.2 to 2.7  $\mu\text{m}$  (black), and 2.7 to 10  $\mu\text{m}$  (blue). The solid lines added for each size range represent a visual guide for the trends. The aerosol was sampled from the reference point (REF).

Finally, in Fig. 3-14 all aerosol data presented in this section are plotted against the sump oil temperature at the respective operating point. As in the preceding figures, the aerosol concentration for the intermediate and fine particles is found to increase, at first slowly and then, beyond about 113  $^{\circ}\text{C}$ , more sharply because condensation starts to take effect due to high oil vapor concentrations. The concentration of coarse particles is not affected by the oil temperature (i.e., by engine workload and blow-by gas flow) but instead, as shown before, by sampling position and engine speed.

This figure re-emphasizes the importance of the (bulk) oil temperature as one of the key parameters for the generation of blow-by aerosol. Moreover, it suggests the possibility of differentiating between a regime of lower temperatures where aerosol generation is dominated by mechanical processes, and higher temperatures where vapor condensation makes an additional contribution. The two temperature regimes become especially noticeable for particles smaller than 2.7  $\mu\text{m}$ .

### 3.4 Experiments to locate aerosol sources within the engine

Blow-by aerosols can arise from several types of sources located in different regions of the engine. A set of experiments was conducted to differentiate between sources located in the upper region of the engine (i.e., between the valve cover and the cylinder head) and sources located in the lower region (i.e., between the cylinder block and the oil pan). Two sampling strategies were pursued for this purpose, both based on measurements with the OPC: In one case, aerosol was sampled from ports located in the respective regions of the engine. While this sounds straightforward, such an approach was complicated in practice by a strong local flow variability, excessively high aerosol concentrations as well as the presence of significant oil films on the walls in the crankcase region. In a second, indirect type of experiments, the OPC sampling port was maintained fixed at the reference sampling point (REF) while changing internal aerosol flow rates by adding defined amounts of particle-free air to either the lower (LOW-1) or the upper (HIGH) aerosol sampling port. The selective addition of particle-free air to one or the other port changes the mixing ratio of aerosols arriving at the OPC from the two engine regions and leads to changes in PSD, which provide information about local blow-by aerosol sources.

***Transfer losses of particles between lower and upper crankcase region:*** A prerequisite to the meaningful interpretation of such data is information about particle losses in the ducts (“risers”, 7 of which were located within the motor block) carrying the aerosol from the lower to the upper region of the engine. The transfer functions of two such riser ducts were determined in a laboratory setup described schematically in Fig. 3-15: Oil aerosol in the size range from about 0.1 to 10  $\mu\text{m}$  was generated in sufficient and stable concentrations by atomizing motor oil (Total Quartz 7000; 10W-40) with a two-fluid nozzle maintained at 40 °C. The connection between the atomizer and the entrance to the riser duct was designed carefully, using relatively wide tubing (ID 25 to 30 mm) and very gentle bends, in order to ensure that the coarse particles would reach the riser

in sufficient concentration. Volume flow rates through the duct were varied by appropriate means. Since the OPC (the usual Palas® OPC) was connected below the duct to minimize unwanted transport losses, the engine block was inverted. Finally, the transfer function of a riser duct, expressed as penetration  $C_{out}/C_{in}$  vs. particle diameter, was determined by comparing the downstream PSD with that from a straight section of tubing of equal length installed vertically next to the motor block.

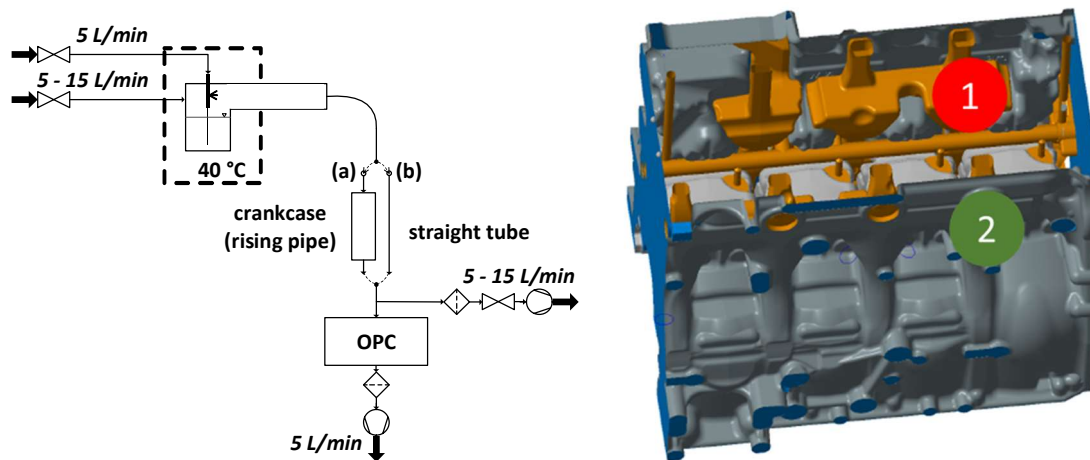


**Figure 3-15:** Schematic of the laboratory setup for measuring the transfer function of an engine riser duct (left) and computer-generated image of the actual crankcase geometry with riser ducts in color (right). Riser ducts no. 1 and no. 2 are identified in the figure.

The right-hand Fig. 3-16 compares the transfer functions (expressed here as penetration) of riser ducts no. 1 and no. 2 in the size range from 0.6 to 40  $\mu\text{m}$ . The left-hand figure shows transfer functions for riser duct no. 1 obtained at volume flows of 10 and 20 Liters/min respectively. Calculated values for the penetration at 10 Liters/min are also included for comparison.

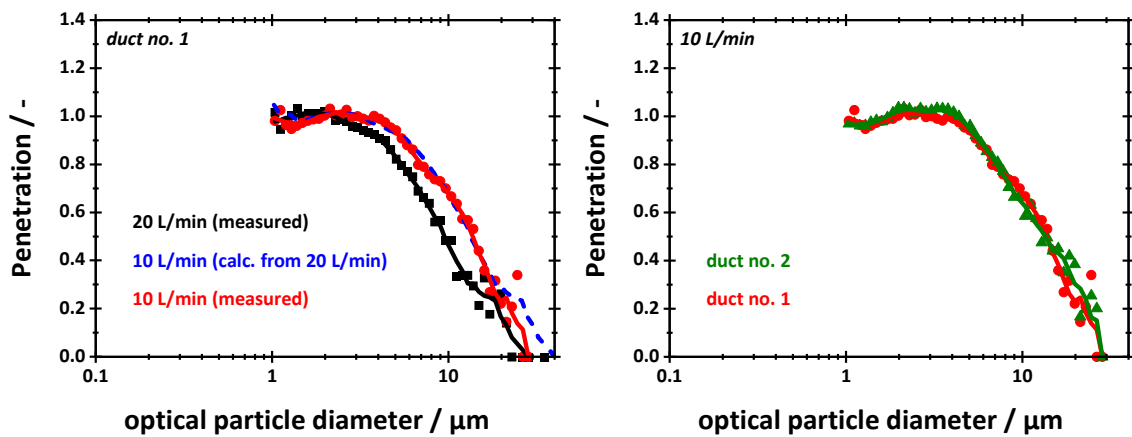


**Figure 3-16:** *Right-hand graph:* Comparison of transfer functions for riser ducts no. 1 and no. 2 at 10 Liters/min. *Left-hand graph:* transfer functions for duct no. 1 at 10 and 20 Liters/min (red and black curves). The theoretical penetration curve at 10 Liters/min (blue) is based on the theoretical shift of the measured curve for 20 Liters/min as described in the text.

Before discussing Fig. 3-16 in detail, a comment regarding the choice of flow rates is in order: The flow rate of 10 Liters/min through a single duct corresponded to a total engine blow-by flow of about 80 Liters/min, which is the flow at nominal power assuming the flow is distributed equally between all ducts and the gear train. Such high flow rates were chosen for test purposes, in order to evaluate (a) the worst-case inertial losses at 10 L/min and (b) to show the sensitivity of the loss function in response to changes in flow rate and Stokes number.

The transfer functions in Fig. 3-16 show clearly that the submicron and micron aerosol fractions are not significantly affected by transfer losses. This was to be expected because diffusional losses in that size are indeed negligible due to short dwell times of only a few tenths of a second. Inertial separation is seen to kick in for particles above about 3 to 4  $\mu\text{m}$  in size; 50% cut points ( $d_{50}$ ) are reached at 10 and 14  $\mu\text{m}$  for flows of 20 and 10 Liters/min, respectively.

Inertial particle losses are known to scale with the dimensionless Stokes number (Hinds, 1999), denoted as  $St$ :

$$St = \frac{\rho_p \cdot x^2 \cdot v}{\mu \cdot L} \quad (3-1)$$

where:

- $\mu$  is the dynamic viscosity of the fluid,
- $\rho_p$  is the density of the particle,
- $x$  is the particle diameter,
- $v$  is the velocity of the flow,
- $L$  is the characteristic length.

Between 20 and 10 L/min one can therefore anticipate an increase in penetration (and thus a shift in the transfer function) by a factor of roughly  $\sqrt{2}$  (see Eq. 3-1). In order to test this relationship, the measurements at 20 L/min were multiplied accordingly to generate a theoretical transfer function curve for 10 L/min (blue curve in Fig. 3-16). The theoretical estimate is in very good agreement with the actual measurement at 10 L/min, clearly indicating that inertial separation is the dominant mechanism here. Differences between riser ducts of slightly different geometries are comparatively negligible.

Considering that 10 L/min corresponds to the blow-by flow at nominal engine power, i.e., to the worst case, the particle penetration at more moderate flow rates should be even better. When reducing the flow rate to, say, 5 L/min, one may assume that >90% of the oil mass below 10  $\mu\text{m}$  will pass unhindered from the lower crankcase of an engine to the valve lid region. Above about 10  $\mu\text{m}$ , there are additional effects to be considered such as the pulsating nature of the blow-by flow and gravitational sedimentation, which may increase actual losses. Such effects were not considered here, however.

**Comparison of blow-by aerosols from the lower and upper engine compartments:** In order to obtain direct PSD information about these respective regions, OPC measurements (with the reference Palas® OPC) were conducted at the sampling locations designated in Fig. 3-3 as REF (near the valve lid cover) and LOW-1 or LOW-2 (oil pan). The

turbocharger was coupled to the engine (standard operation) for all experiments reported in this section. The cooling water temperature was kept at 90 °C, in other words the bulk oil temperature was allowed to vary with the engine operating point.

Note also, that PSD obtained from the lower engine compartment are associated with some (difficult to quantify) uncertainty regarding sampling losses for larger, inertial particles. This has to do with a rather poorly defined (and probably turbulent) air flow inside the oil pan, due to the vicinity of the crankshaft. Also, the length of the sampling line between oil pan and OPC had to be extended to about 2 m, due to space constraints. As a result, it was decided to limit the discussion of PSD from the LOW sampling positions to the size range of 0.3 to 1.3  $\mu\text{m}$ . This size range corresponds to the “fine” faction in previous graphs. It is of special interest, because it contains a significant fraction of the aerosol mass (which is costly to separate).

A first set of data compares blow-by aerosols sampled from the reference measuring point (REF) and from position LOW-1. The engine was operated at 1200 rpm with workloads of 0, 200, 600, and 880 Nm. The resulting PSDs are plotted in Fig. 3-17. In that and the following figures, the particle size region  $>1.3 \mu\text{m}$  is “grayed out” to indicate the uncertainty in sampling losses from the lower engine compartment, and not discussed further.

When operating the engine at 1200 rpm and low workloads of 0 and 200 Nm, the PSDs of the sampling points REF and LOW-1 are in close agreement for “fine” particles (left-hand graph in Fig. 3-17). The degree of agreement clearly indicates that aerosols in the range of 0.3 to 1.3  $\mu\text{m}$  are predominantly formed in the lower regions of the engine and transported with negligible losses from there to the entrance of the blow-by gas ventilation system (located near the reference sampling point). When the engine load is increased to 600 or 880 Nm (right-hand graph), the overall mass concentration of “fine” particles increases substantially (for reasons already discussed in Section 3.3), but also

the difference in concentration increases between the lower and the upper engine compartments. For the highest engine load, the total mass concentration at LOW-1 exceeds that measured below the valve cover (REF) by 43 %.

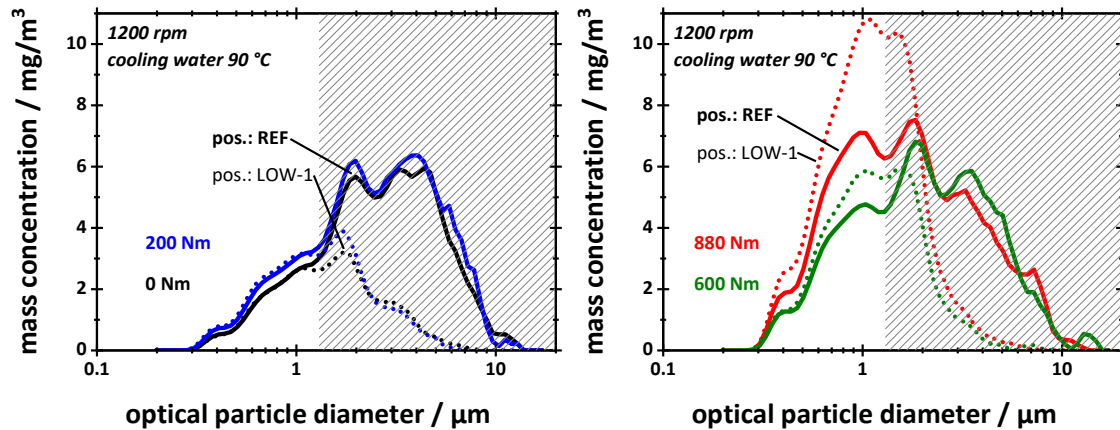


**Figure 3-17:** Blow-by aerosol PSD at 1200 rpm and workloads from 0 to 880 Nm obtained at the position REF (solid lines) and the sampling point LOW-1 (dotted lines). Cross hatching indicates the size range where sampling losses are not well defined due to reasons explained in the text.

The likely cause for the observed difference in concentration between “below” and “above” will now be discussed in more detail: First, transport losses on the aerosol path can be ruled out. Inertial losses in the size range below  $1.3 \mu\text{m}$  are minimal, even at high blow-by flow rates, as shown earlier (compare Fig. 3-16). Diffusion losses are also negligible, because of the high blow-by flow rate. Furthermore, particle-particle interactions leading to coagulation are not expected due to the relatively low total number concentrations on the order  $10^6 \text{ cm}^{-3}$  and short residence time in the ducts. Indeed, the PSDs show no shift in peak at  $1.0 \mu\text{m}$ .

Instead, the observed differences in concentration are probably related to the proximity of the aerosol sources to the sampling ports in the lower region of the crankcase. This proximity can lead to a biased aerosol sample due to the lack of mixing. To verify this non-uniform mixing hypothesis, PSD measurements were conducted at two additional sampling positions LOW-2 and LOW-3. The respective blow-by aerosol spectra, obtained at 1200 rpm with an engine load of 600 Nm, are shown in Fig 3-18.

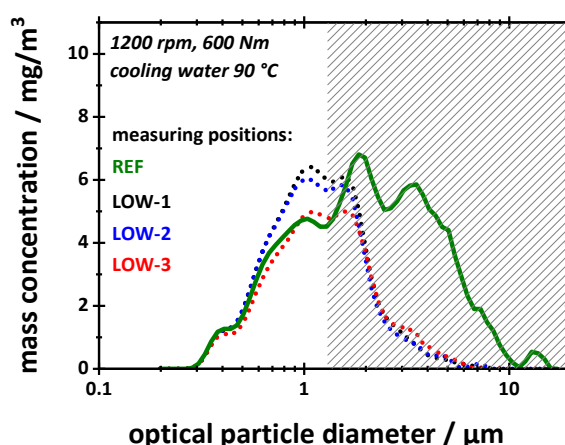


**Figure 3-18:** Blow-by aerosol PSDs at 1200 rpm and 600 Nm for three different sampling locations in the lower engine compartment (dotted lines), compared to the REF PSD (solid green line).

One notices immediately that the two PSD sampled from the front side of the oil pan (LOW-1 and LOW-2) are almost identical and higher in concentration than that from LOW-3, which incidentally matches the PSD from the reference sampling port quite closely. Considering the flow field induced by the rotation of the crankshaft, newly formed particles first pass the front side of the oil pan before reaching the back (LOW-3). This substantiates the supposition that aerosols are not distributed uniformly in that region of the engine and offers a plausible explanation for the differences seen in Fig. 3-18.

Additional OPC measurements were conducted at an engine speed of 2200 rpm and engine loads between 0 and 740 Nm, again using the sampling ports LOW-1 and REF. The resulting aerosol size spectra are plotted in Fig. 3-19.

The size distributions at 2200 rpm show the well-known increase in total concentration aerosol with engine load, which is due to rising oil temperatures and common to all these measurements. As opposed to the experiments at 1200 rpm which did not show significant differences between “above” and “below” (aside from non-uniformities below), the PSDs sampled from the lower region of the crankcase now have a clearly bimodal shape with peaks at 0.7 and 1.9 μm and a dip in concentration around 1.0 μm.

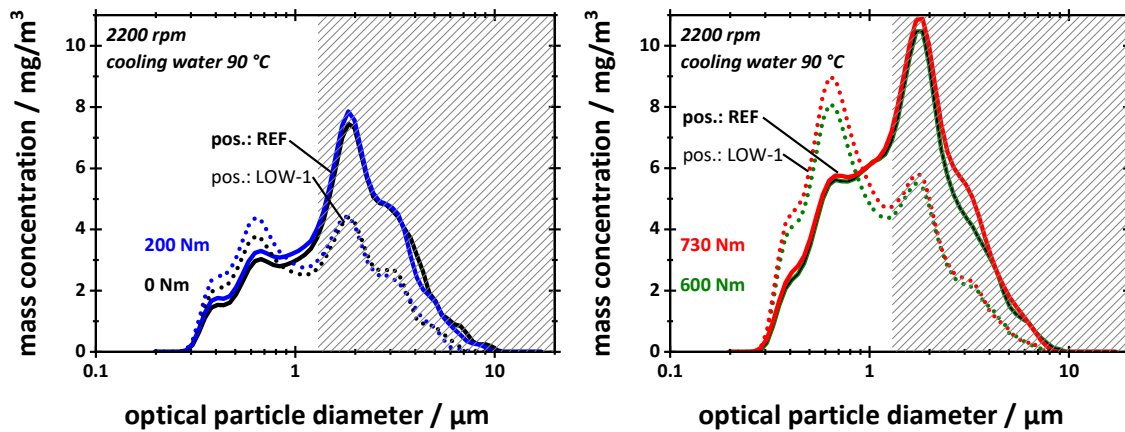


**Figure 3-19:** Comparison of blow-by aerosol PSDs at the position REF (solid lines) and the sampling point LOW-1 (dotted lines) for 2200 rpm and workloads from 0 to 730 Nm.

The main difference between 1200 and 2200 rpm is the flow field in the lower part of the crankcase, which is strongly influenced by the crankshaft speed. Assuming incomplete mixing at LOW-1, a possible explanation for the 0.7  $\mu\text{m}$  peak could be a biased aerosol sample containing submicron aerosol from a nearby source in the lower part of the crankcase.

All these observations point to the lower engine compartment as the most relevant source of submicron blow-by aerosols. To substantiate this even further and to learn more about aerosol flows within the crankcase, a refined experimental procedure was developed. A flow of 50 Liters/min of dry air was added to the engine, either through the lower (LOW-1) or the upper (HIGH) port. The objective of this procedure was to determine whether aerosol sources are primarily located in the lower or upper area of the crankcase. Depending on the location of these sources and where air is introduced, it can either dilute the aerosol or flush out additional particles. The OPC sampling port was maintained at REF. The results of these measurements were then compared with PSDs where no additional air had been added. The additional air flow should have no effect on inertial particle losses in the riser ducts for the particle size range of primary interest, i.e., below about 5  $\mu\text{m}$  (see Fig. 3-16).

Fig. 3-20 shows the measured PSDs with the addition of dilution air (red) and without dilution (black). Also shown in blue is the PSD without dilution air scaled down by the ratio of (blow-by flow)/(blow-by flow + dilution). The left half of the six graphs is for dilution from “above”, while the right half shows dilution from “below”. In total, three engine operating points were used for these experiments: 1200 rpm at 0 Nm, 1200 rpm at 880 Nm and 2200 rpm at 740 Nm (nominal power). Cooling water was kept at 90 °C.

The following outcomes are possible as a result of the addition of an air flow: Either, the aerosol concentration in the respective region is reduced (“diluted”), in which case the PSD obtained without dilution (the black curve) will drop all the way to the blue curve. In other words, the red and blue curves will coincide. Or, additional particles are flushed toward the sampling point by the added air, which compensate for the dilution so that the concentration remains unchanged, or at least well above the blue curve. In other words, the red curve will tend to coincide with the black curve.

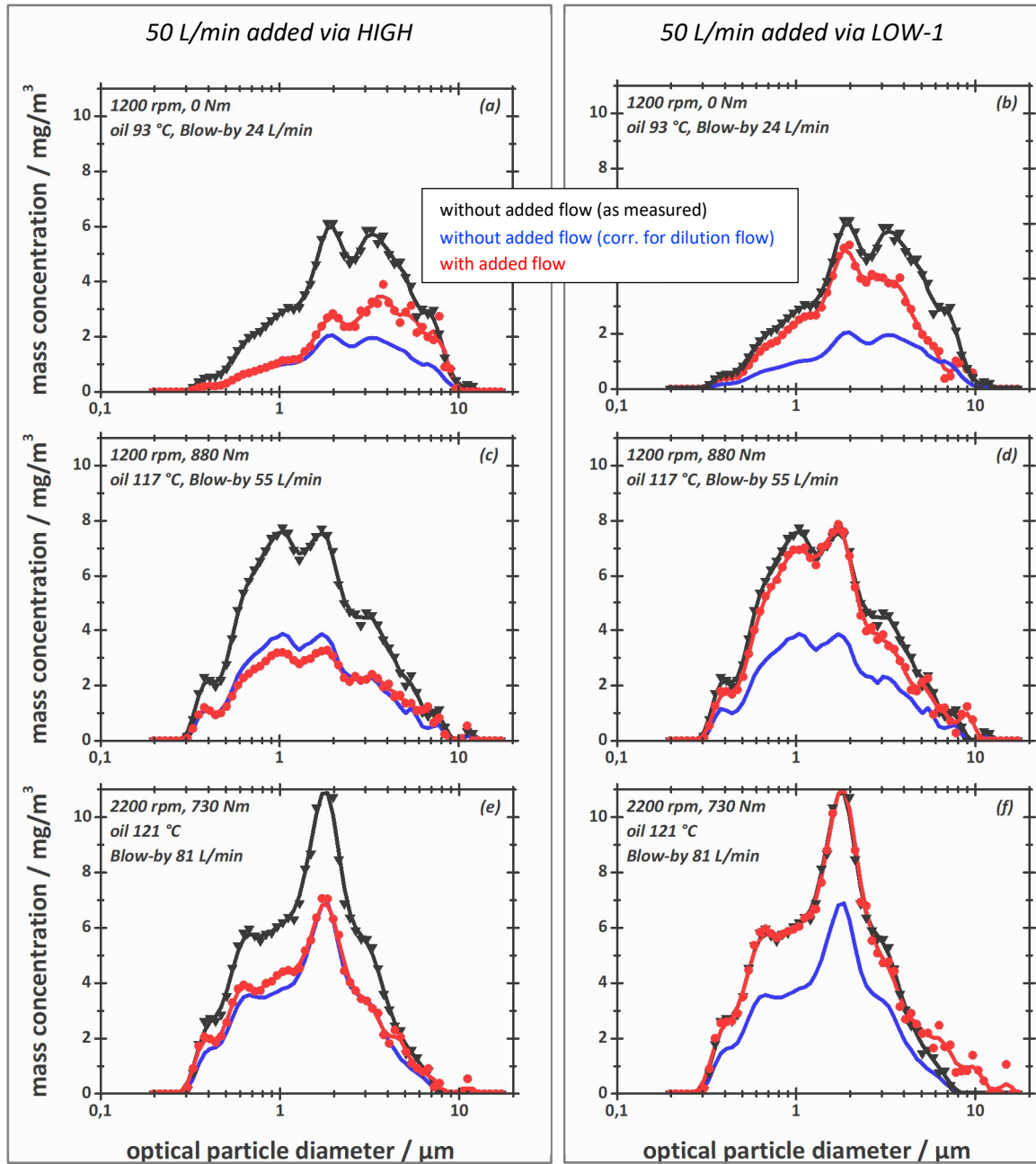


**Figure 3-20:** Blow-by aerosol PSDs with and without the addition of 50 Liters/min of dilution air to the crankcase, either from above (left) or below (right) at three engine operating points. Aerosol was sampled from the reference measuring position (REF). Cooling water constant at 90 °C.

On the left-hand side of Fig. 3-20 the red curves tend to agree with blue curves, while on the right-hand side they tend to agree with the black curves. The respective agreement is in fact excellent for intermediate and high workloads. Thus, for micron and sub-micron particles the addition of dry air *from above* reduces the concentration by the dilution factor. This is a first, clear indication that submicron particles originate primarily from the lower region of the crankcase and are diluted before reaching the OPC probe. With regard to supermicron aerosols, concentrations can be somewhat higher than expected from dilution (for 1200 rpm, 0 Nm), suggesting that the additional flow flushes larger particles out of the upper crankcase and carries them to the reference sampling position.

The addition of air *from below* leaves the concentration of micron sized and submicron particles almost unchanged in the range from 0.3 to 5.0  $\mu\text{m}$ , no matter which operating point is considered. Apparently, the dilution effect is compensated by additional fine particles that either preexist in the lower region of the crankcase and become entrained only with the extra flow, or by the generation of new particles due to vapor condensation. Both scenarios are conceivable, when the dilution air is mixed with the aerosol laden blow-by in the turbulent flow field induced by piston movements and crankshaft rotation. Simultaneously, the added flow is warmed up and saturated with oil vapor. These particles are then flushed out through the riser ducts to the upper crankcase regions and carried to the OPC probe. Inertial particle losses in the riser ducts caused by the added flow are not detectable in the data. This was to be expected and confirms what was found during the transfer function measurements of the riser ducts reported earlier.

In summary, all these findings point to the lower region of the crankcase as the key, and perhaps principal, source of submicron and micron blow-by aerosols. What remains to be clarified is whether all or at least the additional particles are formed by condensation of oil vapor or not. Therefore, a further experiment was conducted at a reduced oil temperature of only 62 °C, where the saturation vapor concentration is definitely negligible.

For this purpose, the cooling water temperature was lowered and the oil pan cooler activated. In all other regards, this experiment followed the same protocol as the measurements shown previously in Fig. 3-20. The results from these OPC measurements at the REF position are shown in Fig. 3-21.

The reduction in oil temperature at an operating point where hot-spot temperatures and oil vapor generation are rather low did not change the system behavior. As observed before, the injection of dilution air to the upper crankcase did reduce aerosol concentrations to the extent of the dilution factor. When adding the same amount of air into the lower crankcase, concentrations remained unaffected. Due to the low temperatures, condensation can be ruled out as an important factor for this behavior. Thus, leading to the conclusion that mechanically formed particles are flushed out from the lower region of the crankcase when air is added here.

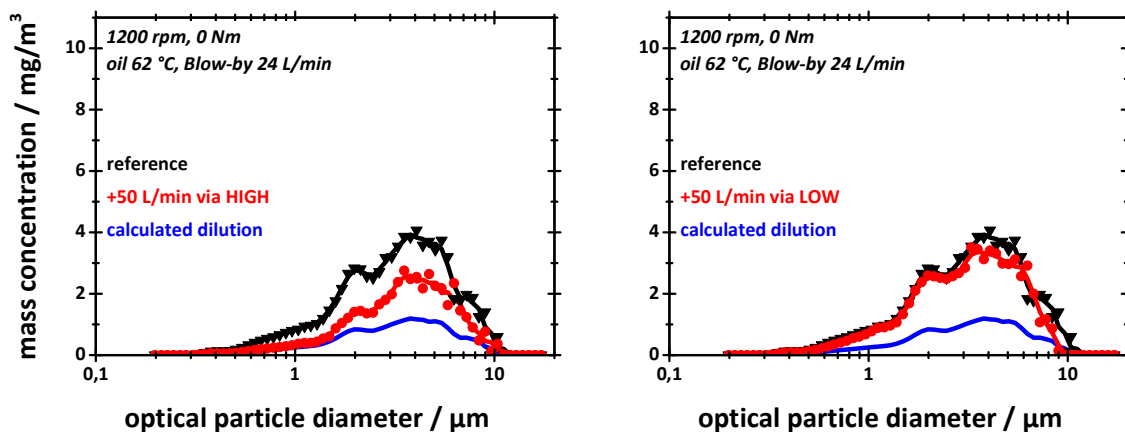


**Figure 3-21:** Blow-by aerosol PSDs with engine operating at 1200 rpm, 0 Nm but at a reduced oil temperature of 63 °C. Measurements are with and without the addition of 50 Liters/min of dilution air to the crankcase, either from above (left) or below (right) at three engine operating points. Cooling water constant at 90 °C. Aerosol was extracted at the reference sampling position (REF).

Generally, the results from this chapter show that adding a dilution gas flow into the crankcase from above (near the entrance to the crankcase ventilation system) can be an effective strategy to reduce blow-by aerosol concentration. But of course, this procedure has negligible impact on the aerosol mass flow rate.

### 3.5 Contribution of the turbocharger to the aerosol load

The turbocharger is a relevant source of blow-by gas and potentially also of aerosols. During engine operation, gases may pass the shaft seals of the turbocharger to reach the crankcase via the turbocharger return pipe. Foaming and spraying during this process can lead to the formation of additional aerosols. Due to high exhaust gas temperatures of up to 550 °C, the oil in the bearings is thermally stressed, decreasing its viscosity and increasing the generation of oil vapor. Both these effects promote aerosol formation by mechanical means or by condensation. Lorenz et al. (2020) have shown that the blow-by aerosol contribution of the turbocharger in the size range of 0.2 to 10 µm depends on the engine-operating point. At high workloads, its contribution reaches up to 21% of the total blow-by aerosol mass concentration. Measurements by Delvigne *et al.* (2010) show that gas leakage in the turbocharger can be responsible for more than 50% of the exhaust gas flow, especially at low and high loads.

To obtain data on the contribution of the turbocharger to the total aerosol, arrangements were made for decoupling the 2-stage turbocharger of the 4-cylinder 5.1-liter test engine from the oil and blow-by paths of the engine. (Section 3.2 gives more details on the decoupling and blow-by compensation procedure.) In the following, the turbocharger contribution is quantified by comparing aerosol spectra obtained by OPC at the reference sampling point (REF) with and without the connected turbocharger (but under identical operating conditions).

Measurements were conducted at a low power operating point of 1200 rpm with zero load and a constant cooling water temperature of 90 °C. It was not necessary to add make-up air when disconnecting the turbocharger, since the latter made no blow-by gas contribution at this operating point. The resulting blow-by aerosol spectra obtained with (red) and without (blue) the turbocharger are shown in Fig. 3-22.

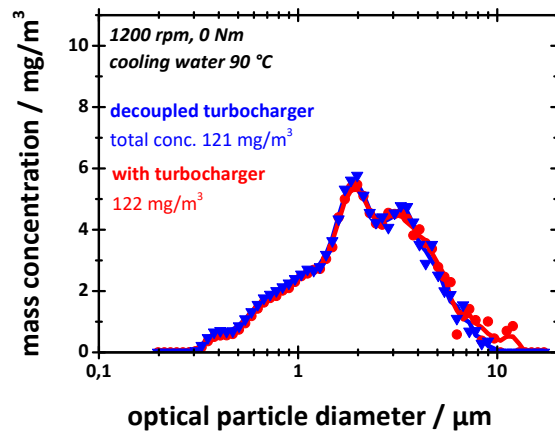


**Figure 3-22:** Comparison of blow-by aerosol PSDs with and without turbocharger at a low power operating point of 1200 rpm with no load and a cooling water temperature of 90 °C. Aerosol was sampled from the reference point (REF).

The two PSDs overlap almost perfectly, indicating that the turbocharger does not contribute to the aerosol at this low-power operating point. The absence of any gas leakage through the turbocharger shaft seals turns the internal volume of the return pipe into a dead zone from which no aerosol is transported into the crankcase. The aerosol contribution of the liquid oil return flow to the crankcase is also negligible because foaming and bubble bursting play a minor role for aerosol concentration (see chapter 4 for more information). More broadly, these data underline the excellent reproducibility of OPC measurements due to well controlled dilution ratios and experimental procedures. However, they are negative with regard to the contribution of the turbocharger-

To gain more insight into the actual contribution of the turbocharger at different operating points of the engine, OPC measurements at the reference point (REF) were conducted at medium to high power operating points, namely at 1200 rpm and 880 Nm; 1800 rpm and 830 Nm; 2200 rpm and 440 Nm; 2200 rpm and 730 Nm. To retain constant conditions of flow and aerosol transfer in the crankcase, compressed air was added to the return pipe of the turbocharger in decoupled operation. The volumetric flow rates corresponding to the above conditions were 11, 15, 13, and 24 L/min, respectively (see Tab. 3-1).

**Table 3-1:** Overview of the examined operating points:

speed / rpm	load / Nm	blow-by from turbocharger / L·min <sup>-1</sup>
1200	880	11
1800	830	15
2200	440	13
2200	730	24

The cooling water temperature was kept at 90 °C resulting in oil temperatures in the range of 110 to 121 °C. The resulting blow-by aerosol spectra with (red) and without the turbocharger (blue) are shown for each operating point in Fig. 3-23.

The four graphs of Fig. 3-23 deliver a surprising picture, in that the turbocharger does not contribute a substantial amount of aerosol mass to the total aerosol emitted from the crankcase, regardless of operating conditions. The maximum contribution to the aerosol mass in the size range from 0.3 to 2 µm is under 20%. Above 2 µm, there is no difference at all between the PSD with and without turbocharger. Even at nominal power, where the temperatures and the blow-by contribution of the turbocharger should reach their maximum, and where the literature suggests a significant contribution (Lorenz et al., 2020), these measurements show a marginal addition of aerosol mass. One must therefore conclude, that for the 4-cylinder 5.1-liter diesel engine and the 2-stage turbocharger investigated, the turbocharger remains a minor source of aerosol.

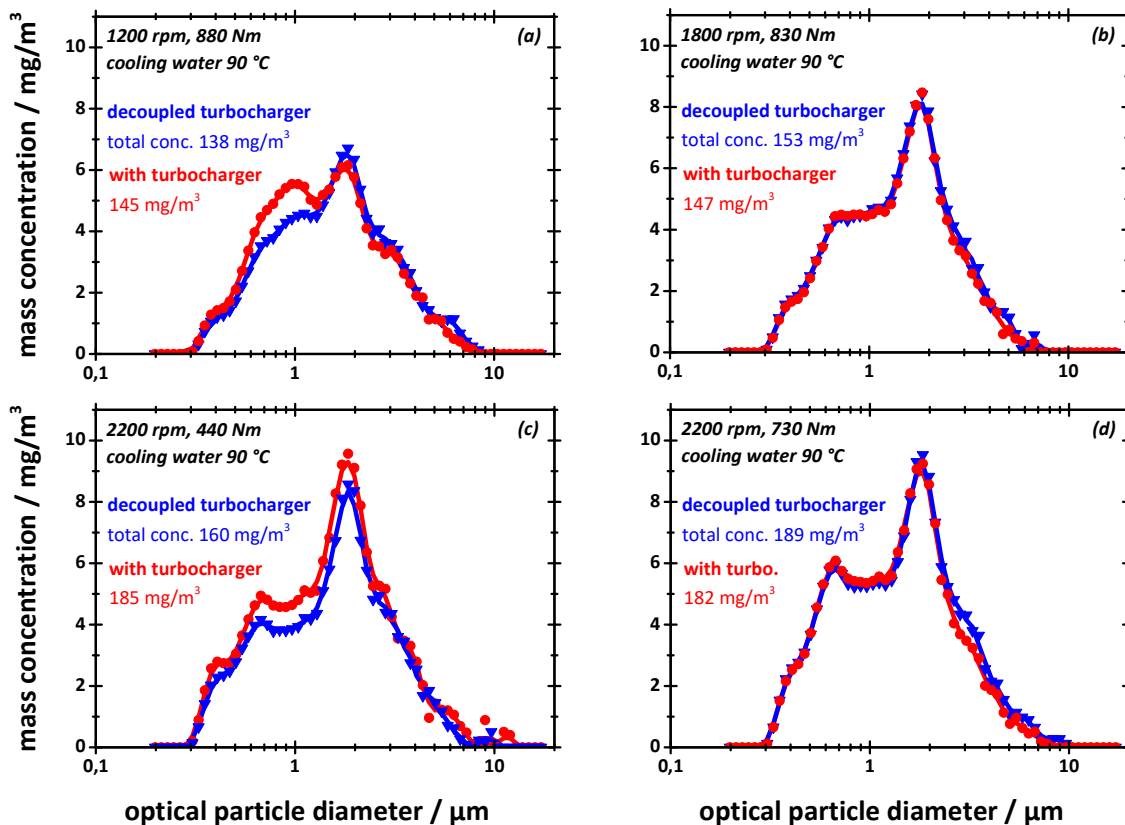


**Figure 3-23:** Blow-by aerosol PSDs with (red) and without (blue) turbocharger aerosol contribution at the operating points of (a) 1200 rpm, 880 Nm; (b) 1800 rpm, 880 Nm; (c) 2200 rpm, 440 Nm; and (d) 2200 rpm, 730 Nm. Compressed air was added in decoupled operation to make up for the flow. Cooling water temperature was kept at 90 °C, the aerosol was sampled from the reference point (REF).

### 3.6 Aerosol sources beyond the optical particle counter measuring range

Complementing information regarding the properties of blow-by aerosols in the size ranges exceeding the upper and lower limits of the OPC-measuring range was obtained using weighted filter samples and electrical mobility analysis, respectively. These experiments were conducted on the same 4-cylinder 5.1-liter diesel engine described in Section 3.2. The engine was operated at 1200 rpm and 0 Nm load (fired mode), with the oil temperature maintained at 93 °C and the cooling water temperature at 90 °C. Due to rapid filter flooding caused by splash oil, testing at other operating points was not possible.

For the particle size range of 5.6 to 560 nm, an engine exhaust particle sizer (EEPS) from TSI was employed. Although this device is primarily designed for measuring particles in the exhaust line, which typically consist of soot agglomerates with an open and branched structure, it is also suitable for characterizing compact, spherical particles such as oil droplets. However, this required the use of the "compact" evaluation profile. Further information comparing this device to other electrical mobility spectrometers can be found in the literature (Michler et al., 2019). Additionally, in Chapter 4, this device is extensively utilized for blow-by aerosol characterization. Both aerosol spectrometers, the OPC and the EEPS, were equipped with the single-stage (1:9) dilution system described in Chapter 2. It should be noted that the OPC aerosol data presented in this section were corrected to account for losses in the sampling and dilution system. Furthermore, the OPC data concentration was uniformly increased by 20% across all particle sizes to address the deviation observed when comparing it with weighted filter samples (Chapter 2; table 2-1). Moreover, to ensure optimal comparability with filter samples, the aerosol probe was positioned in the open face filter housing without a filter element installed.

Gravimetric analysis based on weighed filter samples allowed for the detection of the "entire" blow-by aerosol, particularly particles larger than 10  $\mu\text{m}$ . For this analysis, an open face filter was developed, which incorporated a temperature sensor. The filter consisted of three layers of highly efficient glass fiber media followed by a stabilizing perforated metal plate. This entire filter setup was installed in a spare valve cover, as this setup was ideal for minimizing particle losses during the transfer of the aerosol from the crankcase to the filter. The filter loading time was set at 20 minutes with an airflow rate of 15 L/min. This duration was chosen to ensure that no oil was lost through drainage, and sampling was stopped well before the filter reached a steady state. Furthermore, the filter was loaded for a sufficient period to collect a significant amount of oil, which was approximately 0.2 g per sample. To ensure defined loading conditions, the filter was back-flushed with particle-free compressed air when not actively sampling. This feature was crucial in preventing filter loading during engine warm-up. Fig. 3-24

provides a schematic representation of the filter and photographs of the valve cover with the installed filter housing. The open face filter was positioned directly above an injector and a rocker arm.



**Figure 3-24:** A schematic representation of the open face filter (left) and a photograph of the filter installed in the valve cover of the Daimler OM 934 engine (right).

Fig. 3-25 shows the PSD of blow-by aerosols, obtained by combining results from EEPS, OPC, and filter measurements. At 1200 rpm and 0 Nm, the particle mass concentration of above  $0.56 \mu\text{m}$ , as measured by the OPC with all corrections applied, was  $197 \text{ mg/m}^3$ . The EEPS determined a mass concentration of  $6 \text{ mg/m}^3$  for particles below  $0.56 \mu\text{m}$ . The total gravimetric concentration across all particle sizes, averaged from two filter samples, was  $595 \text{ mg/m}^3$ , leading to a mass concentration of  $392 \text{ mg/m}^3$  for the size range above the OPC. (Since no size information is available from the filter sample, the PSD in that range is represented as flat, with an assumed upper size limit of  $100 \mu\text{m}$ .) Note also that concentrations in Fig. 3-25 are not absolute but normalized to the total concentration (i.e., the concentration from the filter sample).

These data clearly indicate that particles below  $0.5 \mu\text{m}$  contribute only minimally to the overall aerosol mass, particularly at low engine load. This agrees with results published by Scheiber et al. (2021), stating that the bulk of the mass is concentrated above  $0.4 \mu\text{m}$ . Fig. 3-25 also shows that approximately two thirds of the blow-by aerosol mass consist of particles larger than  $10 \mu\text{m}$ . Most of these large droplets originate from aerosol sources located in the upper crankcase region, specifically between the cylinder head

and the valve cover. This conclusion is supported by previous findings indicating that the separation efficiency of the riser ducts starts becoming significant for particles larger than 10  $\mu\text{m}$  (refer to Section 3.4).

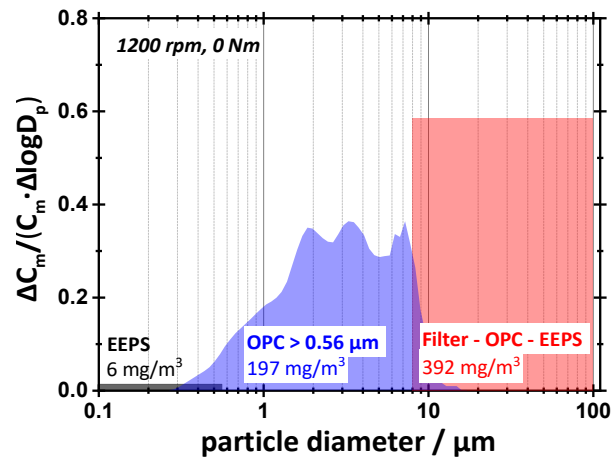


**Figure 3-25:** Normalized blow-by aerosol mass concentration vs. particle size obtained from the OM934 engine operated at 1200 rpm and zero torque. The vertical axis in this representation is non-dimensional.

Moreover, it is crucial to note the detection of a local spray field on the filter media, as shown in Fig. 3-26 (right). This observation suggests that the movement of components such as the camshafts, valve spring cover, and rocker arms generates splash oil, which is a significant source of coarse aerosol. Identifying these sources of splash oil is valuable when determining the optimal location for crankcase ventilation. This is because splash oil creates wall flows that can reach the oil mist filter. The presence of additional oil in the filter would result in increased pressure drop, decreased separation efficiency, and reduced filter lifespan.

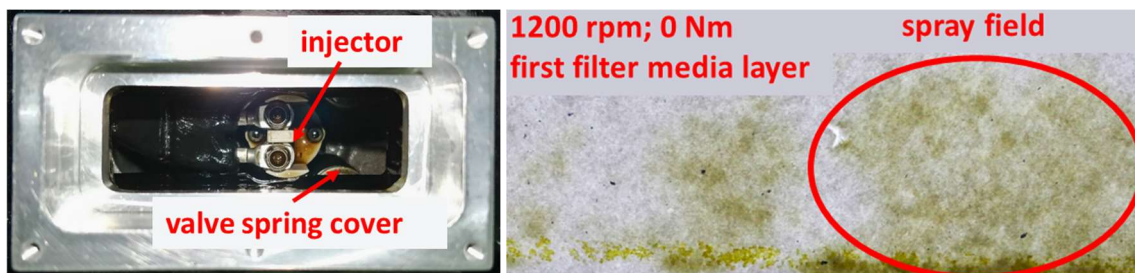


**Figure 3-26:** The photograph (left) displays the components of the Daimler OM934 engine situated directly beneath the open face filter. The photograph (right) captures the first layer of the filter media after it has been loaded with aerosol for 20 minutes at 1200 rpm and 0 Nm.

## 3.7 References

- Delvigne T. (2010). Oil Consumption Sources in a Modern Gasoline Engine Including Contribution of Blow-by Separator and Turbocharger: An Experimental Study Based on the Use of Radiotracers. SAE Technical Paper 2010-01-2256.
- Hinds, W.C. (1999). *Aerosol Technology. Properties, Behavior, and Measurement of Airborne Particles* (2nd ed.). Wiley-Interscience: s.l.
- Lorenz, M., Koch, T., Kasper, G., Pfeil, J., Nowak, N. (2020). Origin and Separation of Submicron Oil Aerosol Particles in the Blow-by of a Heavy-Duty Diesel Engine. SAE Int. Journal of Engines, 13, 363-375.
- Michler, T., Dörnhöfer, J., Erforth, D., Heinz, A., Erforth, D., Heinz, A., Scheiber, K., Weber, P., Nowak, N., Kubach, H., Meyer, J., Koch, T., Dittler, A. (2019). Comparison of Different Particle Measurement Techniques at a Heavy-Duty Diesel Engine Test Bed, SAE Technical Paper 2019-24-0158.
- Scheiber, K., Nowak, N., Pfeil, J., Koch, T., Kasper, G. (2021). Comparison of four diesel engines with regard to blow-by aerosol properties as a basis for reduction strategies based on engine design and operation, AAET, 6, 79–90.



## 4 On blow-by aerosol sources in a single-cylinder crankcase environment

The content of this chapter has been taken from the following publication, which received the best paper award in the track “Powertrain and Emissions Systems”:

Nowak, N., Scheiber, K., Stieler, C., Heller, M.T., Pfeil, J., Koch, T., Kasper, G. (2021). *On Blow-by Aerosol Sources in a Single-Cylinder Crankcase Environment*. Proceedings of the ASME 2021 Internal Combustion Engine Division Fall Technical Conference. <https://doi.org/10.1115/ICEF2021-70947>. © 2021 by ASME.

### 4.1 Abstract

Crankcase aerosol contributes to the particulate matter (PM) emissions of combustion engines equipped with an open crankcase ventilation system. In case of closed crankcase ventilation, the aerosol forms deposits that diminish engine efficiency, performance, and reliability. Such issues are best avoided by highly efficient filters combined with in-engine reduction strategies based on a quantitative understanding of aerosol sources and formation mechanisms in a crankcase environment. This paper reports key findings from a study of aerosol size spectra in the range of 0.01  $\mu\text{m}$  to 10  $\mu\text{m}$  obtained from a 1.3-L single-cylinder engine under well-defined conditions.

Supermicron particles were formed mainly by cooling jet break-up when the piston was positioned in TDC, while at BDC aerosol generation decreased by about 90 % because the oil jet was short and thus stable. Motoring the engine yielded an additional peak around 0.7  $\mu\text{m}$ . It is associated with oil atomization at the piston rings and increased strongly with cylinder peak pressure. No significant contribution of the bearings could be identified at peak pressures below 116 bar. Engine speed had only a minor effect on aerosol properties. Operating the engine in fired mode increased the submicron aerosol concentration substantially, presumably because high(er) peak pressures boost aerosol

generation at the piston rings, and because additional particles may have formed from recondensing oil vapor generated at hotspots. Soot or ash aerosols could not be identified in the crankcase aerosol, because they may have been integrated into the bulk oil.

## 4.2 Introduction

Crankcase aerosol emissions are an undesirable by-product when operating combustion engines. While the emissions from an open crankcase ventilation (OCV) directly pollute the environment, aerosols from closed crankcase ventilation (CCV) systems form deposits on e.g., turbocharger, sensors, and intercooler. These deposits decrease engine efficiency, performance, and reliability. Also, unburned constituents of the aerosol form soot and ash that plug the exhaust gas aftertreatment system.

It is common practice to remove undesirable aerosols by efficient separators such as particle filters but preventing their formation in the first place should be a complementing and more sustainable approach to such issues. In the context of crankcase aerosols this involves the identification of relevant sources to develop in-engine reduction strategies based on the optimization of engine design, process parameters, and operating fluids.

Potential aerosol sources in the crankcase environment require both, liquid oil from which to form particles, and a gas flow to transport these particles out of the engine [1]. The latter is provided by the blow-by that is the sum of all leakage flows that reach the crankcase past piston rings, turbocharger seals, and valve stems. Liquid oil is provided by the lubricating circuit that supplies bearings and cooling nozzles with fluid, engine components predestined to act as aerosol generators. Beyond that, any oil wetted surface can become a droplet source when exposed to sufficient kinetic energy by rotatory (e.g., camshaft, crankshaft, and gears) or quasi-linear motion (e.g., pistons and valves), or by intense shear (e.g., piston rings). Aside from the mechanical atomization and en-

trainment of liquid, re-condensation of supersaturated oil vapor represents another important pathway to the formation of fresh crankcase aerosol or the growth of pre-existing nuclei.

Aerosol generation is influenced by oil properties (e.g., viscosity and volatility) as well as process parameters (e.g., oil temperature, brake mean effective pressure (BMEP), and engine speed) and of course also by engine design aspects. The multitude of parameters and several cross dependencies make it generally difficult to trace back the contribution of a specific source to the over-all crankcase aerosol particle size distribution (PSD) measured somewhere far downstream.

Most crankcase aerosol data published in recent years [2-7] present such global data measured downstream. They give only limited and mostly indirect insights into specific source strengths and spectral characteristics but provide valuable information about global system behavior. For example, it has been shown for diesel engines [5] that the mass concentration of micrometer sized crankcase aerosol (0.4  $\mu\text{m}$  to 1.3  $\mu\text{m}$  to be specific) rises exponentially with engine load, while variations of engine speed have a minor effect on the concentration. This suggests that aerosol generation is influenced strongly by oil temperature and BMEP but less by the motion of engine components.

Lorenz et al. [6] report that the turbocharger contribution to the crankcase aerosol concentration was generally modest, at 21 % or less for an 11-L 6-cylinder engine. However, the turbocharger plays a role also as an important contributor to the blow-by flow (up to  $\sim 40$  %) and, hence, to the aerosol mass rate. Aside from the turbocharger, other specific aerosol sources within the crankcase environment are not discussed in literature. This niche is where we propose to give novel insights.

Experiments were performed on a 1.3-L single-cylinder diesel engine installed on a test bench. The setup permitted variations of boost pressure and independent control of the oil temperatures for different components such as cooling jet nozzle and bearings. It was thus possible to adjust these parameters to study their effect on the crankcase aerosol size spectrum.

Experimental results are presented in three steps. First, the engine is static, and aerosol is only generated by the cooling jet. Second, the engine is motored at various speeds and externally provided boost pressures. Additionally, the local oil temperature is varied to estimate the contribution of individual sources (moving components, bearings, and piston rings) to the total aerosol. Finally, the engine is fired to investigate the role of combustion, soot, and ash on the crankcase aerosol.

Aerosol data were acquired in the range of 0.01  $\mu\text{m}$  to about 10  $\mu\text{m}$ . The aerosol below 0.4  $\mu\text{m}$  was characterized with an engine exhaust particle sizer (EEPS), above 0.4  $\mu\text{m}$  by an optical particle counter (OPC). Both instruments provide highly resolved number size distributions which can be converted accurately to particle mass. Measuring procedures were adopted from [5 and 7] to ensure robust results.

### **4.3 Materials and methods**

This section describes the methods of aerosol characterization and the sampling conditions. It then introduces the single-cylinder research engine and the test bench. It concludes with details on the experimental strategy used to characterize individual aerosol sources in the crankcase environment.

#### ***Characterization of crankcase aerosols***

Aerosol was characterized by two spectrometers that are commercially available. The Optical Particle Counter (OPC; Promo 2000 HP with the Welas 2070 H sensor, by Palas GmbH) characterizes airborne particles individually on the basis of scattered light intensity as they move through a sensing volume. Nominally the OPC detects and counts particles ranging in diameter from 0.3  $\mu\text{m}$  to 17  $\mu\text{m}$  at number concentrations  $<10^6$  per cubic centimeter with a resolution of 32 channels per decade. The complete PSD is refreshed at the rate of 1 Hz. The device offers choices of particle refractive index. Here it was set to 1.47 (paraffin oil), which closely matches the value for engine oil [7]. The bulk density of engine oil (874  $\text{kg}/\text{m}^3$ ) was used for converting particle number to mass.

Where needed, the measuring range of the OPC was extended down to about  $0.01 \mu\text{m}$  by an Engine Exhaust Particle Sizer (EEPS; Model 3090 by TSI Inc.). The EEPS sizes and counts particles in the range of  $0.01 \mu\text{m}$  to  $0.56 \mu\text{m}$  at concentrations of up to  $10^7$  per cubic centimeter on the basis of their electrical mobility with a frequency of 10 Hz and a resolution of 16 channels per decade. Although commonly used to characterize fractal aerosols in tailpipe emissions, this device also offers a calibration option suitable for compact and spherical particles, which was used here for our oily crankcase aerosol.

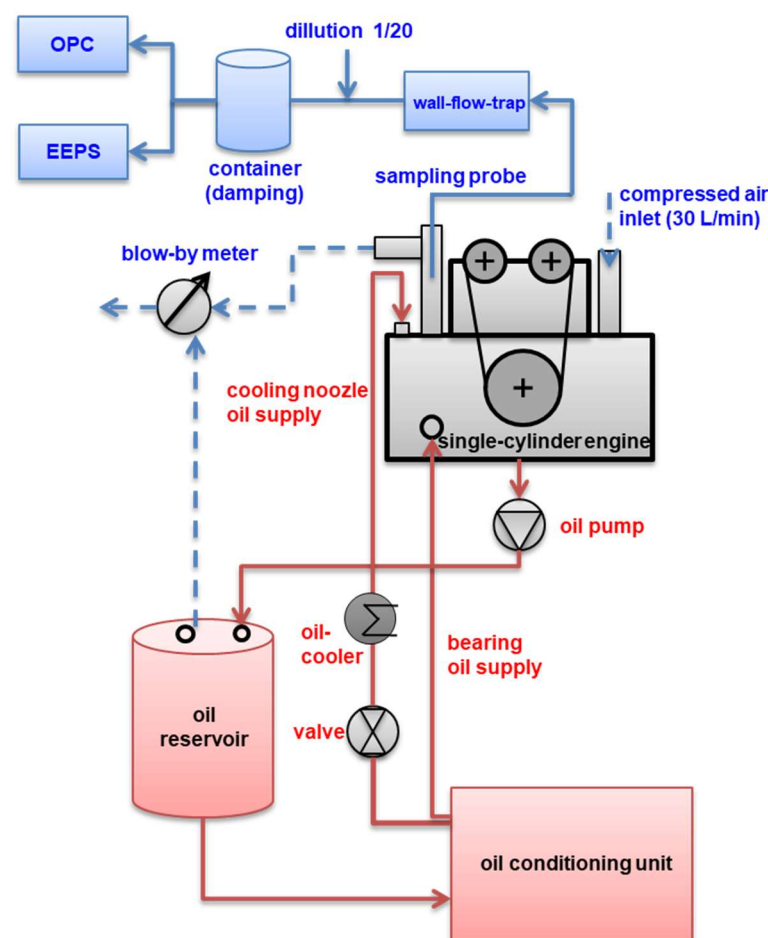


**Figure 4-1:** Schematic of the setup for aerosol measurements and the cooling oil circuit of the single-cylinder engine.

All aerosol data presented in this study refer to a gas temperature of  $21.1 \text{ }^\circ\text{C}$  and a pressure of 1013 mbar. Each measurement was conducted for at least 5 min to ensure representative and robust results.

During all experiments, a constant airflow of 30 L/min (at 20 °C), was fed into the crankcase to flush out aerosol in static operation and keep similar flow conditions for motored and fired operation. Well-defined flow conditions are a pre-requisite for obtaining meaningful aerosol data as the airflow affects aerosol transport, losses, and dilution.

Aerosol was sampled at the entrance of the crankcase ventilation system with an 8 mm sharp-edged probe facing the incoming aerosol flow (Fig. 4-1). It was then diluted with particle free compressed air at a constant ratio of 1:20. A wall-flow trap was installed to prevent oil from entering the spectrometers. In this device, aerosol is transferred from the inlet of a pipe to a coaxial steel probe. The wall-flow is separated as it only wets the surface of the pipe and finally accumulates in a piece of tubing that serves as an oil reservoir. The single-cylinder engine crankcase is characterized by intense pressure pulsations induced by the movement of just one piston. To prevent measuring artifacts from such a pulsatile flow, a 30 L container was installed just upstream of the aerosol spectrometers to dampen the flow.

Measuring artifacts have to be taken into account in case of the broad aerosol distribution present in the crankcase of combustion engines, which ranges from a few nanometers to hundreds of microns. Inertial impaction in the sampling and dilution system reduces the concentration of particles  $>2 \mu\text{m}$ , so that their concentration is underestimated by the aerosol spectrometers. Also, diffusional losses, thermophoretic losses, and condensation effects are known to affect the properties of particles  $<0.1 \mu\text{m}$ . However, these particles only have a minor contribution to the total blow-by aerosol mass concentration. Thus, their influence on the distributions is expected to be negligible. The intermediate range between  $0.1 \mu\text{m}$  and  $2.0 \mu\text{m}$  is expected to be in very good agreement with the actual aerosol in the crankcase.

### ***Engine and test bench properties***

The study is based on a single-cylinder diesel engine laid out specifically for research purposes to emulate one cylinder of a commercial medium-duty four-cylinder engine, with identical geometries for the piston, cylinder, and piston rings. Relevant engine specifications are listed in Tab. 4-1:

**Table 4-1:** Engine specifications:

<b>cylinders</b>	1
<b>displacement</b>	1.3 L
<b>compression ratio</b>	1:17
<b>bore</b>	110 mm
<b>oil type</b>	15W-40

The single-cylinder engine was equipped with low- and high-pressure indication to monitor the cylinder pressure, an important driver for oil atomization at the piston rings. The engine was not equipped with a turbocharger. Boost pressure was supplied by an external air compressor unit. Furthermore, the test bench featured an AVL blow-by meter and analysis options for the tailpipe emission composition, including an AVL AMA4000 and an AVL 415S Smoke Meter. The test bench was also equipped with a dedicated unit for conditioning the lubricant oil to control the oil temperature and pressure at the cooling jet nozzle separately from that at the bearings and independently from engine operation. Amongst other advantages, this feature enables novel strategies for aerosol source characterization addressed below.

### ***Experimental strategy to isolate individual aerosol sources within the crankcase***

Fig. 4-2 resents four potentially important sources of crankcase aerosol, based either on mechanical atomization processes (cooling nozzle, piston rings, and bearings) or on the condensation of oil vapor generated at hotspots. The contribution of these sources as

well as from the main bearings, the valves, the crankshaft, and the camshaft are analyzed by an experimental approach that includes static, motored, and fired engine operation.

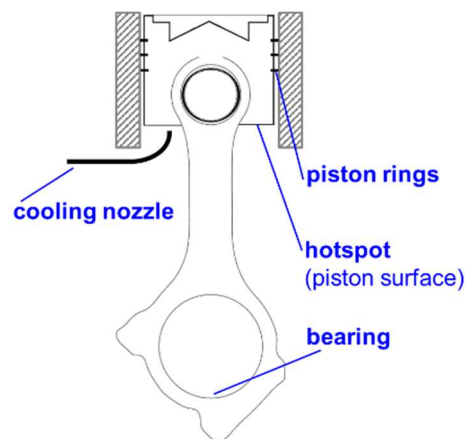


**Figure 4-2:** Aerosol sources in a single piston environment.

In static mode, the cooling nozzle was supplied with oil at 80 °C and an absolute pressure of either 2.6 bar or 4.6 bar. The piston was positioned manually, either at TDC or at BDC to study the effects of length and speed of the oil jet, and thus of its break-up, on aerosol formation. Jet break-up is also affected by the motion of the piston, as shown by experiments with a motored engine. Moreover, motored operation was used to evaluate the effect of various engine speeds and peak pressures on the crankcase aerosol. By additionally controlling the oil temperature at the bearings and the cooling nozzle (see Fig. 4-1), the contribution of selected sources including the piston rings, bearings, and moving components was estimated. This evaluation was based on the thought that the oil viscosity will be a major parameter for oil aerosol generation by mechanical means. Typically, the larger the viscosity, the less aerosol formation is to be expected [8].

Aerosol generation by condensation of oil vapor can be ruled out for static or motored operation because the oil temperature did not exceed 80 °C and in the absence of combustion there are no hotspots. Also, for the same reasons soot and ash are not generated in these operating modes. In fired mode, the peak pressure increases. Aerosol generation at the piston rings and bearings is therefore expected to rise. Additionally, hot

spot temperatures of oil wetted surfaces may rise, thereby increasing the oil vapor concentration locally, potentially leading to condensation effects. Also, the influence of soot and ash was investigated by varying the filter smoke number (FSN) in the range of 0.3 to 2.0.

**Table 4-2:** Overview on the experimental conditions used to obtain information on aerosol sources:

aerosol source	engine operation	engine speed	peak pressure	oil prop. cooling jet
cooling jet	static	0 rpm	0 bar	2.6 bar 4.6 bar 80 °C
cooling jet	motored	1200 rpm	39 bar	2.6 bar 4.6 bar 80 °C
moving components	motored	1200 rpm to 1800 rpm	39 bar	2.6 bar 80 °C
piston rings vs. bearings	motored	1800 rpm	39 bar to 116 bar	2.6 bar 80 °C 50 °C
piston rings bearings hotspots	fired	1800 rpm	100 bar to 183 bar	2.6 bar 80 °C
soot + ash	fired	1800 rpm	140 bar	2.6 bar 80 °C

Tab. 4-2 summarizes potential aerosol sources and the experimental conditions used to estimate their respective contributions. Note that the oil pressure at the bearings was always 5.2 bar and the oil temperature was only changed from 80 °C to 50 °C during the motored “piston rings vs. bearings” experiments.

## 4.4 Results and discussion

This section presents crankcase aerosol data and discusses them with a focus on the contribution of specific sources to the mass-based PSD. Basing the PSD on mass rather than particle number concentration brings the results closer to PM type emission data

and is also relevant for aerosol deposits on critical components such as the turbo-charger. PSD data are presented in terms of a normalized mass concentration on a log scale, i.e., for each size interval the concentration is divided by the logarithmic width of the size class, to account for the different resolutions of the aerosol spectrometers. The experiments are presented in the order of rising complexity (increasing number of active aerosol sources). Thus, first static, then motored, and finally fired experiments are discussed.

### ***Cooling jet – static vs. motored operation***

Fig. 4-3 presents crankcase aerosol data obtained by OPC from the static engine. Oil was fed to the cooling nozzle from an external conditioning unit with pressures of either 2.6 bar (black dashed) or 4.6 bar (blue dashed) while the piston is positioned in TDC. It also shows data obtained with the piston in BDC and oil at 4.6 bar (red dashed).

Evidently, the cooling nozzle is a source of mostly super-micron particles when it is provided with sufficient oil pressure and enough distance between the nozzle and the surface of the piston. Note however that the concentration peak located at 2  $\mu\text{m}$  may not be entirely characteristic of the cooling nozzle but rather the result of inertial particle losses in the sampling and dilution system. When the length of the oil jet is minimized by moving the piston from TDC to the BDC, or when the oil pressure / oil jet speed is decreased, the break-up of the jet is reduced or even prevented. In the case shown here this reduces the aerosol generation by over 90 % (4.6 bar, TDC vs. BDC). These findings are not surprising as the theory on jet break-up and the Ohnesorge diagram predict a significant impact of jet speed on aerosol generation. Lower speeds extend the stable length of the oil jet before break-up because they reduce shearing forces between the liquid and the gaseous phase. Calculations indeed confirm that the break-up mode changes from atomization to wind induced break-up when reducing oil pressure from 4.6 bar to 2.6 bar. Aside from jet break-up, its impact onto the piston surface does not form a significant amount of additional aerosol, nor do the bearings which are also supplied with oil during these static experiments.

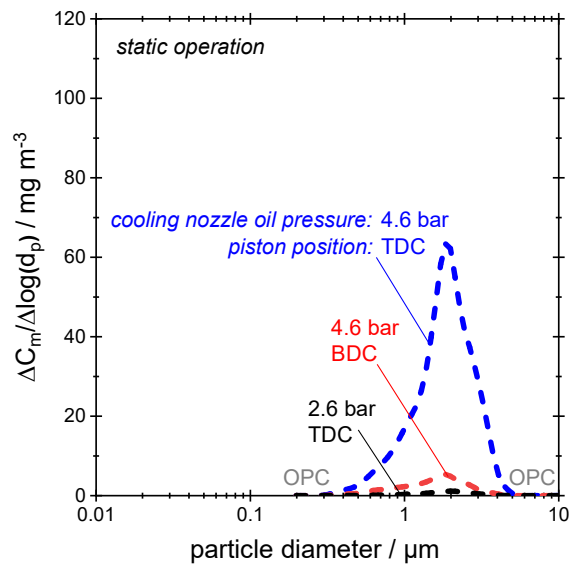


**Figure 4-3:** Aerosol produced by the cooling jet in the static engine.

Fig. 4-4 compares the static engine with data for motored operation. The cylinder is run at 1200 rpm without additional boost pressure (peak pressure of 39 bar); the cooling nozzle is supplied with either 4.6 bar (blue) or 2.6 bar (black). The figure shows that motoring the engine reduces the concentration of larger droplets and increases the sub-micron mode around 0.5  $\mu\text{m}$ . The effect is not large but significant. The decrease on the large end of the PSD is due to enhanced jet break-up by the moving piston. The slight increase in the submicron range is likely to result at least in part from the activation of additional aerosol sources by the moving engine (e.g., piston rings, shafts, and bearings). In contrast to the static engine, changing the nozzle pressure has practically no effect on concentration or shape of the PSD. Jet break-up is either dominated by the interaction with the moving piston, or the cooling nozzle aerosol contributes negligibly compared to other aerosol sources that are activated in motored operation.

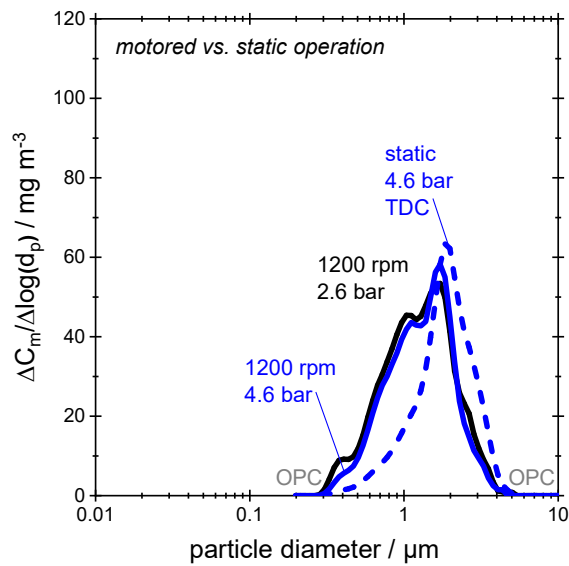


**Figure 4-4:** Crankcase aerosol from static engine compared to motored operation at 1200 rpm.

#### ***Moving components – motored operation***

The effect of engine speed on the crankcase aerosol is shown in Fig. 4-5 (OPC and EEPS combined). The engine is motored at 1200 rpm (blue), 1500 rpm (black), or 1800 rpm (red) with the boost pressure set to 1 bar to ensure similar peak pressures. This makes the stress on bearings and piston rings comparable, so that changes in crankcase aerosol properties can be associated explicitly with moving engine components (e.g., shafts, valves, and piston).

The aerosol concentration below 0.5  $\mu\text{m}$  increases slightly with speed, presumably because more kinetic energy becomes available, and part of this energy is converted to additional surface area of small particles. The concentration of super-micron particles does not change noticeably from 1200 rpm to 1800 rpm. Overall, the effect of engine speed on crankcase aerosol properties is therefore rather small. Aerosol mass flow rates (not shown) are thus also little affected by engine speed because the total blow-by flow changes by less than 10 %.

Fig. 4-5 also contains information about the consistency of the aerosol properties that was generally very good and is shown here in detail for the 1800 rpm data. The error

bars represent the standard deviation of three consecutive measurements of 5 minutes each.

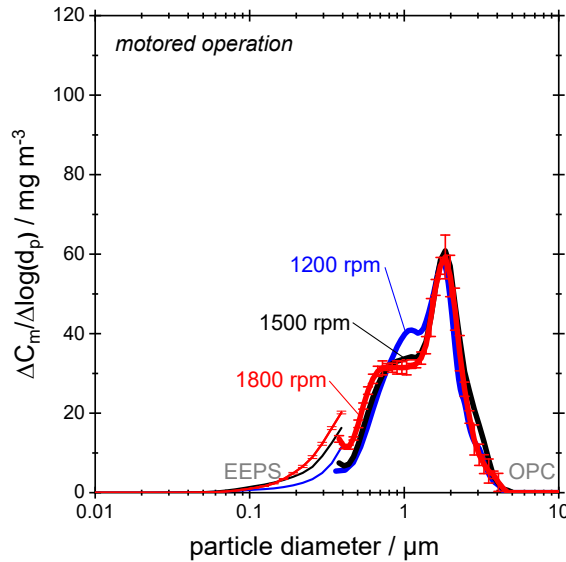


**Figure 4-5:** Effect of engine speed on crankcase aerosol in motored operation.

#### ***Piston rings vs. bearings – motored operation***

Fig. 4-6 presents similar measurements as before in Fig. 4-5 (OPC and EEPS combined) for the engine motored at 1800 rpm, but the boost pressure is now increased in steps from 1 bar (blue) to 2 bar (black) to 3 bar (red), resulting in peak pressures of 39 bar, 76 bar and 116 bar, respectively. Oil temperatures were conditioned to 80 °C for both cooling nozzle and bearings (solid lines); 50 °C for cooling nozzle and 80 °C for bearings (dashed lines); or 50 °C for both cooling nozzle and bearings (dotted lines).

All aerosol size spectra in Fig. 6 exhibit a global maximum at 2 μm that drops off sharply towards larger particles due to losses in the sampling and dilution system. This 2 μm mode is known from further-reaching crankcase aerosol data to be associated with satellite drops arising from oil jet / sheet break-up [7]. When the peak pressure is increased from 39 bar to 116 bar (with oil at 80 °C) the aerosol concentration doubles, and the aerosol flow mass rate (not shown) even triples as the gas flow rises by 50 %. Also, with

increasing peak pressure the shape of the particle size distribution changes as a second mode appears around 0.7  $\mu\text{m}$ .

To distinguish whether this 0.7  $\mu\text{m}$  mode has its origin in oil atomization at the piston rings or at the bearings, the respective oil temperatures were varied separately from each other. When only reducing the oil temperature at the cooling nozzle from 80  $^{\circ}\text{C}$  to 50  $^{\circ}\text{C}$  and thereby also lowering the temperature at the piston rings, aerosol concentration at 0.7  $\mu\text{m}$  decreases notably by up to 33 %. However, when additionally reducing the oil temperature at the bearings from 80  $^{\circ}\text{C}$  to 50  $^{\circ}\text{C}$ , concentrations do not decrease any further.

This is a clear indication that the piston rings are an important contributor to the crankcase aerosol while the bearings are not. The results also point to an effective reduction strategy for crankcase aerosol based on lowering the temperatures in the vicinity of the piston rings, for example via the oil temperature of the cooling jet.

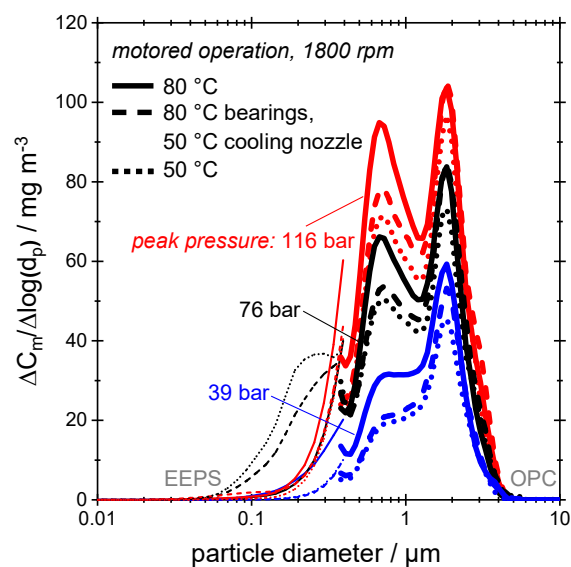


**Figure 4-6:** Effects of peak pressure and oil temperature on aerosol generation by piston rings vs. bearings at 1800 rpm in motored operation.

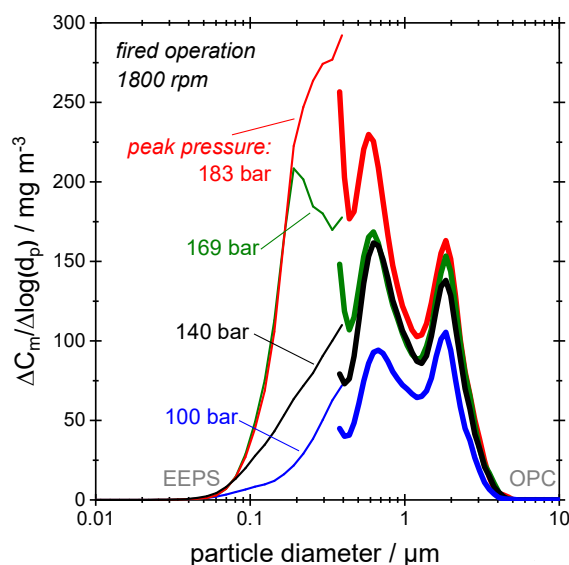
***Piston rings, bearings, and hotspots – fired operation***

Fig. 4-7 presents crankcase aerosol data obtained from the fired engine at 1800 rpm. The engine load was adjusted to 25 %, 50 %, 75 %, and 100 %. These loads correspond to peak pressures of 100 bar (blue), 140 bar (black), 169 bar (green), and 183 bar (red), respectively.

Fired engine operation resulted in similar modal positions as in the motored case, namely the satellite drop mode around 2  $\mu\text{m}$  and the mode around 0.6  $\mu\text{m}$  to 0.7  $\mu\text{m}$  associated with the piston rings. Indeed, particle size distributions agree remarkably well between fired and motored operation for similar peak pressures. This is best seen when comparing the 116 bar motored with 100 bar fired. (Note the different ordinate scales of Fig. 4-6 and Fig. 4-7).

As expected from the trend observed with the motored experiments, the higher peak pressures in fired operation (up to 183 bar) further boost submicron aerosol concentration. However, fired operation does not only increase peak pressure and the stress on the bearings; it also increases the temperature of oil wetted surfaces, thereby increasing the oil vapor concentration and the potential production of submicron condensation aerosol upon cool-down. Newly formed condensation aerosol may explain the additional mode emerging around 0.2  $\mu\text{m}$  to 0.3  $\mu\text{m}$  at the highest loads of 75 % and 100 %.

In addition, the combustion process gives rise to soot and ash. However, these particles do not enter the crankcase as a distinct aerosol, as we show in the following experiments.



**Figure 4-7:** Effects of peak pressure on aerosol generation by piston rings, bearings, and hotspots at 1800 rpm in fired operation.

### ***Soot and ash – fired operation***

The filter smoke number (FSN) was varied in three steps from 0.3 (blue), to 1.3 (black), to 2.0 (red) by changing combustion parameters including the exhaust gas recirculation. To avoid any cross-influences due to other aerosol sources the peak pressure was maintained stable at 140 bar (50 % load); the engine speed was 1800 rpm. Fig. 4-8 shows the effect of a changing soot concentration on the blow-by aerosol.

Increasing the FSN from 0.3 to 2.0 amounts to a tenfold increase in soot mass concentration in the exhaust gas (10 mg/m<sup>3</sup> vs. 100 mg/m<sup>3</sup>), but without any direct effect on the crankcase aerosol PSD. The three PSDs overlap almost perfectly, each with a total aerosol concentration of approximately 150 mg/m<sup>3</sup>. No separate soot peak is visible to suggest the formation of an accumulation mode below 100 nm typical for such particles [9]. We must therefore conclude that soot did not enter - at least in an airborne state - the crankcase of that engine. Since traces of soot are detectable in the oil it must be assumed that soot and ash are integrated into the bulk oil flow as the blow-by gas passes the piston rings or valve stems.

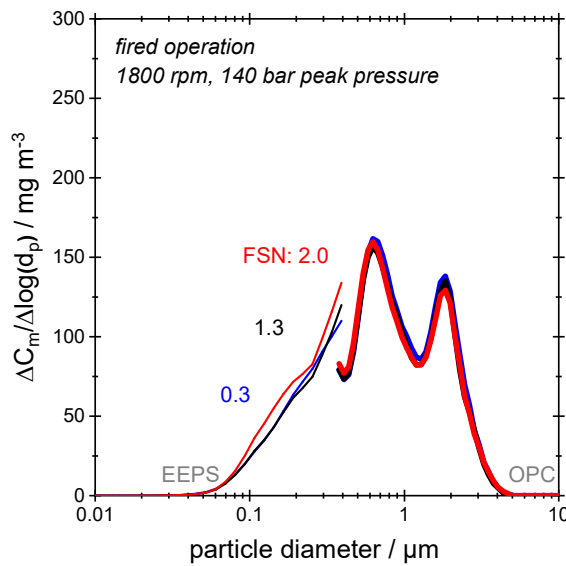


**Figure 4-8:** Effect of soot concentration on crankcase aerosol at 1800 rpm and constant peak pressure of 140 bar in fired operation.

## 4.5 Summary and conclusions

A comprehensive study on blow-by aerosol sources was conducted in a well-defined single-cylinder crankcase environment. Well-defined and recurring peaks in the mass-based droplet spectrum between 0.01  $\mu\text{m}$  and 10  $\mu\text{m}$  could be associated with specific sources of oil aerosol.

A super-micron mode around 2  $\mu\text{m}$  was always present, regardless of whether the engine was static, motored or fired, and associated with satellite drop formation during the break-up of the colling jet. A mode around 0.6  $\mu\text{m}$  to 0.8  $\mu\text{m}$  emerged and grew with increasing peak pressure, both in the motored or fired mode. This peak can be associated with the piston rings; bearings did not appear to contribute significantly to the aerosol. A third peak emerged in the fired engine at loads of 75 % and above and may be associated with the re-condensation of oil vapor generated at engine hotspots. Soot and ash did not form distinct modes in the aerosol PSD, presumably because such particles are integrated into the bulk oil.

An effective reduction strategy for submicron aerosol should focus primarily on the piston rings that have proven to be the most important contributor to the submicron crankcase aerosol. One option in that regard is to improve cooling of the piston, e.g., by lowering the oil temperature of the cooling jet. Reducing the oil temperature of the cooling jet from 80 °C to 50 °C (in the motored mode) lead to a reduction of up to 33% in mass emissions, mainly in the 0.7 µm mode. Aside from piston ring design, the oil properties (mainly viscosity and volatility) are important factors that must be considered in future optimization strategies.

## **4.6 Acknowledgements**

The authors gratefully acknowledge the financial and technical support from Daimler Truck AG, Liebherr-International S.A., MAHLE GmbH, MTU Friedrichshafen GmbH, and UT99 AG, members of the Engine Crankcase Emissions Consortium at the KIT.

## **4.7 UT99 AG**

UT99 is a Swiss manufacturer of high-performance oil mist separators for open and closed crankcase ventilation. UT99 solutions are the industry-standard for large ship, gas, and dual-fuel engines. Systems are available for crankcase flows between 15 m<sup>3</sup>/h and 1050 m<sup>3</sup>/h. UT99 oil mist separators are characterized by a low pressure drop, high efficiency, and a variety of customer-specific options. UT99 is market leader and specialist for the equipment of combined heat and power plants (CHP), whose gas engine - whether operated with natural gas, biogas, or other special gases - benefits considerably from UT99 oil mist separators. UT99 also has extensive know-how and many years of experience in the field of lube oil tank ventilation of turbine bearings in power generation.

## 4.8 References

- [1] Sauter, H.L.; Trautmann, P., Messung und Abscheidung von Ölnabelaerosolen aus der Kurbelgehäuseentlüftung von Verbrennungsmotoren, *MTZ Motortech. Z.* 61 (12), 2000
- [2] Tatli, E., Clark, N., Crankcase Particulate Emissions from Diesel Engines, *SAE Int. J. Fuels Lubr.* 1 (1), 2008
- [3] Johnson, B.T., Hargrave, G.K., Reid, B., Page, V.J., Crankcase Sampling of PM from a Fired and Motored Compression Ignition Engine, *SAE Int. J. Engines* 2 (4), 2011
- [4] Johnson, B.T., Hargrave, G.K., Reid, B., Page, V.J., Wagstaff, S., Optical Analysis and Measurement of Crankcase Lubricant Oil Atomisation, *SAE Int. J. Engines* 2 (4), 2012
- [5] Scheiber, K., Nowak, N., Lorenz, M.-L., Pfeil, J., Koch, T., Kasper, G., Comparison of four diesel engines with regard to blow-by aerosol properties as a basis for reduction strategies based on engine design and operation. *AAET*, 2021
- [6] Lorenz, M.-L., Koch, T., Kasper, G., Pfeil, J., Nowak, N., Origin and Separation of Sub-micron Oil Aerosol Particles in the Blow-by of a Heavy-Duty Diesel Engine, *SAE Int. J. Engines* 13 (3), 2020
- [7] Nowak, N., Scheiber, K., Pfeil, J., Meyer, J., Dittler, A., Koch, T., Kasper, G., Sampling and conditioning of engine blow-by aerosols for representative measurements by optical particle counters, *Journal of Aerosol Science* 148 (2), 2020
- [8] Ohnesorge, W.V., Die Bildung von Tropfen an Düsen und die Auflösung flüssiger Strahlen, *Z. angew. Math. Mech.* 16 (6), 1936
- [9] Burtscher, H., Physical characterization of particulate emissions from diesel engines, *Journal of Aerosol Science* 7 (36), 2005



# 5 On aerosol formation by condensation of oil vapor in the crankcase of combustion engines

The content of this chapter has been taken from:

Nowak, N., Sinn, T., Scheiber, K., Straube, C., Pfeil, J., Meyer, J., Koch, T., Kasper, G., Dittler, A. (2021) *On aerosol formation by condensation of oil vapor in the crankcase of combustion engines*. *Aerosol Science and Technology*, 56 (2), 101–116. <https://doi.org/10.1080/02786826.2021.1976720>

## 5.1 Abstract

The crankcase of combustion engines is a source of undesirable oil vapor and oily aerosols. The roles of nucleation and growth by vapor condensation in their formation (with and without pre-existing nuclei) were investigated both experimentally and by one-dimensional simulation under engine-like conditions using actual motor oil as well as hexadecane. Initial equilibrium saturation levels (at  $T_{\text{sat}} = 100\text{ °C}$  to  $130\text{ °C}$ ) were known and well defined; cooling took place in laminar tube flow at a defined rate.

Nucleation and growth of pre-existing nuclei lead to separate peaks around  $0.25 \pm 0.1\text{ }\mu\text{m}$  and  $0.7 \pm 0.2\text{ }\mu\text{m}$  respectively, that agree remarkably well with actual engine data. The position of the latter peak was quite insensitive to primary nuclei size in the range of  $0.04$  to  $0.2\text{ }\mu\text{m}$ . Increasing either the vapor concentration (via a more volatile oil or higher  $T_{\text{sat}}$ ) or decreasing the cooling rate lead to slightly larger nucleation peaks ( $0.15 \rightarrow 0.35\text{ }\mu\text{m}$ ) but significantly lower peak concentrations (10x). Although counter-intuitive at first, this is explainable by shifts in supersaturation profile during cool-down.

Experiment and simulation limit spontaneous nucleation to pre-existing nuclei concentrations below about  $2$  to  $5 \times 10^5\text{ cm}^{-3}$  at engine oil temperatures  $\geq 100\text{ °C}$ . Significant

vapor losses to system walls during cool-down are an important factor in an actual engine environment as well as in the lab and must be included for realistic simulations. Losses affect actual number concentrations more than peak location.

## 5.2 Introduction

Aside from emissions through the tailpipe, which have been studied extensively (e.g. Kittelson, 1998; Harris & Maricq, 2001; Burtscher, 2005; Maricq, 2007), combustion engines are known also to emit vapors and aerosols from the crankcase, mostly in the form of oil (Sauter, 2004; Agarwal et al. 2011; Johnson, 2012; Ehteram et al. 2013). The crankcase ventilation system represents an important source of such aerosols. Unless they are treated by adequate means, these oily aerosols contribute significantly to the total emissions to the environment or, in case of engines equipped with a closed crankcase ventilation system (CCV), cause a variety of other problems (Xu, 2017; Lakshmanan et al., 2019). Currently, the most common approach is to remove such aerosols with an efficient particle separator (Golkarfard et al., 2019). Another, more sustainable approach is to develop in-engine strategies to reduce aerosol production at the source, based on an understanding of aerosol sources and formation mechanisms in that complex crankcase environment.

Vapor condensation during cool-down of the crankcase flow is mentioned frequently in the context of crankcase aerosol sources. However, the literature does not provide quantitative estimates for its importance or the size range where such aerosols might be found. The current paper addresses the likelihood and importance of heterogeneous or homogenous nucleation explicitly within the range of conditions found in a typical crankcase environment.

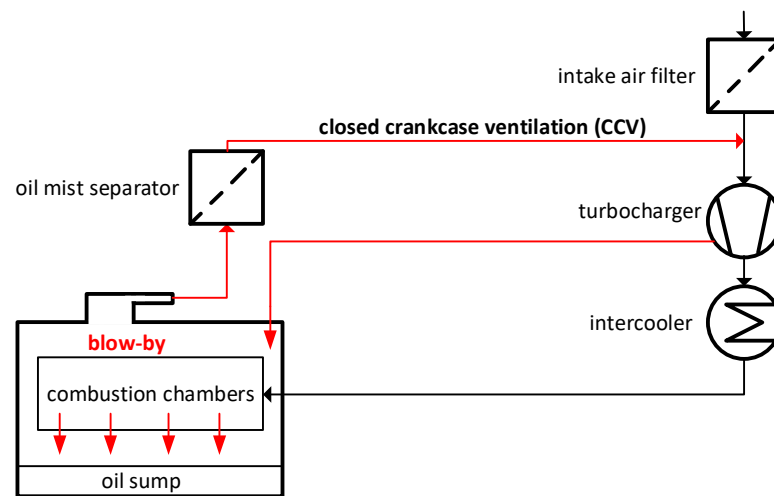


**Figure 5-1:** Schematic of a closed crankcase ventilation system (CCV). The blow-by flow (red arrows) contains oily aerosols. Their concentration is reduced by an oil mist separator before being vented to the intake stroke.

As in many other oil-lubricated machines, crankcase aerosols can arise from mechanical processes, e.g. fast-moving engine components such as shafts and rockers, or by atomization of oil ejected through nozzles (including bearing and piston ring gaps). But aerosol is thought to form also by condensation of oil vapor generated abundantly near engine hot-spots such as pistons or lubricated liners. This all the more as modern combustion engines are designed for increasingly higher power densities and bulk oil temperatures. At present however, there is only scant evidence regarding the true extent of the vapor contribution to the crankcase aerosol detected further downstream in much cooler regions of the engine.

Following well-established concepts of vapor-to-particle conversion, such aerosols may form by homogeneous nucleation and/or by vapor condensation onto pre-existing particles (including freshly nucleated oil droplets), causing their subsequent growth. According to classical theory the mechanisms and kinetics of nucleation and growth are very different, with spontaneous nucleation requiring much higher levels of supersaturation  $S$  than condensational growth, which can operate at levels barely above unity. If nucleation is relevant at all in a given system, it will therefore occur as an initial burst, while condensation takes over as soon as  $S$  relaxes ever so slightly and then carries on

until the vapor is sufficiently depleted by condensation onto aerosol or macroscopic surfaces.

Given that their kinetics and requirements are so very different, the repartition between the two effects must be highly dependent on local conditions, in our case within an engine. Key parameters include the initial amount of vapor available (which in turn depends on temperature and type of oil), the concentration and size range of pre-existing aerosol (e.g. soot from combustion, or fine oil droplets generated mechanically) as well as the mixing and cooling rate(s) further downstream. The body of studies on aerosol formation from condensable vapors by physical or chemical processes is vast, reaching back to the pioneering work of John Aitken in the 19th century (e.g. Fan et al., 2016; Kreidenweis et al., 2019). Unfortunately, the overwhelming majority of these studies concerns the atmosphere, which differs in almost all relevant aspects from those in an engine, including system composition and chemistry as well as the scales of time and space.

With regard to the role of condensation during the formation of crankcase aerosols, it would of course be best to consult the experimental evidence. Much of the published work on crankcase aerosols is concerned with testing the performance of abatement devices (e.g. Kissner et al. 2009) and thus not very helpful for our purposes. A few papers do however present size distribution information in the micron and submicron region of the aerosol spectrum originating mostly from the crankcases of fired or motored truck diesel engines (Tatli & Clark, 2009; Johnson et al., 2011; Lorenz et al., 2019; Nowak et al., 2020; Scheiber et al. AAET, 2021). These truly complex, multi-modal size spectra do not lend themselves to straightforward interpretation. When overlaid they nevertheless shown common features that provide useful clues as to their origin.

Above 1  $\mu\text{m}$ , the “typical” crankcase PSD shows two distinct size ranges: a very broad mode  $>10 \mu\text{m}$  (upward limited only by the measurement technique), and a fairly narrow, sharp satellite drop peak recurring around 2  $\mu\text{m}$  (Nowak et al., 2020) which is also found in re-entrainment spectra from oil mist filters (Wurster et al, 2017) as well as the output

from oil mist nebulizers (Sagot et al., 2017). The 2- $\mu\text{m}$  peak is not very pronounced when based on particle number (and thus sometimes overlooked) but very distinct when the PSD is based on mass. These super-micron peaks are certainly due to mechanical processes such as splashing, atomization, and the bursting of bubbles. This is also supported by the observation (Nowak et al., 2020) that they depend rather weakly on oil temperature (except via changes in oil viscosity) and vapor concentration.

Below the 1  $\mu\text{m}$  cut-off one typically identifies 3 distinct modal size ranges, one around 30 nm (sometimes also a bit higher but always  $<100$  nm), one around 130 - 300 nm, and one in the range of 600 - 900 nm (Tatli & Clark, 2009; Johnson et al., 2011; Lorenz et al., 2019; Nowak et al., 2020; Scheiber et al., 2021). These are indeed “signature modes” in the sense that they recur in many data sets, although with somewhat varying locations on the size axis and strongly varying intensities depending on engine design, engine load (and hence oil temperature and pressure) as well as other factors. Needless to say, some of these modes “appear” or “disappear” when switching between number and volume/mass distributions.

From among the submicron modes – where one would search primarily for signs of vapor condensation – the finest, in the range of a few tens of nanometers, is most likely due to particles from combustion, i.e. soot. It tends to increase dramatically with load and thus with mean effective pressure (Tatli & Clark, 2009; Johnson et al., 2011). Particles in that size range are predestined to serve as condensation nuclei, but it is not clear in which part of the spectrum they re-appear *after* cool-down and growth, and whether homogeneous nucleation can take place concurrently.

The search for clues of vapor to particle conversion effects must therefore concentrate on the region between about 0.1  $\mu\text{m}$  and 1  $\mu\text{m}$ . Lorentz et al. (2020) were the first to point out that both modes in that range are very sensitive to (bulk) oil temperature, with a roughly 50-fold increase in mass concentration between 35 °C and 105 °C. The sensitivity of micron and submicron size crankcase aerosols to oil temperature becomes even more apparent in Fig. 5-2. The figure represents a compilation of data from the same

medium-duty truck diesel engine used later on in this paper. The mass-based size PSD from this engine have a recurring pattern of peaks which permit a fractionation of aerosol mass into different size classes according to Fig. 5-2a. The respective aerosol mass concentrations are then plotted against bulk oil temperature in Fig. 5-2b. One notices the increasing response of oil concentration toward finer particles, and especially the abrupt increase beyond 115 °C where the submicron fraction appears to overtake the larger particles.

Nowak et al. (2020) found that, when cooling a mix of oil vapor and aerosol without adequate dilution, the 0.3  $\mu\text{m}$  peak in engine oil spectra tends to shrink in favor of the next larger peak. While this lends further support to the size interval between 0.1  $\mu\text{m}$  and 1  $\mu\text{m}$  as most interesting for condensation effects, it still leaves the question what condensation and nucleation have to do with these peaks, and whether spontaneous new particle formation can coexist with heterogenous growth under realistic engine-like conditions. The pursuit of this question is the principal topic of this paper

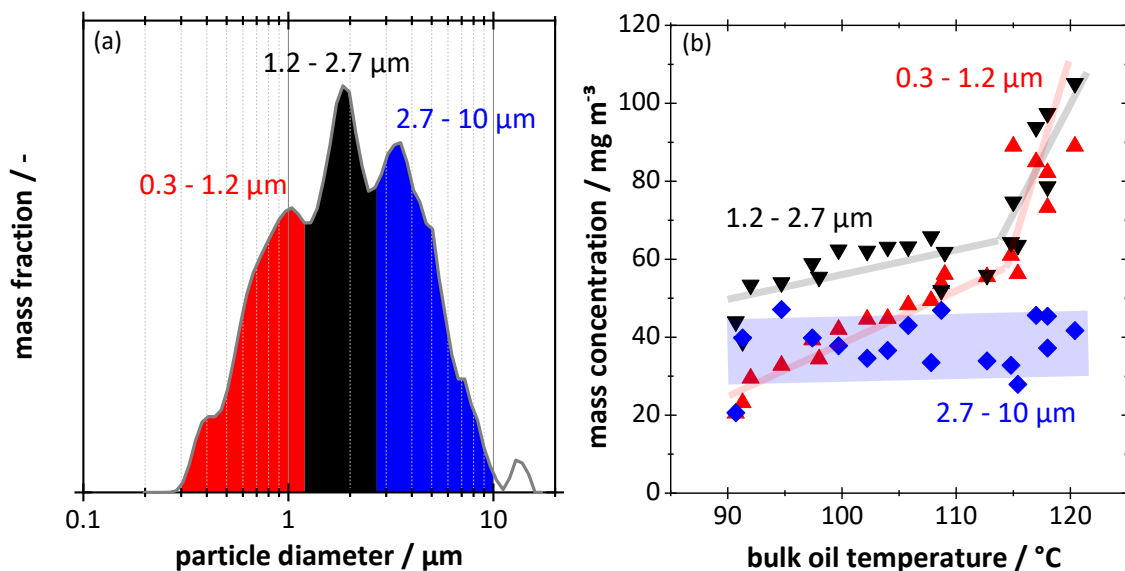


**Figure 5-2:** (a) - Typical crankcase aerosol size distribution to illustrate the choice of particle size ranges. (b) - Oil aerosol concentration vs. bulk oil temperature for three particle size intervals characteristic of crankcase aerosols. Data extracted from OPC measurements across a wide range of operating conditions for a medium duty 4-cylinder 5-Liter diesel engine. Lines inserted to guide the eye.

Since it is practically impossible to vary the relevant parameters independently of each other during operation of a fired (or even motored) engine, these conditions were emulated as closely as possible in a laboratory experiment with actual motor oil as well as hexadecane. Saturated air-vapor mixtures were generated from these liquids in a temperature range between 100 °C and 130 °C and then cooled down at known rates to near ambient, with and without pre-existing oil droplets. Size distributions were recorded by optical particle counter (OPC) in combination with electrical mobility measurements (SMPS) to detect homogeneous nucleation as well growth by condensation.

Separately, nucleation and growth were simulated numerically with a one-dimensional model (Winkelmann et al., 2014) based on classical nucleation theory (Becker and Döring, 1935) in combination with mass transfer by evaporation and condensation to droplets according to Friedlander (1977). The model was extended via MATLAB to deal with pre-existing condensation nuclei as well as multiple droplet size fractions generated along the cool-down tube used in the experiments. The simulations were validated first against the hexadecane experiments, and then used to study the parameter range where experiments are tedious such as cooling rate, vapor concentration, or oil surface tension. Equilibrium vapor data for hexadecane were taken from the literature; for actual motor oil they were measured in the temperature range of interest.

At first, we present GC data showing differences in hydrocarbon composition between sump oil and crankcase aerosol sampled during operation of a combustion engine. These data provide indirect evidence of significant fractionation effects due to evaporation and re-condensation at a high engine load.

### 5.3 Materials and methods

#### Engine characteristics - Composition analysis of submicron crankcase aerosol by GC

For the purpose of composition analysis, the predominantly submicron aerosol fraction was sampled from the crankcase of a 4-cylinder 5.1-liter medium duty diesel engine. The engine was installed on a test bench and operated at nominal power (170 kW, 730 Nm, 2200 rpm). This operating point provides for hot engine components and oil, conditions that boost oil evaporation and favor subsequent particle formation processes by condensation. Hence, it facilitates the identification of evidence for aerosols formed by the condensation of oil vapor. The engine oil used was Shell Rimula R6 LME (5W-30) pre-aged for several hours of medium to high power operation.

The schematic of Fig. 5-3a shows that a sample flow of 12.5 L/min was extracted from the engine with a sharp-edged probe (8 mm ID) inserted vertically through the top of the valve lid cover at a point where the blow-by flow enters the crankcase ventilation system. Then, the sample flow was guided through a wall flow trap before passing through two identical cyclones (URG-2000-30E-5-2.5-S) to remove particles  $>1 \mu\text{m}$ . This was found necessary to avoid flooding the cyclone and obtain a sharp cut off of about 50% at  $1 \mu\text{m}$  (Fig. 5-3b). Finally, the aerosol was collected on a filter consisting of three layers of high-efficiency binder-free glass microfiber (MN 85/90 BF). Filter samples were evaluated visually and by smell and then transferred to the GC in air-tight containers cooled to  $4^\circ\text{C}$  to avoid losing volatile components.

Gas chromatography (GC; Shimadzu Nexis 2030) was used to determine the hydrocarbon index of crankcase aerosols as well as oil sampled from the engine sump according to DIN EN ISO 9377-2. This test method detects oil constituents according to their retention time and compares them to the signals of n-alkanes in the range of C7 to C40. Such compositional information is directly related to oil vapor pressure and thus helpful in tracing the origin and likely formation process of crankcase aerosols by evaporation-condensation vs. mechanical dispersion of sump oil. For example, at a temperature of  $120^\circ\text{C}$  the vapor pressure of a C17 n-alkane is  $10^5$ -fold larger than that of C36 (Lemmon

et al., 2000). As a result, oil droplets formed by evaporation and recondensation are expected to contain significantly more short-chain constituents than the bulk oil.

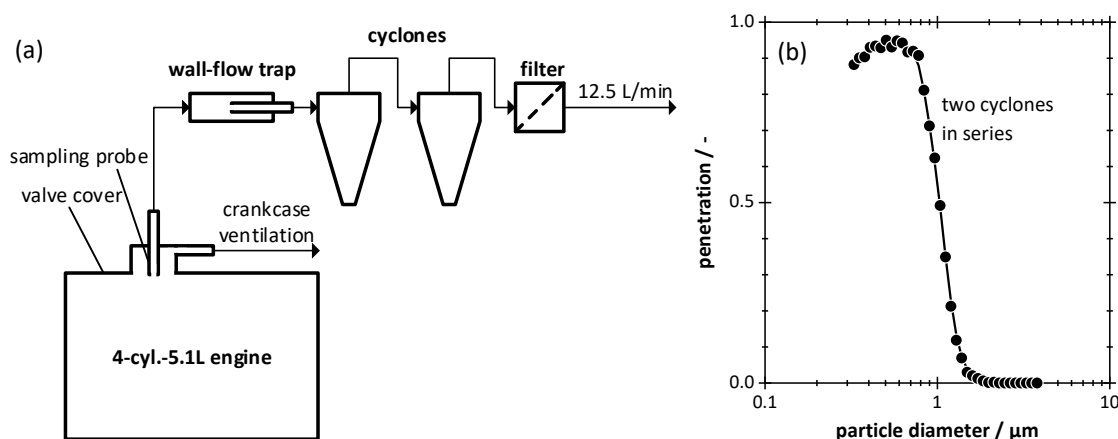


**Figure 5-3:** (a) - Sampling arrangement of submicron crankcase aerosols from a 4-cyl.-5.1L diesel engine. The arrangement is composed of a sampling probe, a wall-flow trap, two cyclones, and a filter to collect the aerosol. (b) - Particle penetration through two cyclones connected in series. These data were obtained by OPC using a flow rate of 12.5 L/min. The compact line is a 3 point adjacent-average that serves as guide to the eyes.

### Generation of oil aerosols by evaporation and recondensation in the laboratory

The main purpose of these laboratory experiments was to provide reliable data generated under well-defined conditions for comparison with and validation of simulations described further down. The aerosol was therefore generated under conditions comparable with those found in the crankcase and subsequent ventilation system of combustion engines, without however trying to emulate the local engine conditions exactly. Once the simulations are validated under these well-defined conditions, they can be extended to study the influence of more extreme parameters on aerosol formation (such as oil vapor temperatures and cooling rates near engine hot-spots) where direct experiments become difficult.

Condensation aerosol was generated by cooling down a vapor-saturated airflow with or without pre-existing particles. The air was saturated either with pure hexadecane or motor oil taken from the engine sump. Hexadecane has the advantage of a well-defined vapor composition (ideal for simulations), while the use of bulk oil bridges the conditions

of the engine and the laboratory. In case pre-existing particles were needed, they were generated by a two-fluid nozzle (May, 1973) placed within the heated chamber. The flow was saturated at temperatures between 100 °C and 130 °C and then cooled down to 25 °C.

According to the set-up shown in Fig. 5-4a an air flow of 5 L/min was saturated in two steps. First, the air passed through a bubbler containing the respective working fluid, in order to obtain a large liquid-air interface and boost mass transport to the gas phase. This vapor laden air stream then passed through a glass microfiber filter pre-loaded with the same liquid, to bring the level of saturation as close to unity as possible. A second, but dry glass fiber filter was installed further downstream to remove droplets that might have penetrated or been re-entrained from the first filter. (Complete saturation at this point was verified as described further down.) This saturated air was then directed out of the heated chamber into a PTFE tube (length 2 m, ID 6 mm) exposed to room temperature, resulting in a temperature profile of the flow as shown in Fig. 5-4b. This temperature profile corresponds to a cooling rate of approximately -380 K/s. At the end of that cooling tube, aerosol was either captured by a filter (three layers of high-efficiency glass microfiber media) for chemical analysis or transferred to an OPC or SMPS for size analysis (see next section).

Vapor concentrations were determined by cooling down a saturated air flow of 5 L/min for 150 min and subsequently weighing the condensate accumulated in cooling tube and filter. As an example, engine oil at 120 °C yielded a mass of about 130 mg, with good reproducibility, corresponding to a vapor concentration of about 120 mg/m<sup>3</sup>. Concentrations did not change measurably even when halving the residence time. Thus, confirming indirectly that the evaporation kinetics sufficed to saturate the air flow under the chosen conditions. This was further confirmed by comparing the experimental values of hexadecane saturated vapor concentrations with the literature (see Fig. 5-6).

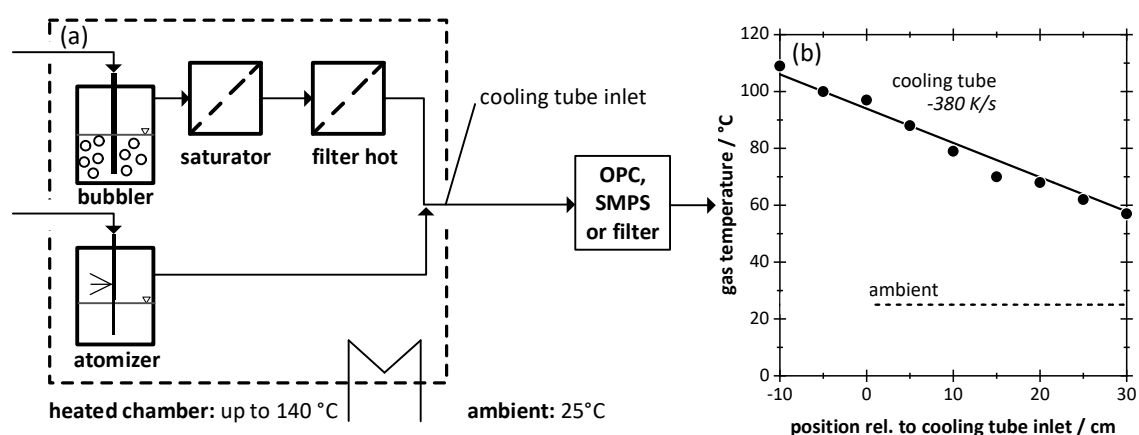


**Figure 5-4:** (a) – Exp. set-up used to saturate and then cool down a flow of vapor laden air or aerosol in a tube exposed to an ambient temperature of 25 °C. Aerosol after cool-down is characterized either by SMPS and OPC or captured on a filter for chemical analysis. (b) - Gas temperature profile in the cool-down tube relative to tube inlet, here for a heating chamber temperature of 120 °C. The ambient temperature is indicated as a dashed line. The linear fit corresponds to a cooling rate of 380 K/s.

### Characterization of laboratory generated aerosol particle size distributions (PSD)

The PSD of oil aerosols was determined by combining a scanning mobility particle sizing system (SMPS) for the submicron portion with an optical particle counter (OPC) for the range from 0.3  $\mu\text{m}$  upward to about 10  $\mu\text{m}$ .

The SMPS system consisted of an  $85^{\text{Kr}}$  neutralizer, a DMA (Hauke model “Vienna Long”) and a CPC (TSI Model 3775). The SMPS sorts the aerosol on the basis of electrical mobility into 64 size bins per decade of logarithmically equal width. A scanning time of 180 seconds was used, with a sheath-air-to-sampling-flow ratio of 35 to 1. The OPC (Palas Promo 2000 H with Welas 2070 HP sensor) sorts particles on the basis of scattered light intensity into 32 size bins per decade of logarithmically equal width. The OPC was operated with the built-in calibration for paraffin oil. Paraffin has a refractive index similar to hexadecane (1.47 vs. 1.43) and almost identical to engine oil. Aerosol sampling and dilution techniques as well as precautions used to avoid soiling of the measurement devices are described by Nowak et al. (2020).

### **Numerical simulation of new aerosol formation and growth from the vapor phase**

Simultaneous nucleation and growth by condensation in the cooling tube were simulated with a one-dimensional model based in part on equations proposed by Winkelmann et al. (2014). Their method calculates new particle formation from classical nucleation theory including the necessary mass and energy balances between carrier gas, vapor and droplets. In its original formulation, the nucleating vapor is assumed to form a single size fraction<sup>1</sup> of monodisperse droplets and is therefore computationally quite efficient. The original model was extended and modified in several aspects to better represent our physical system while still remaining computationally efficient.

An external temperature profile (Fig. 5-4b) along the cooling tube (with corresponding spatial and time coordinates) is imposed on the gas temperature ( $T_{Gas}$ ) which is assumed to be the global temperature for all phases. Energy balances and the heat of condensation are thus omitted for computational reasons. This simplification is known to overestimate the speed of particle growth (Hienola et al., 2001) especially for very small droplets, but still describes general system behavior sufficiently well for our purposes.

As implemented in MATLAB, each population of droplets formed during a given time step, either by nucleation or by injection at  $t=0$ , is maintained as an independent population and grows independently of the others for the remainder of the iteration process. This in effect creates a “true” size distribution width for the nucleation peak (as opposed to an arbitrary assumption made in the Winkelmann Model) and allows also for the existence of a multimodal PSD required in case of pre-existing condensation nuclei. The model implementation furthermore allows for vapor losses to macroscopic surfaces along the cooling tube, which are considerable. These losses are determined experimentally as described in Subsection 5.4, and then distributed linearly along the cooling tube.

The model is based on an oil mass balance computed for each time step for the net mass flow rate from the vapor to the liquid phase,  $\dot{m}_{v \rightarrow l}$ , which consists of the vapor mass

---

<sup>1</sup> The Winkelmann model actually uses a log-normal output size distribution, but with pre-defined geometric standard deviation, and therefore, in effect, generates a single size fraction.

consumed by nucleation,  $\dot{m}_{nuc}$ , minus or plus the vapor mass transferred from or to particles by evaporation or condensation,  $\dot{m}_{c-e}$ , plus the vapor condensing to the walls of the system,  $\dot{m}_{loss}$ :

$$\dot{m}_{v \rightarrow l} = \dot{m}_{nuc} + \dot{m}_{c-e} + \dot{m}_{loss} \quad (5-1)$$

Obviously, these rates scale with the size of the system and thus always refer to a reference volume of  $V_{ref} = 1 \text{ m}^3$ .

The nucleation mass flow rate depends on the nuclei size  $d_{nuc}$ , the nucleation rate  $J_N$ , and the density of the liquid phase  $\rho_l$ , with the common assumption of “twice the critical cluster” mass for  $d_{nuc}$ . The nucleation rate is taken either to equal zero (in case of  $S \leq 1$ ) or, in case of a supersaturated vapor, is calculated following Friedlander (1977), so that

$$\dot{m}_{nuc} = \frac{\pi}{6} \cdot (d_{nuc})^3 \cdot \rho_l \cdot J_N \cdot V_{ref} \quad (5-2)$$

with

$$d_{nuc} = 2^{1/3} \cdot \frac{4 \sigma_{droplet} \cdot m_{Mol}}{\ln(S) \cdot k_B \cdot T_{Gas} \cdot \rho_l} \quad (5-3)$$

and for a supersaturated vapor ( $S > 1$ ) that exceeds a pre-defined threshold  $J_N = 10^7 \text{ m}^{-3}\text{s}^{-1}$

$$J_N = \sqrt{\frac{2 \sigma_{droplet}}{\pi \cdot m_{Mol}} \cdot \frac{\rho_{tot}^2 \cdot Y_v^2}{m_{Mol} \cdot \rho_l}} \cdot \exp\left\{\frac{(-16)\pi \cdot \sigma_{droplet}^3}{3 \cdot (k_B \cdot T_{Gas})^3} \cdot \left(\frac{m_{Mol}}{\rho_l \cdot \ln(S)}\right)^2\right\} \quad (5-4)$$

The saturation  $S$  is given by

$$S = \frac{p_v}{p_v^{S=1}} = \frac{\rho_{tot} \cdot k_B \cdot T_{Gas}}{m_{Mol} \cdot p_v^{S=1}} \cdot Y_v = \frac{Y_v}{Y_v^{S=1}} \quad (5-5)$$

with  $Y_v^{S=1}$  designating the vapor mass fraction at equilibrium vapor pressure,  $S = 1$ . Transition to dimensioned variables requires the introduction of the total density  $\rho_{tot}$  equal to the ratio of total mass to total system volume.

The condensation or evaporation mass flow of each particle size class is calculated according to a balance of the vapor and the liquid phase:

$$\dot{m}_{c-e} = -N \cdot 2\pi \cdot d \cdot D_{oil-air} \cdot \rho_{tot} \cdot (1 - Y_l) \cdot \ln\left(\frac{1 - Y_v}{1 - Y_v^{S=1}}\right) \cdot V_{ref} \quad (5-6)$$

Therein  $d$  represents the droplet diameter calculated from the liquid mass and  $D_{oil-air}$  is the binary diffusion coefficient of oil in air. The dimensionless mass inside the system boundaries consists of a liquid mass fraction in the form of droplets  $Y_l$  plus the mass fractions of vapor  $Y_v$  and air ( $Y_a = 1 - Y_l - Y_v$ ). While  $Y_a$  remains unaffected, condensation or evaporation lead to a mass transfer between liquid and vapor phase and consequently to changes in vapor and liquid mass fractions with time.

Vapor losses to macroscopic surfaces, especially along the walls of the cooling tube, are significant. The total vapor loss from beginning to end of the tube is known experimentally from the difference between equilibrium vapor concentration and total aerosol mass. But the variation of these losses along the tube, i.e. over time, is not known and challenging to model accurately. For simplicity sake it was therefore assumed that losses scale linearly with  $(\dot{m}_{nuc} + \dot{m}_{c-e})$  with a constant dimensionless factor of  $W$ :

$$\dot{m}_{loss} = W \cdot (\dot{m}_{nuc} + \dot{m}_{c-e}) \quad (5-7)$$

Based upon the above considerations, the following set of differential equations was derived for the mass balances of vapor and liquid droplets in the system:

$$\frac{dY_v}{dt} = -\frac{\dot{m}_{v \rightarrow l}}{\rho_{tot}} \quad (5-8)$$

$$\frac{dY_l}{dt} = \frac{\dot{m}_{v \rightarrow l}}{\rho_{tot}} - \frac{\dot{m}_{loss}}{\rho_{tot}}$$

$$\frac{dN}{dt} = J_N$$

Note that the overall number of droplets  $N$  only changes according to the nucleation rate. Aerosol loss mechanisms such as coagulation or diffusion to the walls are neglected in the model, because overall residence times in the cooling tube are too short to be relevant.

The numerical stability of the system was ensured by reducing the duration of the time steps to a level where a further reduction only had a negligible effect on the results. In practice, subdividing the cooling process into time steps with a length of 0.3 ms each was sufficient.

The computational procedure is as follows:

- Each time step begins by calculating one global temperature (gas, vapor, and liquid) according to a given cool-down ramp.
- Then,  $J_N$  is calculated according to Eq. 5-4 for the momentary system state. For the sake of computational efficiency,  $J_N = 0 \text{ m}^{-3}\text{s}^{-1}$  as long as  $J_N$  remains below a user-defined threshold of  $10^7 \text{ m}^{-3}\text{s}^{-1}$ .
- When  $J_N$  exceeds that threshold, nucleation and condensational growth are included by solving the set of differential equations of Eq. 5-8 for that time step by solvers available in MATLAB based on Runge-Kutta methods.
- All nuclei formed during that time step are placed into one size class with diameter  $d_{nuc}$  and number  $N$ . Other size classes that may already exist at that point in time are subject to the condensation routine and increase in diameter according to  $Y_1$  in Eq. 5-8 but without a change in number. This is of course solved individually, for each size class.

- Once  $J_N$  drops below the threshold again due to vapor depletion (but with at least one droplet size class existing), the nucleation routine is stopped, hence  $J_N = 0 \text{ m}^{-3}\text{s}^{-1}$ , and droplet growth is considered for all existing size classes.
- Pre-existing droplets are considered a separate size class undergoing the same condensation growth routine.
- Finally, all droplet populations are sorted into pre-determined size intervals to obtain a PSD. Size classes were typically chosen to resemble those of a given measurement, i.e. with equal interval width on the logarithmic scale.

## 5.4 Results and discussion

### Evidence of aerosol formation by vapor condensation in a crankcase environment

Engine oils are a complex blend of base oils and additives, often consisting of more than 100 different chemical compounds with greatly differing vapor pressures. In a hot engine environment this must lead to significant differences in the composition of the liquid vs. the gaseous oil phases. Uy et al. (2016) had already noticed from GC measurements, that engine oil mist separators removed some higher-boiling, larger molecules from the blow-by aerosol. More generally, particles formed by condensation of engine oil vapor should have a chemical composition resembling more closely that of the vapor phase, i.e. with a significantly higher fraction of volatiles than the bulk oil. This chemical fingerprint allows a qualitative identification of any contribution of condensation to crankcase aerosol formation.

Fig. 5-5 compares the GC spectra of three oil samples, submicron aerosol emitted from the crankcase of the medium-duty diesel engine (red), submicron motor oil aerosol generated in the lab by evaporation-condensation (blue), as well as a sample of bulk sump oil (black) from the engine. Note that the oil had been “broken in” by engine operation for several hours as described in the experimental section. The spectra are represented as mass fraction vs. equivalent n-alkane chain length and normalized for unit area.

According to Fig. 5-5 the sump oil contains components with retention times corresponding to the range of C14 to beyond C40 with a broad maximum between C25 and C30. The same sump oil was used in the laboratory to generate droplets by cooling down the saturated oil vapor flow from 130 °C to 25 °C. The composition of these droplets differs significantly from that of the sump oil, in that they contain a much larger fraction of volatile components up to about C25 while the content of heavier components above C30 is negligible. This enrichment is presumably due to a fractionation process.

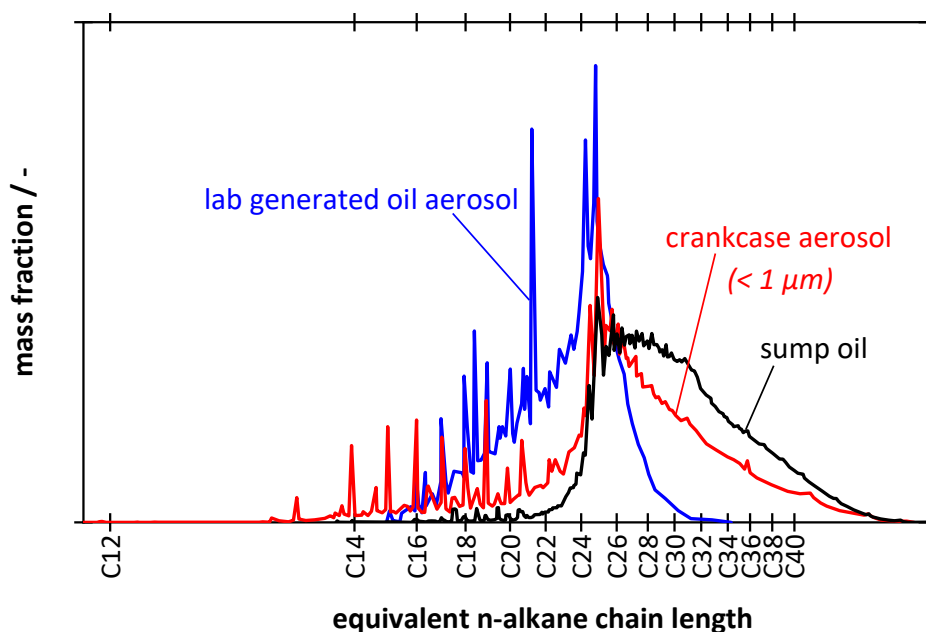


**Figure 5-5:** GC-spectra of sump oil (black), aerosol generated from sump oil by evaporation-condensation in the lab (blue), and crankcase aerosol from the fired engine (red).

The third GC spectrum (red curve) is for actual submicron crankcase aerosol sampled from the diesel engine at nominal power using the same bulk oil as for the other spectra. It lies between those of the lab-generated pure condensation aerosol and the sump oil. There is still a noticeable enrichment of short-chained components in the crankcase aerosol when compared to the bulk, but not as pronounced as for the pure condensation aerosol. Both the crankcase aerosol and the lab-generated aerosol were clear in visual appearance, and both had a more aggressive smell than the much darker sump oil. How-

ever, the peaks C14 to C16 (amounting to 5% of the total sample mass) are over-represented in comparison to the other two spectra, indicating the likelihood of some carry-over of diesel fuel via the piston rings.

Vapor condensation appears to make a significant contribution to the submicron crankcase aerosol. However, these data do not tell us whether the crankcase aerosol represents an external or an internal mixture. In other words, the aerosol may consist of separate fractions of homogeneously nucleated and mechanically redispersed bulk oil; or it may have been formed entirely by vapor condensation onto redispersed (perhaps partially evaporated) droplets. This raises the question whether homogeneous nucleation can play a significant role in the crankcase, perhaps under extreme conditions near hotspots and under typical cooling rates.

The other question is, how a few mass percent of diesel fuel in the crankcase might alter the overall processes of condensation and nucleation. If fuel enters the crankcase as a spray of fine droplets, these droplets will add to the pre-existing aerosol population. If the fuel is present as short-chained vapor, this will increase the overall concentration of condensables. Both these issues are covered by the experiments and simulations described in the following. A third issue concerns the influence of a few percent of shorter-chain molecules on the simulations, via the average mass diffusion coefficient and the surface tension. The latter will also be addressed.

### **Aerosol formation by nucleation and growth of hexadecane and engine oil vapor**

***Equilibrium vapor concentrations:*** Aerosol formation and/or growth by condensation requires vapor concentrations above the thermodynamic equilibrium. Equilibrium vapor concentration data are shown in Fig. 5-6 for hexadecane (in blue) and for two engine oils, Rimula R6 (in black) and Quartz 7000 (in red). The experimental data points were determined using the cold trap setup described earlier. For hexadecane, the error bars represent  $\pm$  one standard deviation for 3 measurements each, while the blue curve is based on readily available literature data (Lemmon et al., 2000). Agreement is very good for hexadecane, and this validates our experimental technique sufficiently to apply it

also to engine oils for which vapor data can generally not be found in the open literature. For engine oil, an exponential function (solid curves) was fitted to the data points to estimate concentrations at intermediate temperatures as required for the simulations. Hexadecane has a shorter chain structure and a lower molar mass of 226 g/mol compared to the oils (approximately 354 g/mol for Quartz 7000 and 381 g/mol for Rimula R6). Hence, the motor oils require higher temperatures (about 80 °C higher) to reach comparable vapor concentrations.

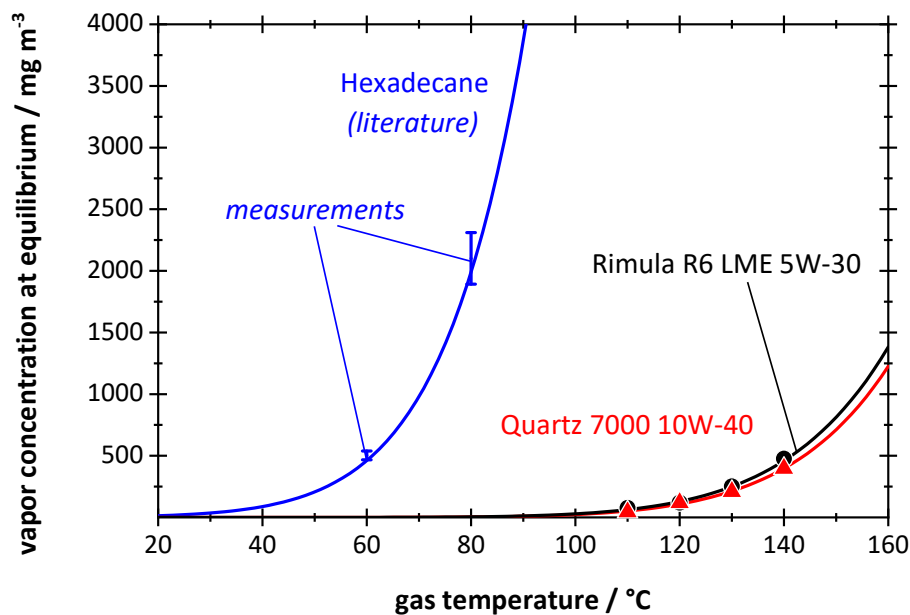


**Figure 5-6:** Equilibrium vapor concentrations for hexadecane and two engine oils. Data points are based on measurements according to Section 5.3. Error bars for hexadecane represent the standard deviations of three measurements each. Solid curve for hexadecane from Lemmon et al., 2000; solid curves for engine oils are exponential fit functions.

**Nucleation:** Tab. 5-1 gives an overview of the nucleation experiments and includes information on vapor properties that were used for the simulations. Section 5.3 describes the actual experimental set-up used for these experiments and introduces the numerical simulation. The diffusion coefficient for vapor in air was obtained according to Poling et al. (2001), the surface tension of droplets was calculated according to Tolman (1949). A density of 773 kg/m<sup>3</sup> was used for hexadecane and 874 kg/m<sup>3</sup> for engine oil to convert

between aerosol number and mass. The cooling rate was taken according to actual experimental conditions as  $-380$  K/s (see Fig. 5-4b). Vapor losses were derived from the experimental data from the difference in measured aerosol mass concentration (obtained by SMPS or OPC) and vapor mass concentration at equilibrium (see Fig. 5-6).

**Table 5-1:** Conditions for cool-down experiments without pre-existing particles and vapor data used for simulation:

cool-down	material	vapor conc. at STP	vapor losses
100 °C → 25 °C (Fig. 7a)	hexadecane	10600 mg/m <sup>3</sup>	99.98 %
110 °C → 25 °C (Fig. 7b)	hexadecane	19000 mg/m <sup>3</sup>	90.72 %
120 °C → 25 °C (Fig. 8a)	Quartz 7000 10W-40	170 mg/m <sup>3</sup>	99.67 %
130 °C → 25 °C (Fig. 8b)	Quartz 7000 10W-40	310 mg/m <sup>3</sup>	56.56 %

The following figures show number-based PSDs for aerosols formed by cooling down the particle-free vapors of either hexadecane (Fig. 5-7) or Quartz 7000 oil (Fig. 5-8) to 25 °C from saturation temperatures between 100 °C and 130 °C. Numerical results are in black, measurements by OPC in blue. Note that the numerical data were calculated using the same particle size classes as for the measurements. Total number concentrations are included to give an impression of actual concentrations obtained.

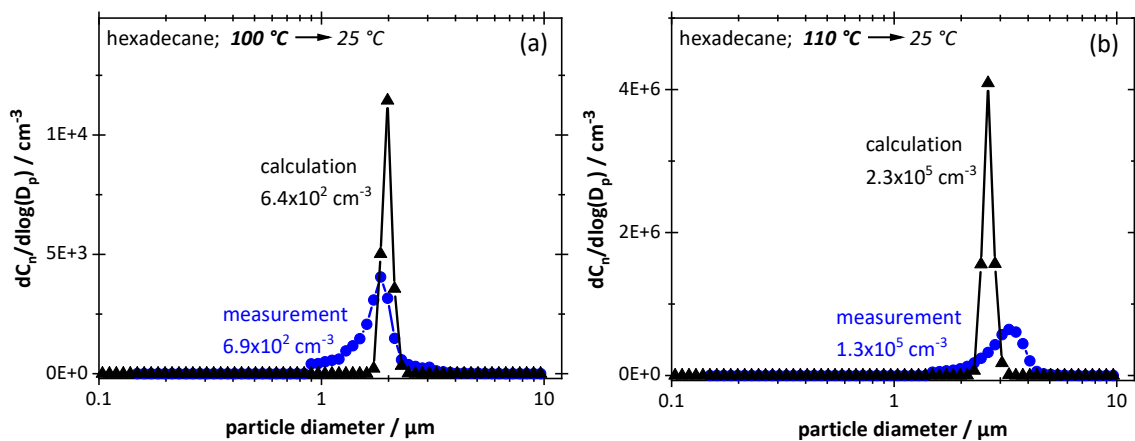


**Figure 5-7:** Number based PSDs obtained by cooling down saturated particle-free hexadecane vapor from 100 °C (a) or 110 °C (b) to 25 °C. Concentrations stated at STP. OPC measurements (blue) and numerical simulation (black) use the same size classes (32 logarithmically equal bins per decade).

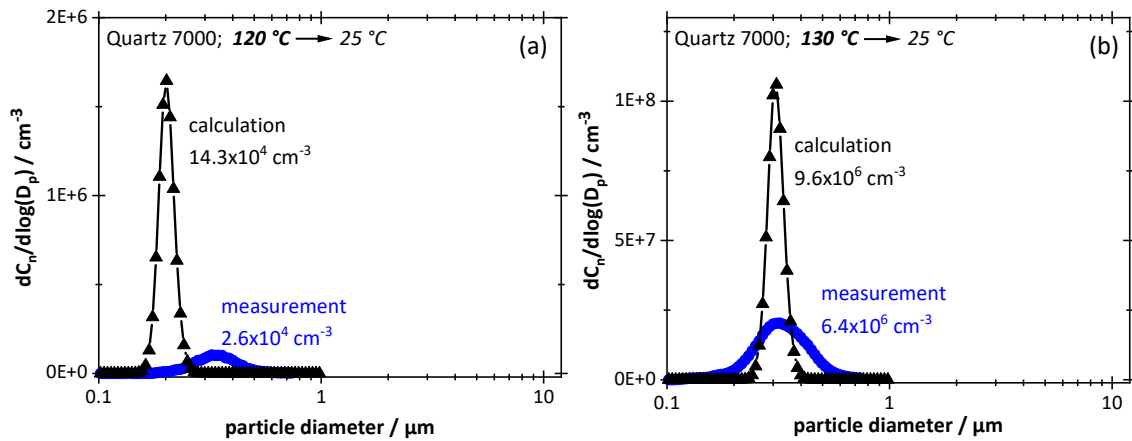


**Figure 5-8:** Number based PSDs obtained by cooling down saturated particle-free engine oil vapor from 120 °C (a) or 130 °C (b) to 25 °C. Concentrations stated at STP. SMPS measurements (blue) and numerical simulation (black) use the same size classes (64 logarithmically equal bins per decade).

Two features are immediately apparent in Figures 5-7 and 5-8: the numerical PSDs are narrower than the experimental PSDs, but the modal values agree remarkably well. The difference in width is hardly surprising, given that the real system is not as perfectly uniform in terms of flows, temperature, vapor distributions, etc. as the simulated one. However, the overall agreement of simulated and measured size spectra confirms the relevance of homogenous nucleation in the absence of a pre-existing aerosol.

Given the difference in equilibrium vapor concentrations between the two working fluids (Tab. 1), droplet sizes as well as concentrations in case of hexadecane are understandably much higher than for engine oil, even though the starting temperature of hexadecane is lower. Modal diameters are about one order of magnitude higher; concentrations also when comparing them on a mass basis for 110 °C hexadecane (1760 mg/m<sup>3</sup>) and 130 °C engine oil (130 mg/m<sup>3</sup>).

On the other hand, the increase in total aerosol concentration from the lower to the higher starting temperature (for the same working fluid) is too drastic to be justified by simple thermodynamic arguments. In case of hexadecane, the concentration jumps from 2 mg/m<sup>3</sup> at 100 °C to 1760 mg/m<sup>3</sup> at 110 °C. That is far more than the exponential characteristic of the vapor concentration curve would suggest, namely from

10600 mg/m<sup>3</sup> to 19000 mg/m<sup>3</sup>, an 80 % increase. For motor oil the increase in mass concentration by a factor of 240 is similarly strong.

Such a jump can only be explained by the kinetics of vapor transport onto system walls during cool-down. The fraction of vapor lost to the walls is by no means constant or even linear with starting temperature. For hexadecane at 100 °C and 110 °C losses amount to a staggering 99,98 % and 90,72 %, respectively. Yet, nucleation still occurs at these temperatures, while experiments below 100 °C produced no measurable aerosol at all because too much vapor was lost.

The observed decrease in vapor loss fractions with increasing vapor concentration is reasonable. Similar issues have been observed and simulated in the laminar cooling section of condensation particle counters, where vapor is depleted radially inward at a rate that depends on the vapor diffusion coefficient (as well as the concentration of particles), while the build-up of supersaturation near the core is driven also by the inward cooling rate and hence the thermal conductivity of the carrier fluid. For our system the dependence on cooling rate, a key factor, will be discussed in the next section. Beyond that, the wall loss issue will not be pursued further because no new understanding could be gained regarding the processes in a crankcase.

***Effects of pre-existing particles on nucleation:*** The crankcase environment is characterized not only by large amounts of hydrocarbon vapor but also pre-existing airborne particles in significantly varying concentration. These particles consume vapor during cool-down and thereby slow down the build-up of supersaturation, leading to delays or even prevent nucleation. The effect of such condensation nuclei in a crankcase environment is largely unknown and we have no good feeling for their influence on nucleation.

Numerical simulations were therefore conducted at first to understand the sensitivity of the crankcase system to nuclei concentration  $N_0$  and size  $d_0$ , and then compared to a few cool-down experiments using parameters and techniques described earlier. The simulation is based on initial nuclei sizes of 30 nm, which corresponds to a typical crankcase aerosol mode (cf. introduction), as well as 200 nm. The motor oil temperature was

chosen at the high end of our range to account for the existence of hotspots typical for an engine at high loads. Fig. 5-9 presents PSDs based on number (a) and mass (b) calculated for three different starting concentrations  $N_0$  between  $0.2$  and  $3 \times 10^6 \text{ cm}^{-3}$  and  $d_0 = 30 \text{ nm}$ , which is realistic for a crankcase. For better readability, each PSD is split into a red portion that represents the nucleation mode and a blue portion representing the growth of preexisting nuclei.

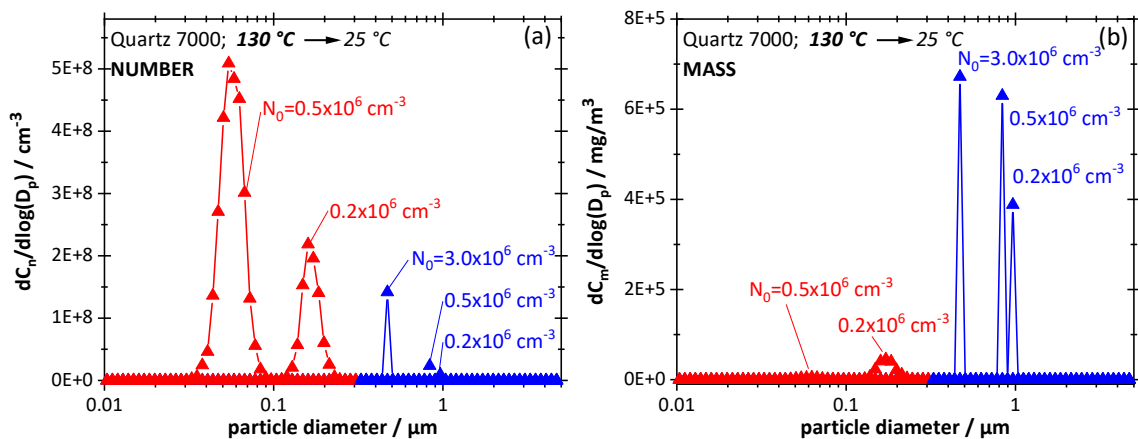


**Figure 5-9:** Simulated PSDs based (a) on number and (b) on mass for three different initial nuclei concentrations with  $d_0 = 30 \text{ nm}$ . The nucleation part of the PSD shown in red, the pre-existing nuclei in blue.

In Fig. 5-9a note first of all that condensation nuclei always grow far beyond their initial size, to between about  $500 \text{ nm}$  and  $900 \text{ nm}$ , becoming smaller of course with increasing nuclei concentration because the vapor supply remains constant. The nucleation peak for  $N_0 = 0.2 \times 10^6 \text{ cm}^{-3}$  appears around  $200 \text{ nm}$  and then also moves toward smaller sizes for higher  $N_0$  while the peak height increases, and then disappears abruptly around  $0.5 \times 10^6 \text{ cm}^{-3}$ . (Not shown in the graphs.) That behavior of the nucleation peak can be explained by a delay in the onset of nucleation in the presence of nuclei. Vapor is at first depleted (because the nuclei begin to grow much sooner) but not enough to prevent the development of a rather high supersaturation further down the line. The higher the supersaturation at the moment of nucleation on-set, the smaller and more copious the droplets. (This will become clearer in the following section when the effect of the cooling rate is explored.) Simulations were also performed using larger nuclei with  $d_0 = 200 \text{ nm}$ .

The PSDs were practically indistinguishable in terms of peaks heights and location of peaks from those with  $d_0 = 30$  nm. They are therefore not shown here.

Needless to say, the nucleation peaks “disappear” visually when presenting these PSD in terms of particle mass (Fig. 5-9b), thereby illustrating the problem with comparing crankcase aerosol data between publications.

Nucleation experiments in the presence of condensation nuclei were performed with motor oil (Fig. 5-10), using the same parameters as for Figs. 5-8 and 5-9 but in a much more limited range, due to experimental constraints. The initial size of the condensation nuclei was  $< 600$  nm. These data also show a nucleation peak at 300 nm for  $N_0 = 0.2 \times 10^{-6} \text{ cm}^{-3}$ . (The actual peak location is probably closer to 200 nm, but this is no longer resolved by the OPC.) However, the peak disappears almost completely when increasing  $N_0$  to  $0.3 \times 10^{-6} \text{ cm}^{-3}$ . The experiment is thus more sensitive to variations of  $N_0$  than the simulations, but this is not entirely surprising.

Although not fully representative of the crankcase environment, the experiment nevertheless confirms that nucleation is possible at high vapor concentrations and significant cooling rates, even in the presence of considerable number concentrations of pre-existing aerosol.

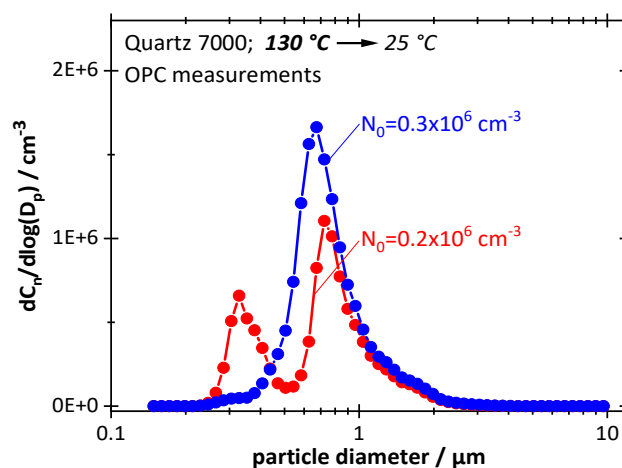


**Figure 5-10:** Measured PSDs for two concentrations  $N_0$  of pre-existing aerosol with  $d_0 < 600$  nm. Other parameters are the same as for Fig. 8.

### **Influence of cooling rate and oil properties on aerosol generation**

The influence of cooling rate and oil properties (surface tension, vapor pressure) on nucleation and growth of aerosol from engine vapor are discussed on the basis of simulations using the model already introduced earlier. For simplicity and comparability, it was assumed that only vapor but no particles were present before cool-down. Vapor losses to system walls were set to zero.

Fig. 5-11 shows the influence of cooling rate on aerosol number concentration (a) and number-weighted median particle diameter (b) for starting temperatures of 120 °C, 130 °C, and 140 °C. equilibrium vapor concentrations of the engine oil (Total Quartz 7000 10W-40) at the respective temperatures and peak supersaturations at the respective cooling rates have also been added. Calculations are based on an oil surface tension of 30 mN/m. Note that the intermediate cooling rate of -380 K/s (black curve) corresponds to the conditions during the lab experiments and is our reference. The other two cooling rates were chosen as respectively 4x higher and lower than the reference rate.

The two graphs of Fig. 5-11 show, not surprisingly, that higher cooling rates produce more and smaller particles. Considering the linear concentration scale, the *number concentration* increases about 50-fold (in case of the 120 °C experiments) from about  $1 \times 10^7 \text{ cm}^{-3}$  at -95 K/s to about  $56 \times 10^7 \text{ cm}^{-3}$  at -1520 K/s, while the mean particle size drops by a factor of about 3.5. This general behavior is due to the increase in theoretical peak saturation with cooling rate, e.g. from  $S=100$  at -95 K/s to  $S=145$  at -1520 K/s for a starting temperature of 140 °C. According to classical theory the nucleation kinetics speed up considerably when increasing the supersaturation (e.g. Hinds, 1999), thereby converting more of the vapor mass to particles while leaving less vapor for subsequent condensation and growth.

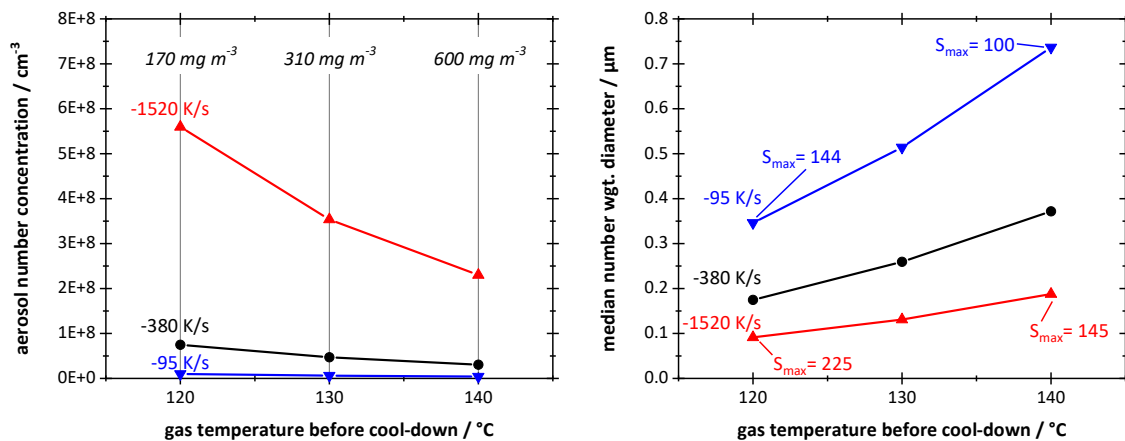


**Figure 5-11:** Total aerosol number concentrations (a) and number-weighted median particle diameters (b) plotted against gas temperature before cool-down at three different cooling rates. Equilibrium vapor concentrations and peak saturations during cool-down are added. Simulated for Total Quartz 7000 10W-40 with a surface tension of 30 mN/m. Lines connecting data points serve as a guide to the eye.

Fig. 5-11 also shows that rising the initial equilibrium vapor concentration (i.e. the starting temperature) at constant cooling rate produces larger but fewer particles. This is due to a boost in vapor consumption by condensation onto newly formed particles which reduces the peak supersaturation and hence the nucleation rate. Note however, that aerosol *mass concentrations* are determined solely by the equilibrium vapor concentration which is only a function of temperature (see Fig. 5-6).

The effect of the initial vapor concentration on aerosol number concentrations and number-weighted median particle diameters is further illustrated by Fig. 5-12. Oil type (Total Quarz 7000 10W-40, surface tension 30 mN/m) and cooling rate (-380 K/s) remain unchanged in relation to the previous graphs. Hence the black curves are based on the same reference values as before. The red and blue curves, denoted as 2Ps and 0.5Ps respectively, represent calculations for twice and half the saturation vapor pressure of the oil. The trends seen in Fig. 5-12 reinforce the findings already derived from Fig. 5-11: Regardless of whether the initial saturation vapor concentration is increased via a higher temperature or via a (hypothetical) oil with larger volatile content, the effect on aerosol number concentrations and particle diameters is always the same, namely a decrease of the former and an increase of the latter.

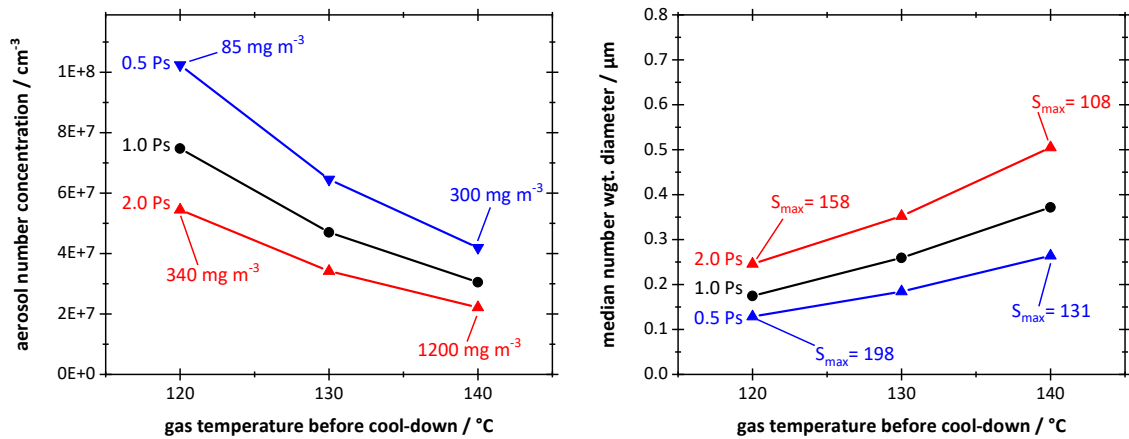


**Figure 5-12:** Total aerosol number concentrations (a) and number-weighted median particle diameters (b) plotted against gas temperature before cool-down. For each starting temperature, equilibrium vapor concentrations are scaled by factors of 0.5 (blue) and 2.0 (red) relative to the black reference curve. Actual vapor concentrations and peak saturations during cool-down have been added. Surface tension of 30 mN/m and cooling rate of -380 K/s remain unchanged. Straight lines connecting data points as a guide to the eye.

Finally, the role of the surface tension in the context of nucleating oil vapor is investigated in Fig. 5-13, again using the same graphical representation as before. Simulations were performed for three different surface tensions, namely 25 mN/m (blue), 30 mN/m (black), and 35 mN/m (red). These values bracket the variability of this parameter more than sufficiently, because the surface tension of oils varies little in general. The data are again based on cooling rates of -380 K/s and vapor concentrations corresponding to Quartz 7000 oil. For some data points the peak saturation value was added for information.

Fig. 5-13 indicates that the surface tension has a minor impact on aerosol formation when cooling down saturated oil vapor. This was unexpected as classical nucleation theory suggests a major negative influence of surface tension on nucleation rates (see Eq. 5-4). The simulations have shown however, that higher surface tensions also delay the start of nucleation during cool-down, thus permitting the build-up of higher peak saturations before the on-set of particle formation. (In our simulation, the delay was from about 14 ms to 20 ms, leading to an increase in  $S$  from 40 to 383!) Ultimately both factors

seem to neutralize each other, resulting in similar aerosol nucleation rates, number concentrations, and diameters after cool-down.

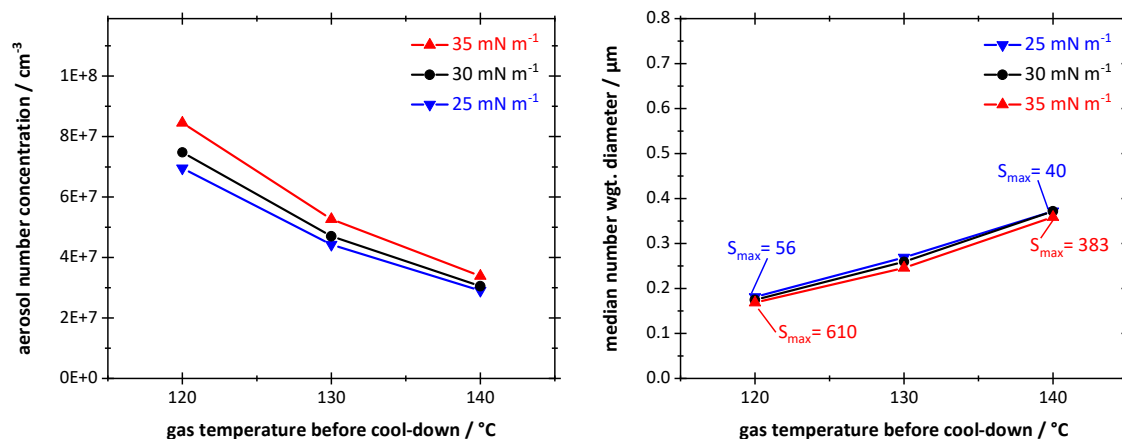


**Figure 5-13:** Total aerosol number concentrations (a) and number-weighted median particle diameters (b) plotted against the gas temperature before cool-down for three different values of surface tension. Cooling rate  $-380$  K/s, equilibrium vapor concentration corresponding to Total Quartz 7000 10W-40. Straight lines connecting data points are a guide to the eye.

## 5.5 Summary and conclusions

The roles of nucleation and growth by oil vapor condensation (with and without pre-existing nuclei) during the formation of submicron crankcase aerosols were investigated both experimentally and by simulation under engine-like conditions using actual motor oil as well as hexadecane.

The chemical composition of the submicron crankcase aerosol fraction from a commercial 4-cylinder 5-Liter diesel engine, analyzed by GC, suggests vapor-to-particle conversion mechanisms are likely to play a role in its formation. GC spectra of the submicron aerosol had a significantly higher volatile hydrocarbon content ( $\leq C_{25}$ ) than the bulk engine oil (up to  $C_{40}$ ).

Experimentally, air-vapor mixtures were saturated between  $100$  °C and  $130$  °C (equivalent to vapor concentrations between  $0.2$  g/m<sup>3</sup> and  $20$  g/m<sup>3</sup>) and then cooled down at a defined rate to near ambient, with and without pre-existing submicron oil droplets. Aerosols were characterized by OPC and SMPS. For engine oil, and in the absence of

nuclei, nucleation peaks appeared near 300 nm in number concentrations that decreased with vapor supply and vanished completely below 100 °C due to vapor losses onto cooling tube walls. Addition of nuclei in concentrations above about  $2 \times 10^5 \text{ cm}^{-3}$  quickly suppressed spontaneous aerosol formation. This confirms observations on fired engines that the submicron blow-by aerosol concentration is very sensitive to bulk oil temperature.

Separately, nucleation and growth were simulated numerically in MATLAB with a one-dimensional model based on classical nucleation theory in combination with mass transfer between liquid and vapor phase. Model equations are based on Winkelmann et al. (2014) with computationally efficient extensions to allow for progressive cooling and vapor loss to tube walls as well as pre-existing nuclei. Simulations were validated first against the hexadecane experiments, and then used to study the effects of cooling rate, vapor concentration, nuclei concentration and oil surface tension in parameter ranges difficult to reach experimentally. Equilibrium vapor data for hexadecane were taken from the literature; for actual motor oil they were measured in the temperature range of interest.

Simulations agreed well with homogenous nucleation experiments in the absence of nuclei, especially with regard to peak location. Increasing the equilibrium saturation level for a given temperature (equivalent to using a more volatile oil) shifts nucleation toward fewer but larger droplets. This is consistent with measurements on hexadecane vs. motor oil. Upon addition of increasing nuclei concentrations upward of  $0.2 \times 10^6 \text{ cm}^{-3}$ , nucleation peaks gradually increased in height while diminishing in asymptotic droplet size from about 200 nm to 40 nm, then vanished completely beyond about  $1 \times 10^6 \text{ cm}^{-3}$  in favor of purely condensational growth of pre-existing nuclei. Growth of nuclei was less sensitive to vapor concentration, with asymptotic sizes between about 500 nm to 900 nm. Increasing the oil surface tension from 25 to 35 mN/m had almost no effect on nucleation rates, because the delayed start of nucleation due to an increased surface energy barrier was compensated by a large increase in supersaturation during cool-down.

In sum, experiments and simulation confirm the important contribution of both nucleation and condensational growth of preexisting aerosols to the submicron crankcase aerosol spectrum. The nucleation peak can be expected to lie between about 100 and 300 nm, while condensational growth of pre-existing nuclei is usually completed between 500 and 900 nm. The two mechanisms thus appear to form distinct peaks which agree remarkably well in their respective size ranges with peaks found in the literature on crankcase aerosols.

The temporal evolution of supersaturation that goes hand in hand with vapor depletion by condensation onto pre-existing nuclei as well as macroscopic surfaces during the cooling process, a characteristic of any engine environment, is key to understanding the role of nucleation for crankcase aerosol.

Applied to practical reduction strategies, it appears obvious that lower bulk oil temperatures and fewer engine hotspots have a key role to play in reducing the aerosol mass output from the crankcase. The role of less volatile engine oils, although intuitively desirable, is less straightforward because a higher vapor pressure (at otherwise constant temperatures) leads to the formation of fewer but larger droplets by nucleation and to more growth of pre-existing aerosols. And larger droplets are the easier to remove by most abatement devices. Finally, the results suggest that lower cooling rates (although difficult to control in engine design) would be equally beneficial for the same reasons.

## 5.6 References

- Agarwal, A.K., Goyal, S.K., Srivastava, D.K. (2011). Time resolved numerical modeling of oil jet cooling of a medium duty diesel engine piston. *International Communications in Heat and Mass Transfer*, 38, 1080-1085.
- Becker, R., Döring, W. (1935). Kinetische Behandlung der Keimbildung in übersättigten Dämpfen. *Annalen der Physik*. 416(8):719–752.
- Burtscher, H. (2005). Physical characterization of particulate emissions from diesel engines. A review. *Journal of Aerosol Science*, 36, pp. 896–932.
- Ehteram, M.A., Tabrizi, H.B., Ahmadi, G., Safari, M., Mirsalim, M.A. (2013). Investigation of fine droplet generation from hot engine oil by impinging gas jets onto liquid surface. *Journal of Aerosol Science*, 65, 49-57.
- Fan, J., Wang, Y., Rosenfeld D., Liu, X. (2016). Review of Aerosol-Cloud Interactions: Mechanisms, Significance and Challenges. *Journal of the Atmospheric Sciences* 73, 4221.
- Friedlander, SK. (1977). *Smoke, Dust and Haze*. Wiley, New York.
- Golkarfard V., Subramaniam R., Broughton J., King A, Mullins B. (2019). Comparative Performance of 12 Crankcase Oil Mist Separators. *SAE International Journal of Engines* 12, 5–14.
- Harris, S.J., Maricq, M.M. (2001) Signature size distributions for diesel and gasoline engine exhaust particulate matter. *Journal of Aerosol Science* 32, 749-764.
- Hienola, J., Kulmala, M., Laaksonen, A. (2001). Condensation and evaporation of water vapor in mixed aerosols of liquid droplets and ice: numerical comparison of growth rate expressions. *Journal of Aerosol Science*, 32, 351-374.
- Hinds, W.C. (1999). *Aerosol Technology. Properties, Behavior, and Measurement of Airborne Particles* (2nd ed.). New York: Wiley.
- Johnson, B.T. (2012). Experimental analysis of crankcase oil aerosol generation and control. Loughborough University. Thesis. <https://hdl.handle.net/2134/10968>.
- Johnson, BT., Graham K. Hargrave, Benjamin A. Reid, and Vivian J. Page (2011) Crankcase Sampling of PM from a Fired and Motored Compression Ignition Engine. SAE paper 2011-24-0209
- Kissner, G., Ruppel, S. (2009). Highly Efficient Oil Separation Systems for Crankcase Ventilation. SAE International, 01-0974.

- Kittelson, D. B. (1998). Engines and nanoparticles. *Journal of Aerosol Science*, 29(5-6), 575–588.
- Kolb, H.E., Watzek A.K., Francesconi V.Z., Meyer, J., Dittler, Kasper, G. (2018). A mesoscale model for the relationship between efficiency and internal liquid distribution of droplet mist filters. *Journal of Aerosol Science*, 123, 219-230.
- Kreidenweis, S.M., Petters, M., Lohmann, U. (2019). 100 Years of Progress in Cloud Physics, Aerosols, and Aerosol Chemistry Research. *Meteorological Monographs Vol. 59*.
- Lakshmanan, M., Maddali, V., Natrajan, R., Muthyam, R., Balasubramanian, N. (2019). Insight into Effect of Blow-By Oil Mist Deposits on Turbocharger Performance Deterioration in a Diesel Engine. *SAE Technical Paper 2019-26-0340*.
- Lemmon E.W., Goodwin, A.R. (2000). Critical Properties and Vapor Pressure Equation for Alkanes  $C_nH_{2n+2}$ : Normal Alkanes With  $\{less\ then\ or\ equal\ to\}36$  and Isomers for  $n=4$  Through  $n=9$ . *Journal of Physical and Chemical Reference Data* 29(1), 1-39.
- Lorenz, M., Koch, T., Kasper, G., Pfeil, J., Nowak, N. (2020). Origin and Separation of Submicron Oil Aerosol Particles in the Blow-by of a Heavy-Duty Diesel Engine. *SAE Int. Journal of Engines*, 13, 363-375.
- Maricq, M.M. (2007). Chemical characterization of particulate emissions from diesel engines: A review. *Journal of Aerosol Science* 38, 1079-1118.
- May, K. (1973). The Collison nebulizer: description, performance and application. *Journal of Aerosol Science*. 4, 235-243.
- Nowak, N., Scheiber, K., Pfeil, J., Meyer, J., Dittler, A., Koch, T., Kasper, G. (2020). Sampling and conditioning of engine blow-by aerosols for representative measurements by optical particle counters. *Journal of Aerosol Science*, 148, 105452.
- Penner, T., Meyer, J., Kasper, G., Dittler, A. (2019). Impact of operating conditions on the evolution of droplet penetration in oil mist filters. *Journal of Separation and Purification Technology*, 211, 697-703.
- Poling, B.E., Prausnitz, J.M., O'Connell, J.P. (2001). *The properties of gases and liquids*. 5th ed. New York : McGraw-Hill.
- Sagot, B., Forthomme A., Wojda M., De La Bourdonnaye G. (2014). Tuning of an oil mist generator for the performance evaluation of oil separators used in blow-by applications. *Proc. 1st European Conference on Fluid-Particle Separation, Lyon, France*.
- Sauter, H. (2004). *Analysen und Lösungsansätze für die Entwicklung von innovativen Kurbelgehäuseentlüftungen*. Berlin: Logos-Verlag.

- Scheiber, K., Nowak, N., Pfeil, J., Koch, T., Kasper, G. (2021) Comparison of four diesel engines with regard to blow-by aerosol properties as a basis for reduction strategies based on engine design and operation, AAET. (Status: accepted)
- Tatli, E., Clark, N.N. (2009) Crankcase Particulate Emissions from Diesel Engines. SAE Int. Journal of Fuels and Lubricants , 1, 1334- 1344
- Tolman, R.C. (1949). The Effect of Droplet Size on Surface Tension. The Journal of Chemical Physics, 17, 333–337.
- Uy, D., Storey, J., Sluder, C., Barone, T. et al. (2016). Effects of Oil Formulation, Oil Separator, and Engine Speed and Load on the Particle Size, Chemistry, and Morphology of Diesel Crankcase Aerosols. SAE Int. Journal of Fuels and Lubricants 9, 224-238.
- Winkelmann, C., Nordlund, M., Kuczaj, A.K., Stolz, S., Geurts, B.J. (2014). Efficient second-order time integration for single-species aerosol formation and evolution. International Journal for Numerical Methods in Fluids, 74, 313-334.
- Wurster, S., Meyer, J., Kasper, G. (2017). On the relationship of drop entrainment with bubble formation rates in oil mist filters. Journal of Separation and Purification Technology, 179, 542-549.

## 5.7 List of symbols

### Roman

$d$	droplet diameter	$m$
$d_{nuc}$	nucleus diameter	$m$
$D_{oil-air}$	binary diffusion coefficient of oil in air	$m^2 s^{-1}$
$J_N$	nucleation rate	$m^{-3} s^{-1}$
$k_B$	Boltzmann constant	$J K^{-1}$
$m_{Mol}$	molecular mass	$kg$
$\dot{m}_{c-e}$	Mass flow rate of condensation minus evaporation	$kg s^{-1}$
$\dot{m}_{v \rightarrow l}$	net mass flow rate from vapor to liquid phase	$kg s^{-1}$
$\dot{m}_{nuc}$	mass flow rate of nucleating oil vapor	$kg s^{-1}$
$N$	number concentration of droplets	$m^{-3}$
$p_v$	vapor pressure	$Pa$
$p_v^{S=1}$	vapor pressure at equilibrium	$Pa$
$S$	saturation	–
$T_{gas}$	gas phase temperature	$K$
$T_l$	liquid phase temperature	$K$
$W$	vapor loss scaling factor	–
$Y_a$	mass fraction of air	$kg kg_{tot}^{-1}$
$Y_l$	mass fraction of liquid	$kg kg_{tot}^{-1}$
$Y_v$	mass fraction of vapor	$kg kg_{tot}^{-1}$
$Y_v^{S=1}$	mass fraction of vapor at equilibrium	$kg kg_{tot}^{-1}$

### Greek

$\rho_l$	density of liquid phase	$kg m^{-3}$
$\rho_{tot}$	total density	$kg m^{-3}$
$\sigma_{droplet}$	surface tension of droplet	$N m^{-1}$





## 6 Summary and conclusions

A comprehensive understanding of the sources and formation mechanisms of blow-by aerosols is crucial for ensuring sustainable engine operation as well as a minimized impact on the environment. To obtain reliable aerosol data, two dilution systems were developed, and an optical particle counter (OPC) was extensively tested to establish a robust measurement procedure. This procedure allowed for the characterization of blow-by aerosols on two engines: a medium-duty 4-cylinder 5.1-liter diesel engine and its one-cylinder counterpart. The study evaluated the influence of engine speed, engine load, and oil temperature on aerosol properties. Additionally, the contribution of specific sources such as cooling nozzles, turbocharger, and piston rings was assessed. The results revealed that, in addition to the mechanical atomization of oil, the condensation of oil vapor also played a significant role in aerosol generation. Consequently, a study on aerosol formation through the condensation of oil vapor in the crankcase of combustion engines was conducted. Based on the findings from the various experiments, strategies to reduce aerosol emissions were formulated at the end of this chapter.

The **reliability of size and concentration measurements** by OPC was studied extensively for a typical engine blow-by environment characterized by a mixture of oil aerosol and saturated oil vapor at temperatures up to 120 °C. The study utilized an OPC Promo 2000 H device from Palas GmbH. A single-stage (1:9) and a double-stage (1:80) sampling and dilution system were developed, and their particle transfer functions determined by OPC measurements in the size range of 0.3 to 10 µm. The results showed that losses below 2 µm ranged from negligible to 10%, while losses above that size range progressively increased, reaching values of over 90% around 10 µm. The  $d_{50}$  cut-points were approximately 7 µm and 6 µm for the single-stage and double-stage systems, respectively. Based on these transfer functions, a correction function was derived to account for particle losses up to 8 µm.

The study also investigated droplet growth by vapor condensation during the cooling process. This was done with well defined mixtures of aerosol and saturated oil vapor at temperatures ranging from 80 °C to 120 °C, where saturation vapor concentrations increased from 9 mg/m<sup>3</sup> to about 110 mg/m<sup>3</sup>. Theoretically, substantial growth can occur due to the vapor mass exceeding the aerosol mass. However, experimental measurements of droplet growth during the cooling process of an undiluted mixture of vapor and aerosol indicated that growth was negligible below approximately 100 °C, likely due to the condensation of virtually all the vapor on the system walls. Above 100 °C, the cool-down process generated sufficient supersaturation to activate growth and cause significant changes in particle size distribution (PSD), particularly in the size range from the lower limit of OPC detection to about 2 µm. Even at a temperature of 120 °C, over 95% of the total vapor mass condensed on the walls. Diluting the aerosol sample with 20 °C air in a 1:20 ratio effectively suppressed condensational growth at all starting temperatures, indicating that a heated OPC sensor is not necessarily required for blow-by aerosol measurements.

The same study also examined the accuracy of converting OPC-based number distributions to total aerosol mass through a comparison with filter samples. Two OPC sensor ranges were investigated: 0.2 to 10 µm and 0.3 to 17 µm. The results showed that the 0.2 to 10 µm range provided more accurate measurements, generally agreeing to within -10%, while the 0.3 to 17 µm range agreed to within -20%. It was also shown that the contamination of the OPC sensor optics was a problem caused by the deposition of oil droplets and/or oil vapor. If left uncontrolled, this issue resulted in a significant decrease in effectively recorded mass. Rather than clean the optics regularly, the better strategy devised to address this issue was to reduce the sampling time intervals significantly. Also, the calibration of the OPC was found to be sensitive to pulsations in the sampling flow. The best way to overcome such issues is by calibrating with an aerosol in a steady flow. However, the exact nature of these problems has not been fully understood.

The entire process of sampling, diluting, conditioning, and measuring, along with the various loss corrections and experimental precautions derived in the laboratory, was

---

finally tested under field conditions with actual crankcase aerosol from a modern 4-cylinder 5.1-liter combustion engine. The engine aerosol was sampled from a port installed in the valve cover before it entered the crankcase ventilation system. Additionally, OPC measurements were obtained with undiluted aerosol, requiring the engine to run in a low-torque mode with relatively low aerosol concentrations to obtain a reference particle size distribution (PSD) for comparison. For the particle size range where a loss correction function was applied ( $\leq 8 \mu\text{m}$ ), it was found that the correction amounted to approximately 17% of the total aerosol mass. Measurements of the undiluted blow-by aerosol within the OPC sensor range of 0.6 to 40  $\mu\text{m}$  revealed that the PSD was actually much broader and exceeded the sensor's size range on both ends. Two prominent modes were detected in the volume-based PSD visible to the OPC: one in the range of 2 to 4  $\mu\text{m}$  and another around 20  $\mu\text{m}$ .

Based on these findings and with the above tools, a ***comprehensive study on a medium-duty 4-cylinder 5.1-liter diesel engine*** was conducted. The influence of oil temperature, engine load and engine speed on the blow-by aerosol properties was investigated. Increasing the engine load at 1200 rpm from 0 to 880 Nm at a free-moving oil temperature of up to 117 °C resulted in a 64% higher concentration of particles smaller than 1.2  $\mu\text{m}$ . At a constant oil temperature of 93 °C, the same test resulted in a 50% higher concentration. Similar results were obtained at 2200 rpm. Lowering the oil temperature to 48 °C almost completely prevented the formation of submicron particles. When increasing the engine speed from 1400 to 2400 rpm, the concentration below 2.7  $\mu\text{m}$  increased significantly. Both the increase in engine load and the increase in engine speed resulted in an increase in the blow-by gas flow rate and thus more aerosol emissions from the crankcase. To determine the aerosol contribution of the turbocharger, experiments were conducted by coupling and decoupling the turbocharger. The results show, surprisingly, that the turbocharger at nominal engine power was a negligible aerosol source, but contributed up to 30% to the blow-by gas flow. At medium load operation its aerosol contribution was always below 20%. The location of the blow-by aerosol

sources within the engine was determined by varying the OPC sampling points and introducing dilution air into different sections of the crankcase. The lower crankcase compartment was found to be the major source of submicron aerosols. Introducing air into this compartment caused particles to be flushed through the riser ducts into the upper crankcase section. This did not result in the dilution of the aerosol, but the mass rates increased in proportion to the dilution factor. Analysis of the separation characteristics of the risers showed inertial behavior and very low efficiencies of less than 10% at 10  $\mu\text{m}$ , resulting in most particles  $<10 \mu\text{m}$  passing through the ducts unhindered. The upper part of the crankcase proved to be a source of particles larger than 2.7  $\mu\text{m}$  and even larger than 10  $\mu\text{m}$ . These particles were captured by a filter integrated directly into the lid cover. Complementary measurements with an electrical mobility spectrometer showed that the mass contribution of aerosols smaller than 0.5  $\mu\text{m}$  at 1200 rpm and no-load operation is only about 1% (6 mg/m<sup>3</sup>).

An additional study was conducted in a controlled *single-cylinder crankcase environment* to investigate the sources of blow-by aerosol. The study revealed specific and recurring peaks in the droplet spectrum between 0.01 and 10  $\mu\text{m}$ , which could be attributed to distinct sources of oil aerosol. Regardless of whether the engine was static, motored, or fired, a super-micron mode around 2  $\mu\text{m}$  was consistently present. This mode was associated with the formation of satellite drops during the break-up of the cooling jet. Another mode around 0.6 to 0.8  $\mu\text{m}$  emerged and grew as peak pressure increased, both in the motored and fired modes. This peak could be linked to the piston rings, while bearings did not seem to contribute significantly to the aerosol below 116 bar peak pressure. In the fired engine, a third peak around 0.2  $\mu\text{m}$  to 0.3  $\mu\text{m}$  appeared at loads of 75% and above, which may be attributed to the re-condensation of oil vapor generated at engine hotspots. Soot and ash did not exhibit distinct modes in the aerosol particle size distribution (PSD), likely because such particles are integrated into the bulk oil.

---

Finally, the *roles of nucleation and growth through oil vapor condensation* in the formation of submicron aerosols in the crankcase were investigated under engine-like conditions by both experiments and simulations. The experiments utilized actual engine oil as well as hexadecane; simulations were performed using a one-dimensional MATLAB model based on classical nucleation theory and mass transfer between the liquid and vapor phases.

Chemical analysis of the submicron fraction of crankcase aerosols from the same 4-cylinder diesel engine using gas chromatography (GC) indicated that vapor-to-particle conversion mechanisms likely contribute to their formation. The GC spectra of the submicron aerosols revealed a significantly higher content of volatile hydrocarbons (up to C<sub>25</sub>) compared to the bulk engine oil (up to C<sub>40</sub>).

In the experimental setup, air-vapor mixtures were saturated within the temperature range of 100 °C to 130 °C (corresponding to vapor concentrations between 0.2 g/m<sup>3</sup> and 20 g/m<sup>3</sup>) and then cooled down to near ambient temperature at a defined rate, with and without pre-existing submicron oil droplets. The aerosols were characterized using an OPC and a scanning mobility particle sizer (SMPS). For engine oil without pre-existing nuclei, nucleation peaks appeared near 300 nm in the number concentrations. These peaks decreased with vapor supply and disappeared below 100 °C due to vapor losses onto cooling tube walls. The addition of nuclei at concentrations above approximately  $2 \times 10^5 \text{ cm}^{-3}$  suppressed spontaneous aerosol formation, consistent with observations from fired engines that the concentration of submicron blow-by aerosols is highly sensitive to bulk oil temperature.

Separately, nucleation and growth were simulated using a MATLAB model based on classical nucleation theory, combined with mass transfer between the liquid and vapor phases. The model equations account for progressive cooling, vapor losses to tube walls, and pre-existing nuclei. The simulations were first validated against the hexadecane experiments and then utilized to study the effects of cooling rate, vapor concentration,

nuclei concentration, and oil surface tension within parameter ranges that are challenging to explore experimentally. Equilibrium vapor data for hexadecane were obtained from the literature, while for actual motor oil the equilibrium vapor data were obtained by measurements in the relevant temperature range.

With regard to homogeneous nucleation, the simulations aligned well with condensation experiments in the absence of nuclei, particularly in terms of peak location. Increasing the equilibrium saturation level at a given temperature (equivalent to using a more volatile oil) shifted nucleation towards fewer but larger droplets, consistent with the observations comparing hexadecane and engine oil. As the nuclei concentration increased beyond  $0.2 \times 10^6 \text{ cm}^{-3}$ , nucleation peaks gradually increased in height while diminishing in asymptotic droplet size, ranging from about 200 nm to 40 nm, and eventually vanished beyond approximately  $1 \times 10^6 \text{ cm}^{-3}$  in favor of purely condensational growth on pre-existing nuclei. The growth of nuclei was less sensitive to vapor concentration, resulting in sizes between approximately 500 and 900 nm. Increasing the oil surface tension from 25 to 35 mN/m had a minimal effect on nucleation rates because the delayed initiation of nucleation due to an increased surface energy barrier was compensated by a significant increase in supersaturation during cool-down.

In conclusion, the combination of experimental findings and simulations substantiates the significant role played by both nucleation and condensational growth in the formation of submicron aerosols in the crankcase. The nucleation process is characterized by a peak in the size range of approximately 100 to 300 nm, whereas the condensational growth of pre-existing nuclei typically reaches completion between 500 and 900 nm. These two mechanisms give rise to distinct peaks in the aerosol size distribution, aligning remarkably well with previous studies on crankcase aerosols.

## **6.1 Strategies for reducing blow-by aerosol formation**

In order to reduce submicron blow-by aerosol emissions from an engine effectively, the primary focus should be on optimizing the design of piston rings. The rings have been

identified as the most significant contributors to submicron crankcase aerosol. Experiments with a single-piston engine showed that the rings are in fact both a source of blow-by gas which sweeps submicron aerosol out of the crankcase compartment, and a source of fine droplets in the 0.6 to 0.8  $\mu\text{m}$  range. In this context, reducing the brake mean effective pressure (BMEP) of the engine to a minimum would be equally advantageous because crankcase emission concentrations increase exponentially with BMEP.

Another reduction strategy hinges on the role of oil vapor in generating fine droplets. Enhanced piston cooling, e.g., by reducing the oil temperature of the cooling jet, may be a viable option in this regard. In experiments conducted on a single-cylinder engine, decreasing the oil temperature of the cooling jet from 80 to 50  $^{\circ}\text{C}$  (in motored mode) resulted in a 33% reduction in mass emissions, particularly in the 0.7  $\mu\text{m}$  mode. Similarly, on a 4-cylinder diesel engine (in fired mode), reducing the oil temperature from 93  $^{\circ}\text{C}$  to approximately 70  $^{\circ}\text{C}$  led to a 50% decrease in the concentration of particles smaller than 1  $\mu\text{m}$ . This temperature reduction also caused a shift in the particle size distribution towards larger particles, which can be separated more effectively by efficient oil mist filters.

The oil cooling nozzle itself generates a droplet mode around 2  $\mu\text{m}$ , which is associated with the formation of satellite drops during the break-up of the oil jet. By reducing the distance between the nozzle and the piston and thereby improving jet stability, the impact of this source can be minimized.

The turbocharger was found to contribute less than 20% to the aerosol mass but up to 30% to the blow-by gas flow. Its contribution to the total aerosol concentration at nominal engine power was negligible. However, the increased gas flow in the turbocharger return line to the crankcase can significantly affect emissions, just like the blow-by from the rings. Introducing this gas flow in the lower region of the crankcase, between the cylinder block and the oil sump, does not dilute the blow-by aerosol but rather flushes out additional particles. Alternatively directing the turbocharger gases to the upper region of the crankcase between the valve cover and cylinder head would be preferable

because this dilutes the blow-by aerosol. A prerequisite for this approach is that the entrance to the ventilation system must be in the upper region of the crankcase.

The crankcase, being a saturated environment, contains a significant amount of oil vapor. At temperatures around 120 °C, the vapor concentration exceeds 100 mg/m<sup>3</sup>. When this vapor condenses, it forms new particles and substantially increases the aerosol mass concentration. Therefore, it is evident that lower bulk oil temperatures and fewer engine hotspots play a key role in reducing aerosol mass emitted from the crankcase. The use of less volatile engine oils, although intuitively desirable, is less straightforward with regard to lowering the blow-by aerosol output, because higher a vapor pressure (at constant temperatures) results in the formation of fewer but larger droplets through nucleation and increased growth of existing aerosols. Larger droplets are easier to remove using most abatement devices. Lastly, the results suggest that lower cooling rates (though challenging to control in engine design) would be equally beneficial for the same reasons.

In summary, the following aerosol sources were found to be major contributors to blow-by aerosol in the range of 0.3 to 2.7 µm:

- Oil atomization at the piston rings/cylinder liners is the main source of PM.
- The break-up of the oil jet from the cooling nozzles forms satellite droplets.
- The blow-by gas flow (not PM) from the turbocharger is significant.
- Recondensing oil vapor from engine hot spots adds mass to airborne particles.

In contrast, the sources listed below contributed only slightly to aerosol in the 0.3 to 2.7 µm range. This knowledge is equally important to avoid efforts that do not result in benefits.

- No relevant atomization was detected at the main bearings.
- Valves, camshaft, and crankshaft mainly form coarser aerosol.
- No ash or soot mode (also below 0.3 µm) was detected in the crankcase.
- Aerosols from bursting oil bubbles/foam are negligible.
- The impaction of the oil cooling jet on a static piston forms almost no particles.

These findings point to meaningful in-engine reduction strategies that could be implemented during engine design and operation. They involve optimizing specific engine components, reducing oil temperature, reducing oil volatility, and increasing oil viscosity. This, of course, conflicts with other optimizations for engine operation. Therefore, finding a suitable solution to this trade-off is key to improving sustainable engine operation.







# List of publications

- Michler, T., Dörnhöfer, J., Erforth, D., Heinz, A., Erforth, D., Heinz, A., Scheiber, K., Weber, P., Nowak, N., Kubach, H., Meyer, J., Koch, T., Dittler, A. (2019). Comparison of Different Particle Measurement Techniques at a Heavy-Duty Diesel Engine Test Bed, SAE Technical Paper 2019-24-0158.
- Lorenz, M., Koch, T., Kasper, G., Pfeil, J., Nowak, N. (2020). Origin and Separation of Submicron Oil Aerosol Particles in the Blow-by of a Heavy-Duty Diesel Engine. SAE Int. Journal of Engines, 13, 363-375.
- Nowak, N., Scheiber, K., Pfeil, J., Meyer, J., Dittler, A., Koch, T., Kasper, G. (2020). Sampling and conditioning of engine blow-by aerosols for representative measurements by optical particle counters. Journal of Aerosol Science, 148, 105452.
- Nowak, N., Scheiber, K., Stieler, C., Heller, M.T., Pfeil, J., Koch, T., Kasper, G. (2021). On Blow-by Aerosol Sources in a Single-Cylinder Crankcase Environment. Proceedings of the ASME 2021 Internal Combustion Engine Division Fall Technical Conference.
- Nowak, N., Sinn, T., Scheiber, K., Straube, C., Pfeil, J., Meyer, J., Koch, T., Kasper, G., Dittler, A. (2021) On aerosol formation by condensation of oil vapor in the crankcase of combustion engines Aerosol Science and Technology, 56 (2), 101–116.
- Scheiber, K., Nowak, N., Pfeil, J., Koch, T., Kasper, G. (2021). Comparison of four diesel engines with regard to blow-by aerosol properties as a basis for reduction strategies based on engine design and operation, AAET, 6, 79–90.
- Scheiber, K.-M.; Nowak, N.; Lorenz, M. L.; Pfeil, J.; Koch, T.; Kasper, G. (2022). Impact of engine oil volatility and viscosity on blow-by aerosol formation, AAET, 7, 153–163.
- Nowak, N., Sirtl, C., Ryman, O., Flynn, P., Stieler, C, & Heller, M. (2022). Aerosol Separation and Pressure Control of a Smart Crankcase Ventilation System. Proceedings of the ASME 2022 ICE Forward Conference.
- Nowak, N., Roller, N. & Stieler, C. (2023). Future-proof Crankcase Ventilation Systems. MTZ Worldw 84, 62–67.

